Title
Control of Meiotic Entry by Dual Inhibition of the Key Mitotic Transcription Factor SBF

Author
Su, Amanda Jasmine

Publication Date
2023

Peer reviewed|Thesis/dissertation

Control of Meiotic Entry by Dual Inhibition of the Key Mitotic Transcription Factor SBF

By

Amanda J Su

A dissertation submitted in partial satisfaction of the

requirements for the degree of

Doctor of Philosophy

in

Molecular and Cell Biology

in the

Graduate Division

of the

University of California, Berkeley

Committee in charge:

Professor Elçin Ünal, Chair
Professor Nicholas Ingolia
Professor Rebecca Heald
Professor Kathleen Ryan

Summer 2023

Control of Meiotic Entry by Dual Inhibition of the Key Mitotic Transcription Factor SBF

Abstract

Control of Meiotic Entry by Dual Inhibition of the Key Mitotic Transcription Factor SBF

by

Amanda J Su

Doctor of Philosophy in Molecular and Cell Biology

University of California, Berkeley

Associate Professor Elçin Ünal, Chair

Transcription factors induce dynamic changes in gene expression to drive cellular differentiation. During the mitotic G1/S of budding yeast when the cell irreversibly commits to divide, transcription factors SBF(Swi4-Swi6) and MBF(Mbp1-Swi6) play essential roles by activating the expression of the G1/S transcriptome. While SBF and MBF act in parallel to mediate the mitotic G1/S transition, their regulation and function in meiosis have remained elusive. Here we characterize both the functional impact of SBF activation on meiotic entry and the molecular mechanisms restricting SBF activity in meiosis.

We first elucidated the functional significance of SBF activity restriction in meiosis and found that elevation of Swi4 protein levels was sufficient to activate SBF, resulting in mis-expression of SBF targets in meiosis. Further experimentation led us to discover that untimely SBF activation caused downregulation of early meiotic genes and delayed meiotic entry. Meiotic entry delays were caused by reduction in the function of Ime1, a master transcriptional regulator of meiosis. Among the SBF targets, G1 cyclins were the main driver of meiotic delays. We further found that G1 cyclins blocked the interaction between Ime1 and its cofactor Ume6.

We next investigated how SBF activity is restricted during meiosis and identified two parallel mechanisms: repression of the SBF-specific Swi4 subunit through LUTI-based regulation and inhibition of SBF by Whi5, a homolog of the Rb tumor suppressor. Our study provides insight into the role of *SWI4*^{LUTI} in establishing the meiotic transcriptional program and demonstrates how the LUTI-based regulation is integrated into a larger regulatory network to ensure timely SBF activity.

For my family, Mom, Dad, Madison and Maypo, and for my partner Dan.

Table of contents

List of Figures

List of Tables

Acknowledgements

Thank you to my family for all your love, support, and understanding – I would not have made it this far without you all. I am immensely grateful for all my parents sacrificed in raising me and giving me the privilege to pursue my passions and interests. Thank you to my sister – you are my other half and I would not be here without you.

Graduate school was made truly worthwhile since I met my lifelong partner Dan here. Thank you, Dan, for helping me through every day with so much love and laughter. I cannot adequately thank you enough to express how grateful I am for all your selfless support. Thank you for all the yummy food, for playing games with me, and for always taking me on new adventures in the Bay and beyond.

Thank you Elçin for your patience, passion, and generosity throughout my time in graduate school. You have supported me throughout difficult challenges in both graduate school and personally and I cannot imagine getting through graduate school without you as my mentor.

Thank you to all the current and former members of the Brar and Ünal lab. The supportive and friendly environment fostered in this lab is like no other and I am so grateful to have been a part of. Thank you to my second mentor Gloria for your thoughtful feedback and support throughout the years. Kate, my bay mate, I am deeply grateful for finding your friendship in graduate school. Thank you for always making me laugh and for always being there to support me through both the highs and lows of lab and life. Thank you, Christiane, for all your hard work keeping the lab running – we would all be lost without your skillful organization and handiness in the lab. You have also been such a wonderful friend to me and seeing and talking to you in lab always brightened my day. Thank you to my amazingly hardworking and kind technician Siri. It was an honor to work with you and thank you for your dedication and patience.

Finally, I want to thank all my friends both in and out of graduate school. I have met so many wonderful and supportive people throughout my time in Berkeley. From griding ranks in games online with me to exploring the food of the Bay Area you all have been amazingly generous friends who have brought invaluable balance and joy to my life.

Chapter 1: Introduction

Gametogenesis is a conserved and fundamental process by which sexually reproducing organisms undergo a specialized cell division known as meiosis, which is coupled with major cellular remodeling to form reproductive cells called gametes. In the budding yeast *Saccharomyces cerevisiae*, many of the gametogenic events are conserved with metazoans, making this a simple and highly- tractable model system. In budding yeast, gametogenesis is also known as sporulation and the gametes are often referred to as spores. Entry into gametogenesis requires multiple external stimuli and internal cues that which trigger waves of gene expression. This chapter will introduce the regulatory mechanisms governing entry into gametogenesis. The terms “meiotic program” and “meiotic differentiation” will be used interchangeably with “gametogenesis” throughout this dissertation.

1.1: Overview of meiosis

In the budding yeast *Saccharomyces cerevisiae*, gametogenesis occurs under nutrient-depleted conditions whereby a diploid cell differentiates into haploid gametes. This reduction in ploidy occurs as a result of the two meiotic nuclear divisions that follow a single round of DNA replication and is coordinated with major morphogenic changes to produce haploid spores (reviewed in Neiman, 2011).

A diploid yeast has two copies of each chromosome, one from each parent chromosome. These pairs are called homologous chromosomes or homologs. Upon entry into meiosis the cell undergoes synthesis phase or ‘S phase’ (Figure 1.1) when a single round of DNA replication produces identical copies of each chromosome. These identical copies are referred to as sister chromatids, which are joined together by the cohesin protein complex.

S phase is followed by Prophase I when DNA recombination is initiated via programmed double stranded breaks (DSBs) throughout the genome by the meiosis-specific endonuclease Spo11. In budding yeast and mammals this recombination step is how homologs are “find one another” and pair while also introducing genetic diversification (reviewed in Keeney et al., 2014). During recombination DSBs are repaired by homologous recombination, resulting in genetic exchange between the homologous chromosomes. Formation of the synaptonemal complex further pair the homologous chromosomes. Homologous recombination is essential for proper meiotic divisions as it aids in the formation of physical linkages between the homologs. Linkage between each pair of homologs is necessary for their proper orientation and subsequent segregation on the meiosis I spindle. Failure at this step can lead to meiotic arrest or chromosome segregation failure which is often linked with fertility defects (reviewed in Hassold T and Hunt P, 2001). Spo11 and other key proteins involved in meiotic recombination, such as Rad51, and Mre11, are conserved between yeast and humans (reviewed in Handel and Schimenti, 2010). Studying meiosis in budding yeast has added to field’s understanding of the regulation of meiotic recombination, including the strict spatial and temporal control of DSB formation and repair.

Following recombination, the cell undergoes two consecutive rounds of chromosome segregation. In meiosis I, the homologous chromosomes separate, followed by meiosis II, where the sister chromatids split. Since there is no additional round of DNA replication, the result is four haploid gametes. Accurate chromosome segregation is essential to ensure the proper distribution of genetic material into the haploid daughter cells. During meiosis II the prospore membrane begins to encapsulate the four spores, in a structure called a tetrad. Coupled to meiosis are other major morphological changes such as organelle remodeling (reviewed in Sing et al., 2022), as the haploid gametes inherit a single copy of the genome and organelles.

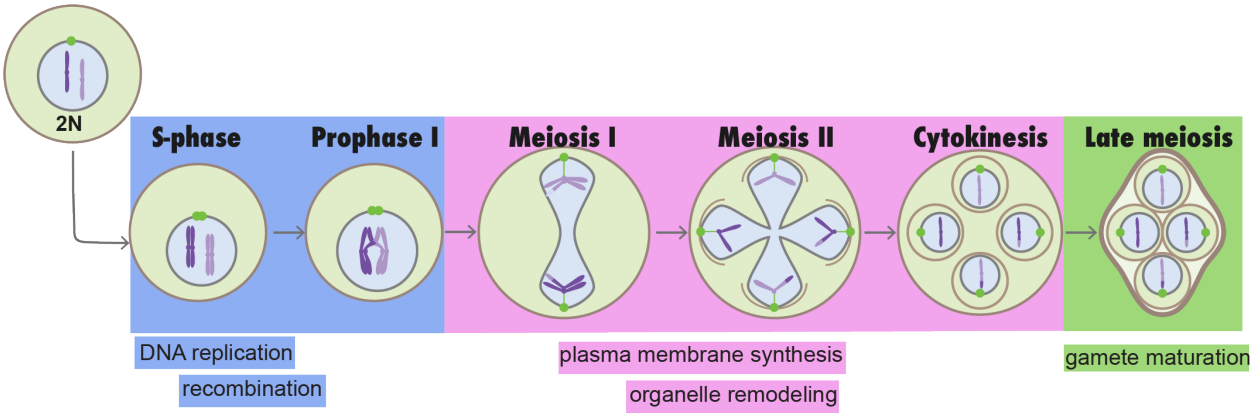

Figure 1.1. Overview of yeast gametogenesis.

Birth defects and aneuploidies, conditions characterized by an abnormal number of chromosomes in the cell, occur when there are errors in meiosis. As women age, the quality of their oocytes declines, resulting in an increased likelihood of errors during meiosis. Studies have shown the incidence of aneuploidies, such as Down syndrome and other chromosomal disorders, is higher in children born to older mothers (reviewed in Hassold T and Hunt P, 2001). These conditions can have significant developmental and health consequences, highlighting the importance of understanding the mechanisms underlying successful meiosis.

1.2: Regulation of meiotic differentiation

Gametogenesis is controlled by a cascade of regulatory events to ensure proper coordination of meiotic progression. Key factors involved in this regulation are transcription factors (TF) controlling the expression of genes critical for meiosis. Microarray studies first characterized the regulation of meiotic progression in budding yeast involving a coordinated series of expression of early, middle, and finally late genes, (Chu et al., 1998). Early genes are involved in meiotic DNA replication, middle genes regulate the meiotic divisions and spore formation, while late genes are involved in spore maturation. Strict temporal regulation of these transcriptional waves by key TFs ensures the proper advancement of meiosis.

Entry into gametogenesis impinges on the TF Ime1, which regulates the first wave of early meiotic genes involved in DNA replication and recombination (Williams et al., 2002; Chu et al., 1998; Brar et al., 2012). Due to it being the gatekeeper of meiosis many signals converge on the ~two kilobase long *IME1* promoter; namely a diploid *MAT***a**/*MAT*α mating type, presence of a non-fermentable carbon source, respiration-competent mitochondria, and nitrogen depletion (Honigberg, 2003; reviewed in van Werven and Amon, 2011; Kassir et al., 1988). Additional work has shown that *IME1* expression requires downregulation of G1 cyclins known as Clns as well as cAMP-protein kinase A (PKA) and TORC1 pathways (Weidberg et al., 2016; Colomina et al., 1999). Understanding the regulation of *IME1* therefore is important to understanding meiotic entry.

Next, we will explore the details of how mating type and nutritional signals are integrated at the *IME1* locus to control *IME1* expression. Mating type in yeast is defined at the MAT locus and there are two versions of the MAT locus, *MAT**a*** and *MAT*α. At the *MAT**a*** or *MAT*α loci DNA binding protein a1 or α*2* are expressed respectively. In a diploid cell, when both are expressed, the two proteins form a1/α*2* a transcriptional repressor complex that binds the *RME1* (repressor of Ime1) promoter to inhibit *RME1* expression (Covitz et al., 1991). Therefore, haploid cells express Rme1 and prevent expression of *IME1* while diploid cells inhibit *RME1* and thus express *IME1*. This mechanism was further characterized at the *IME1* locus involving two long non-coding RNA (lncRNA) whose expression regulate *IME1* levels and the propensity of meiotic entry (Moretto et al., 2018; van Werven et al., 2012). The first lncRNA *IRT1* is within the *IME1* promoter and expressed from the same strand as *IME1*. When *IRT1* is expressed co-transcriptional repressive histone modifications H3 lysine 4 demethylation (H3K4me2) H3 lysine 36 trimethylation (H3K36me3) are laid down as well as changes in nucleosome positioning turning off expression of *IME1* (Van Werven et al., 2012). The repressive *IRT1* transcript is regulated by Rme1 and therefore is only expressed in haploid cells. A second lncRNA called *IRT2* was later discovered. Its expression is on the same strand as *IRT1* and *IME1* (Moretto et al., 2018). *IRT2* expression occurs during starvation conditions in diploid cells and its expression represses *IRT1* to help further induce *IME1* transcript levels. *IRT2* expression is regulated by Ime1 itself as it has URS1 site in its promoter driving its expression. Altogether, there is a feed-forward loop whereby expression of Ime1 drives more robust expression of *IME1* increasing the probability of entering meiosis.

Depletion of fermentable carbon sources is an additional requirement for meiotic entry which is regulated at the level of *IME1* expression. In the presence of a fermentable carbon source such as glucose yeast will primarily undergo fermentation which activates the Ras/PKA signaling pathway. High PKA levels have been shown to regulate *IME1* expression by at least three mechanisms. Firstly, high PKA levels inactivate TFs Msn2 and Msn4 via phosphorylation (Smith et al., 1998). Msn2 and Msn4 induce expression of genes with a stress-response element (STRE), one of which is *IME1* (Görner et al., 1998; Martínez-Pastor et al., 1996; Sagee et al., 1998). *IME1* expression is thus repressed by high PKA levels. Additionally, high PKA levels results in phosphorylation of the transcriptional repressor Sok2 to downregulate *IME1* expression. Finally, the AMP kinase

Snf1 activates *IME1* expression in response to glucose level by inhibiting repressor Tup1-Ssn6 (Mizuno et al., 1998).

In addition to regulation of *IME1* transcript levels, there are also post-translational mechanisms in place to regulate Ime1 and in turn entry into meiosis. Namely Ime1 protein stability as well as localization are regulated during meiosis. Ime1 protein is degraded by the proteasome and its stability is regulated by the kinase Ime2, which destabilizes Ime1 (Guttmann-Raviv et al., 2002). Localization of Ime1 is regulated by nutritional cues through TORC1 and G1 cyclins, as well as an unidentified mechanism that involves ammonia (Colomina et al., 1999, 2003). In these studies, high G1 Cyclin-CDK dependent kinase (Cln-CDK) activity or nitrogen availability resulted in cells with reduced nuclear Ime1 and decreased sporulation efficiency.

Ime1 cannot bind to DNA or chromatin itself, but instead activates its targets via its association with its cofactor Ume6 (Smith et al., 1993; Williams et al., 2002; Strich et al., 1994). Ume6 is bound to upstream regulatory sequence 1 (URS1) motif in the promoters of early meiotic genes (EMGs). During mitotic growth, in the absence of Ime1, Ume6 functions as a transcriptional repressor of EMGs due to its association with the Sin3/Rpd3 histone deacetylase complex (Kadosh and Struhl, 1997) and the Isw2 chromatin remodeling complex (Goldmark et al., 2000). Ime1's binding to Ume6 results in the activation of EMGs and initiation of meiotic entry. Two protein kinases, Rim11 and Rim15, phosphorylate Ime1. Both kinases are inhibited by the presence of glucose via the PKA pathway (Pedruzzi et al., 2003; Rubin-Bejerano et al., 2004; Vidan and Mitchell, 1997). The Rim11/Rim15-dependent phosphorylation of Ime1 regulates its interaction with Ume6, and therefore assists in the activation of EMGs (Vidan and Mitchell, 1997; Pnueli et al., 2004; Malathi et al., 1999, 1997).

Ime1-Ume6 additionally regulates the expression of an important target gene called *NDT80*, which encodes a TF regulating the middle meiotic genes (MMGs). Expression of *NDT80* occurs during pachytene of meiotic prophase, culminating in the meiotic divisions where cells are now irreversibly committed to meiosis (Tsuchiya et al., 2014; reviewed in Winter, 2012). Regulation of *NDT80* expression is also tightly controlled and while having a URS1 site in its promoter where Ime1-Ume6 is bound, NDT80 is not expressed with the EMGs. This is due to a repressor protein Sum1 that has overlapping binding specificity to Ndt80 and is bound to an extended MSE element (Xie et al., 1999). Sum1 recruits and binds histone deacetylase Hst1 to represses gene expression (Xie et al., 1999). Other Ndt80-regulated genes have Sum1-Hst1 complex bound to their MSE elements to repress expression in mitotically growing cells (McCord et al., 2003). Therefore, the expression of *NDT80* is regulated by both Ume1-Ime1 and removal of Sum1-Hst1 via phosphorylation (Pak and Segall, 2002; Shin et al., 2010). Ndt80 goes on to regulate the expression of MMGs, which include genes that regulate the meiotic divisions as well as genes that function during spore wall formation (reviewed in Neiman 2005).

1.3: Overview of the G1/S transition

The general mechanisms regulating the eukaryotic cell cycle, including those regulating the G1/S transition, are functionally conserved from yeast to metazoans (reviewed in Bertoli et al., 2013; Eser et al., 2011). Progression through the cell cycle is tightly regulated to ensure proper ordering of molecular events as the cell divides. A major driver promoting progression through the mitotic program are cyclin-dependent kinases (CDKs). CDKs are protein kinases that require a subunit cyclin to activate and specify their enzymatic activity. Budding yeast has a single CDK, Cdk1 (also known as Cdc28) that works in complex with nine different cyclins. Each cyclin acts in a specific stage of the cell cycle when in complex with Cdk1. In brief there are three G1 cyclins, Cln1 through Cln3 which form Cln-CDK complexes to progress the cell through the G1 phase and G1/S transition (reviewed in Bertoli et al., 2013). B-type cyclins Clb5 and Clb6 regulate S phase and B-type cyclins Clb1-4 regulate M phase (reviewed in Bloom and Cross, 2007). Each cyclin-CDK complex phosphorylates a specific group of substrates which are necessary for the cell cycle to progress. Finally, it is thorough the strict regulation of cyclin synthesis and degradation that allows for this carefully regulated series of molecular events to occur properly.

Here we will compare and contrast how these cyclin-CDKs regulate mitotic versus meiotic G1/S. The G1/S transition which in budding yeast is referred to as the commitment point or 'Start' is the point where the cell is irreversibly committed to DNA replication and subsequent division (Hartwell et al., 1974). Accumulation of Cln-CDK results in the activation of the SBF (SCB-binding factor) and MBF (MCB-binding factor) TFs. Cln3-CDK relieves repression of SBF by Whi5 via phosphorylation of Whi5. This partial activation of SBF leads to expression of G1 cyclins *CLN1* and *CLN2* whose protein product, when complexed with CDK, hyperphosphorylates Whi5 promoting its nuclear export, thereby fully activating SBF (Costanzo et al., 2004; De Bruin et al., 2004; Wagner et al., 2009). This positive feedback loop, whereby SBF activates expression of Cln1 and Cln2 which results in further de-repression of SBF, drives the commitment to Start (Doncic et al., 2011). SBF and MBF activate the expression of hundreds of genes including S-phase cyclins Clb5 and Clb6 (Spellman et al., 1998; Iyer et al., 2001; Ferrezuelo et al., 2010). Finally, during the mitotic G1/S phase, late G1 promotion into S phase requires Cln-CDK triggered degradation of Sic1 (Verma et al., 1997) which inhibits B-type cyclins Clb5 and Clb6. Degradation of the S-phase CDK inhibitor Sic1 is how mitotic cells move from G1 to S phase where DNA replication occurs.

G1 cyclins have been shown to be repressive for meiotic entry (Colomina et al., 1999) so how is the G1/S transition accomplished for meiotic G1/S where Clb5 and Clb6 still direct premeiotic S phase? As reviewed in Section 1.2, upon meiotic entry Ime1 and Ime2 are expressed and both promote entry into meiotic S phase. *IME2* is an EMG regulated by Ime1 itself, which is a meiosis-specific kinase with homology to CDKs (reviewed in Honigberg, 2004). During the meiotic G1/S transition, Cln-CDK complex is replaced by Ime2 protein kinase where Ime2 drives cells into premeiotic S phase by promoting degradation of the S phase CDK inhibitor Sic1 (Dirick et al., 1998; Brush et al., 2012). After S phase, Clb-CDK activities are diversely regulated to achieve meiotic recombination and the divisions (Carlile and Amon, 2008).

1.4: Transcriptional activation of G1/S transition

As reviewed in section 1.3, cells enter a new cell cycle during G1 via activation by Cln-CDKs, which promote expression of the G1/S transcriptome. The mechanisms of G1/S transcriptional activation are functionally conserved from yeast to humans. In budding yeast, the G1/S transcriptome of the mitotic cell cycle is regulated by SBF and MBF. SBF is a heterodimeric TF comprised of Swi4 and Swi6 while Mbp1 and Swi6 make up MBF. Swi4 and Mbp1 are the DNA binding components for each TF and bind to SCB (Swi4 cell cycle box) and MCB (MluI cell cycle box) consensus sequences, respectively. During the G1/S transition, SBF and MBF are bound to sequence-specific promoter elements in order to activate a transcriptional program involving around 200 genes (Spellman et al., 1998; Simon et al., 2001; Iyer et al., 2001). Improper regulation of the G1/S transition can lead to cancer due to uncontrolled cell proliferation.

Whi5 is nuclear and bound to SBF to repress its activity during early G1 (Argüello-Miranda et al., 2018). This repression is relieved via three main mechanisms: Whi5 dilution (Schmoller et al., 2015), phosphorylation of Whi5 by Cln-CDKs (Costanzo et al., 2004; De Bruin et al., 2004; Wagner et al., 2009), and activation of SBF-regulated transcription via Cln3 (Kõivomägi et al., 2021). Cln3 is the most upstream activator of SBF via phosphorylation of repressor Whi5. Cln3 protein levels are regulated via nutritional availability through transcription, translation, as well as protein stability. CLN3 transcript levels are induced by glucose and *CLN3* is translationally repressed during nitrogen limitation(Parviz and Heideman, 1998; Gallego et al., 1997).

During the G1/S transition, activation of SBF and MBF is required for budding and DNA replication. SBF regulates genes involved in budding and cell morphogenesis while MBF regulates genes involved in DNA replication (Iyer et al., 2001). Although SBF and MBF act in parallel during the G1/S transition, it has been observed that they activate functionally specialized subsets of genes (Iyer et al., 2001; Simon et al., 2001; Ferrezuelo et al., 2010). This partitioning of SBF and MBF regulated plays an important role during induction of different transcriptional programs like responses to DNA stress (Travesa et al., 2013). Despite the well characterized function in budding yeast mitotic growth, the regulation and function of SBF and MBF in meiosis remains largely unknown. During mitotic growth, SBF and MBF act in conjunction since DNA replication and budding occur simultaneously. In contrast, because the meiotic program requires DNA replication but not bud formation, the regulation and subsequent activity of SBF and MBF must be divergent in meiosis. Additionally, during early meiosis SBF targets are suppressed while MBF targets are upregulated (Iyer et al., 2001). While this pattern does not demonstrate a direct role for SBF and MBF in regulating meiotic gene expression, it supports the proposed functional specialization of SBF and MBF playing a role in establishing the meiotic G1/S regulon. For example, downregulation of SBF could be crucial during meiotic entry since SBF regulates cyclins *CLN1* and *CLN2,* which have been shown to repress early meiotic gene expression (Colomina et al., 1999). Understanding the functional consequence of the specialized functions of SBF and MBF in meiosis will unravel an important aspect of meiosis- how the meiotic transcriptional program can be established by SBF and MBF.

1.5: LUTI-based gene regulation

The advent of high throughput sequencing and ribosome profiling revealed the gene regulation of budding yeast meiosis to dynamic and complex. High-resolution transcriptome analysis revealed non-canonical transcript isoforms expressed in yeast during meiosis (Brar et al., 2012; Cheng et al., 2018; Lardenois et al., 2011; Kim Guisbert et al., 2012; Chia et al., 2021). Additionally, paired RNA-seq and ribosome profiling of the meiotic program revealed an enrichment of non-canonical translation in meiosis with 30% of ribosome footprints mapping outside of annotated open reading frames (ORFs) in meiosis (as compared to 5% in mitosis). Many of these footprints mapped to novel start sites using AUG or near-cognate (non-AUG) codons revealing new protein products as well as translationally repressive upstream ORFs (uORFs). From these observations we can posit two general functions these non-canonical gene expression mechanisms are adding: 1) novel or alternative protein products 2) modulation of gene expression.

What mechanisms regulate how these novel meiosis specific proteins are made? A subset of footprints mapping outside of annotated ORFs in meiosis produce short ORFs or short peptides, which contain a canonical start and stop codon. These ORFs were previously not annotated due to their short length when the *S. cerevisiae* genome was first sequenced. The second group are synthesized due to non-canonical translation occurring in meiosis. The use of translation start site initiation mapping in meiosis (Eisenberg et al., 2020) revealed many N-terminally extended proteins initiate at upstream near-cognate start codons to generate alternative protein isoforms and have been observed in yeast and other organisms (reviewed in Higdon and Brar, 2021; Kearse and Wilusz, 2017). In addition, there are truncated proteins which occurs through the use of an in-frame downstream start codon often due to alternative transcription start site usage. Overall, these non-canonical translation events occurring in meiosis result in the production of short peptides, N-terminally extended or truncated proteins with potentially altered meiosis specific functions. Even though the functional significance of these alternative protein products is unknown, their pervasive expression in meiosis suggest potential contributions to gamete development.

Aside from alternative protein products these non-canonical transcription and translation events can function to toggle gene expression. It has been well characterized that there is dynamic expression of non-canonical transcript isoforms in yeast meiosis. Many non-canonical transcript isoforms have been characterized to regulate gene expression. For example, expression of two lncRNAs results in the recruitment of methyltransferases and histone deacetylases, altering the chromatin context and resulting in transcriptional interference of nearby gene *IME1* (Moretto et al., 2018; van Werven et al., 2012). Additionally, transcriptional interference also occurs in meiosis via anti-sense transcription at the *IME4* locus to regulate *IME4* expression at the onset of meiosis (Hongay et al., 2006).

Finally, a non-canonical form of gene expression that combines uORF translational repression as well as transcriptional interference is LUTI-based repression. LUTI-

mediated gene regulation was first characterized at the *NDC80* locus (Chen et al., 2017; Chia et al., 2017). LUTI-based gene regulation occurs when expression from an upstream distal promoter (*NDC80*^{LUTI} promoter) produces a 5′ extended LUTI mRNA. Expression of *NDC80*^{LUTI} mRNA results in combined act of transcriptional and translational interference, ultimately resulting in downregulation of Ndc80 protein synthesis.

The transcriptional interference is achieved during expression of the LUTI mRNA where co-transcriptional repressive histone modifications H3 lysine 4 demethylation (H3K4me2) and H3 lysine 36 trimethylation (H3K36me3) are deposited over the previously active *NDC80* canonical promoter (Chia et al., 2017; reviewed in Li et al., 2007). Deposition of H3K4me2 and H3K36me3 results in increased nucleosome occupancy, which inhibits transcription initiation at the *NDC80* canonical promoter. In summary, *NDC80*^{LUTI} expression results in decreased canonical *NDC80* transcript due to transcriptional interference. Secondly, translational interference occurs due to uORFs contained within the 5′ extended leader of the LUTI mRNA. Since scanning for a start codon by the ribosome occurs in the 5′ to 3′ direction, these uORFs are translationally repressive due to translation initiation and termination occurring within the upstream uORFs, thus outcompeting initiation at the original canonical ORF.

While both transcriptional and translational interference have been characterized forms of gene regulation (reviewed in Gullerova and Proudfoot, 2010; reviewed in Andrews and Rothnagel, 2014), the LUTI based mechanism uniquely couples the two together. The LUTI mRNA is the black sheep of the canonical central dogma as increased expression mRNA leads in this case does not result in increased protein output. Additionally, it is proposed that LUTI mediated regulation evolved from changes in cis regulatory regions of target genes resulting that co-opted existing transcription factors to produce LUTI mRNA to tune gene expression (reviewed in Tresenrider and Ünal, 2017). Furthermore, cell differentiation programs such as meiosis are well characterized as initiated through temporal activation of gene waves. The evolution of LUTI-based gene regulation uniquely allows for coordinated gene repression during these waves of gene activation.

LUTI expression is highly tunable and allowing for dynamic changes in gene expression. At least 380 LUTIs are expressed at distinct times throughout the budding yeast meiotic program (Cheng et al., 2018; Tresenrider et al., 2021). Additionally, 15 LUTIs, which are regulated by the evolutionarily conserved transcription factor Hac1, have been identified during the unfolded protein response (Van Dalfsen et al., 2018). LUTI-based regulation is not restricted to yeast as it occurs in fruit flies and human cells (Jorgensen et al., 2020; Hollerer et al., 2019). While LUTIs have been identified in various contexts of cellular stress and differentiation, their effect on cellular physiology during these processes is poorly understood.

The work described in this thesis, identifies the function of SBF's downregulation during meiotic G1/S. Using two orthogonal methods, RNA-seq and time-lapse fluorescent microscopy, we discover that increased SBF activity delays meiotic entry due to the expression of G1 cyclins, *CLN1* and *CLN2*. Additionally, we found that G1 cyclins suppress meiotic entry by blocking the interaction between Ime1 and its binding partner

Ume6. Finally, we uncover two parallel working mechanisms regulating SBF activity during meiosis. We first characterize an Ime1-regulated meiotic LUTI expressed from the *SWI4* locus (*SWI4*^{LUTI}), which through paired transcriptional and translational interference results in decrease Swi4 abundance during meiotic entry. Further investigation revealed a second regulator, Whi5, which is a well characterized suppressor of SBF in mitotic growth. Only when we combined loss of LUTI-based repression and removal of Whi5 did we observe a meiotic delay. These data together suggest an important functional role for *SWI4*^{LUTI} during the switch from mitotic growth to meiotic differentiation.

Chapter 2: SBF downregulation is required for timely meiotic entry

This chapter is adapted from the following publication:
Su, A.J., S.C. Yendluri, and E. Ünal. (2023). Control of meiotic entry by dual inhibition of a key mitotic transcription factor. *bioRxiv*. https://doi.org/10.1101/2023.03.17.533246

2.1 Introduction

A key aspect in understanding developmental programs and cell state transitions is mapping the interplay between transcription factors and their associated gene regulatory networks. In the budding yeast *Saccharomyces cerevisiae*, the transition from mitotic growth to meiotic differentiation is a crucial decision that is regulated by multiple inputs, such as nutrient availability, respiration competence, and cell identity. Under nutrient-limiting conditions, a diploid cell enters the meiotic program to produce four haploid gametes. The process of meiotic entry is tightly controlled by the master transcriptional regulator Ime1, as both extrinsic (e.g. nutrient status, extracellular pH) and intrinsic (e.g. mating type, mitochondrial function) cues are integrated at the *IME1* promoter (Kassir et al., 1988; Honigberg, 2003; reviewed in van Werven and Amon, 2011). Once translated, Ime1 is phosphorylated by the Rim11 and Rim15 kinases to promote its nuclear localization and interaction with Ume6 (Vidan and Mitchell, 1997; Pnueli et al., 2004; Malathi et al., 1999, 1997). In mitotically dividing cells, Ime1 target genes are repressed by Ume6 through its association with the Sin3-Rpd3 histone deacetylase complex (Kardosh and Struhl, 1997; Rundlett E. et al., 2003). However, under nutrient starvation, entry into the meiotic program is initiated by the interaction between Ime1 and Ume6, which together function as a transcriptional activator, culminating in the induction of early meiotic genes (Bowdish et al., 1995). Mitosis to meiosis transition requires dynamic remodeling of the gene regulatory networks to maintain the mutual exclusivity of these programs. While entry into the mitotic program is initiated by the central transcription factors SBF and MBF (Spellman et al., 1998; Iyer et al., 2001), whether and how these complexes are regulated during meiotic entry is unknown.

The molecular mechanisms regulating entry into the mitotic cell cycle, also known as G1/S transition, are functionally conserved from yeast to metazoans (reviewed in Van Den Heuvel and Dyson, 2008). SBF and MBF are heterodimeric transcription factors composed of Swi4-Swi6 and Mbp1-Swi6 subunits, respectively (Figure 2.1).

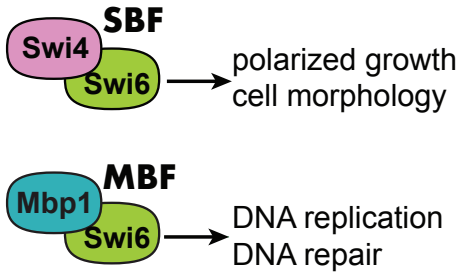

Figure 2.1. A schematic of SBF and MBF complexes.

These transcription factors are homologous to the mammalian E2Fs (reviewed in Bertoli et al., 2013). E2Fs are negatively regulated by the tumor suppressor protein Rb, which is homologous to the budding yeast Whi5 that inhibits SBF in early G1 (De Bruin et al., 2004; Costanzo et al., 2004; Hasan et al., 2014). Whi5-based SBF inhibition is relieved by cyclin/CDK-dependent phosphorylation and subsequent re-localization of Whi5 from the nucleus to the cytoplasm (Wagner et al., 2009). Although SBF and MBF act in parallel during the G1/S transition (Spellman et al., 1998; Iyer et al., 2001), they activate functionally specialized subsets of gene targets. SBF regulates the expression of genes involved in budding and cell morphogenesis, while MBF-regulated genes are involved in DNA replication and repair (Iyer et al., 2001; Simon et al., 2001). Despite the well-characterized function in budding yeast mitotic growth, the regulation and function of SBF and MBF during meiotic entry remains largely unknown. In contrast to mitotic divisions where budding and DNA replication occur simultaneously, the meiotic program requires DNA replication and repair, but not bud morphogenesis or asymmetric growth. Accordingly, the regulation and subsequent activity of SBF and MBF are likely to be divergent to establish meiotic entry.

The activity of SBF and MBF is regulated in part through subunit abundance, which in turn controls expression of the G1/S regulon (Dorsey et al., 2018). For example, overexpression of a hyperactive allele of *SWI4* can trigger premature entry into the cell cycle (Sidorova and Breeden, 2002). Additionally, *SWI4* has also been shown to be haploinsufficient and rate limiting during G1/S progression (Mcinerny et al., 1997). These results suggest that the precise levels of SBF and MBF subunits are important for activating the G1/S regulon at the correct time.

Three key observations support differential regulation of SBF and MBF during the meiotic program: First, a meiotic mass spectrometry dataset suggests that Swi4 has dynamic protein behavior, which is not observed for its counterparts Swi6 and Mbp1 (Cheng et al., 2018). Second, two SBF-specific targets, namely the G1-cyclins *CLN1* and *CLN2*, have been shown to repress early meiotic gene expression (Colomina et al., 1999). Third, meiotic cells express a repressive non-canonical mRNA from the *SWI4* locus called LUTI (Brar et al., 2012; Tresenrider et al., 2021), which stands for Long Undecoded Transcript Isoform (Chen et al., 2017; Chia et al., 2017). This last point will be further investigated in Chapter 3.

Here we investigate differential regulation of SBF and MBF during the meiotic program and determine how the untimely activation of SBF impacts meiotic entry. We found that overexpression of Swi4 results in the activation of SBF targets and concomitant downregulation of the early meiotic genes. SBF targets Cln1 and Cln2 inhibit meiotic entry by blocking the interaction between Ime1 and its cofactor Ume6. Overall this our work provides mechanistic insights into how SBF misregulation impedes transition from mitotic to meiotic cell fate.

2.2 Results

2.2.1 Swi4 is the sole downregulated subunit within the SBF and MBF complexes during meiosis

While the SBF and MBF transcription factors have been heavily studied in the context of the mitotic cell cycle, their involvement in regulating the meiotic transcriptional program is not well understood. To understand the regulation and function of these complexes during meiosis, we first monitored the levels of SBF and MBF subunits throughout a meiotic time course. Cells were first grown in rich media overnight and were then transferred to pre-sporulation media. After additional overnight growth, cells were shifted to sporulation media (SPO) to induce meiosis, and samples were taken hourly for protein extraction and immunoblotting to monitor the abundance of each subunit. Unlike the mitotic G1/S transition (Kelliher et al., 2018), meiotic entry resulted in ~30% decrease in Swi4 levels after 2 hours, while Mbp1 and Swi6 levels were increased (Figure 2.2*).* These data indicate that Swi4 is the sole subunit within SBF and MBF whose level declines during meiotic entry and are consistent with a published mass spectrometry dataset (Cheng et al., 2018).

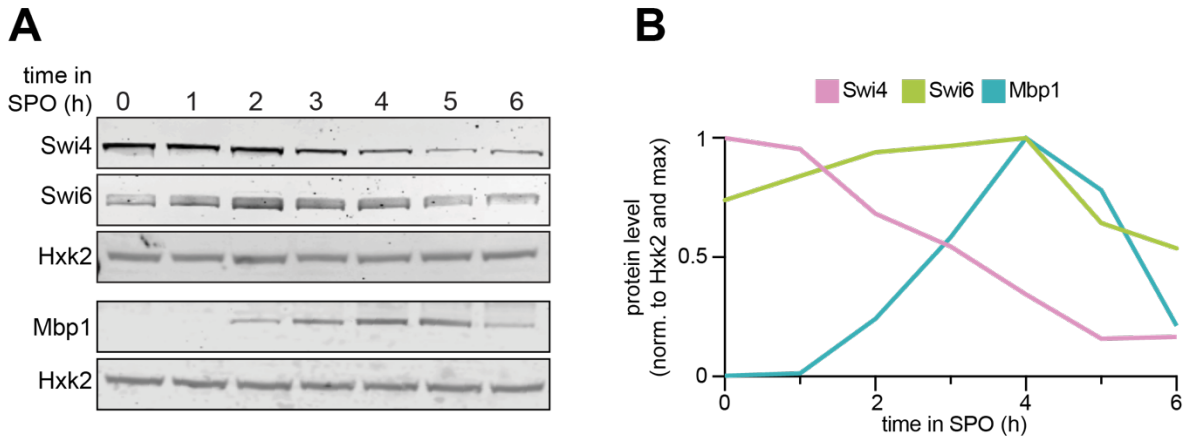

Figure 2.2. A. Abundance of SBF and MBF subunits in meiosis. Samples from strain UB35246 were collected between 0-6 hours (h) in sporulation medium (SPO) and immunoblots were performed using α-Swi4, α-Swi6, and α-Mbp1 respectively. Hxk2 was used a loading control. Representative blots from one of two biological replicates are shown. **B.** Quantification of the immunoblots in (A). The signal at each time point was first normalized to Hxk2 loading control and then to the max signal.

We next examined the expression of a set of well-characterized transcripts that are regulated by SBF or MBF (Iyer et al., 2001; Simon et al., 2001; Bean et al., 2005; Harris et al., 2013; Smolka et al., 2012) using a published meiotic RNA-seq dataset (Brar et al., 2012). This analysis revealed that compared to mitotically dividing cells, most of the SBF-specific target genes had either low or no expression during early meiosis (Figure 2.3). In contrast, most of the MBF targets displayed increased expression upon meiotic entry (Figure 2.3).

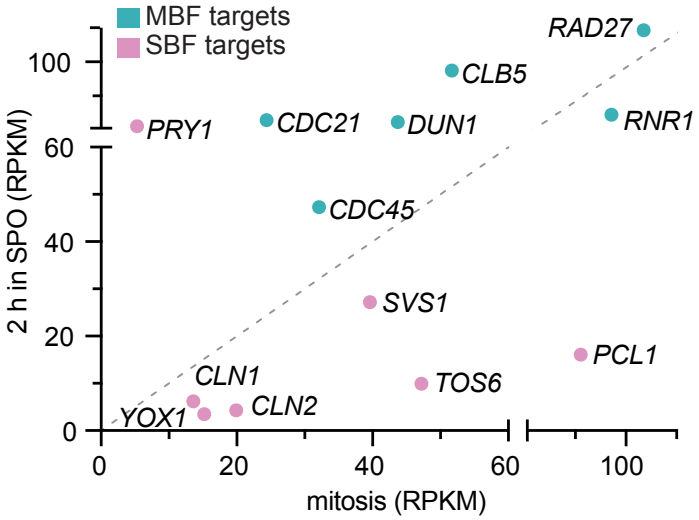

Figure 2.3. Expression of select SBF and MBF targets in meiosis versus mitotic entry. Scatterplot of RNA-seq data (RPKM) from (Brar et al., 2012) comparing 2 h in SPO vs. mitotic growth of well characterized SBF targets (pink) and MBF targets (teal).

Based on our findings thus far, we propose that Swi4 levels are tightly regulated in meiosis to ensure that SBF targets, including *CLN1* and *CLN2*, are turned off during meiotic entry. If Swi4 is indeed limiting for meiotic SBF activity, then higher Swi4 levels should lead to increased expression of SBF targets. To test this possibility, we overexpressed *SWI4* by placing it under the regulation of the *ATG8* promoter (*pATG8-SWI4*), which is highly expressed in meiosis (Brar et al., 2012). The steady-state level of *pATG8*-driven Swi4 was 5 times higher than wild type (Figure 2.4).

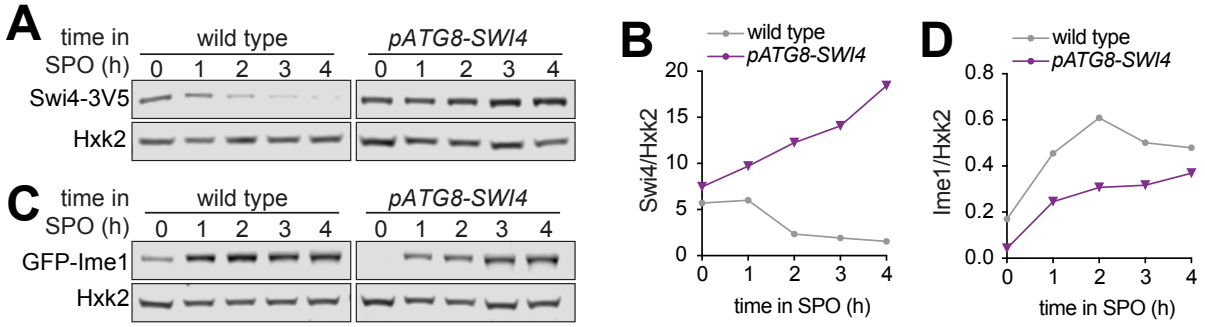

Figure 2.4. A. Abundance of Swi4 and Ime1 levels in meiosis. Wild type (UB22199) and pATG8-SWI4 (UB22226) cells collected between 0-4 h in SPO. Immunoblot performed using α-V5 to quantify Swi4-3V5 abundance. Normalized to Hxk2 loading control. **B.** Quantification of the immunoblot in (A). **C.** Immunoblot using α-GFP to quantify GFP-Ime1 abundance. Normalized to Hxk2 loading control. **D.** Quantification of the immunoblot in (C).

Using reverse transcription coupled with quantitative polymerase chain reaction (RT-qPCR), we measured the transcript levels of well-characterized SBF targets and observed a significant increase in the expression of *CLN1* and *CLN2* in *pATG8-SWI4* cells relative to wild type (Figure 2.5, p = 0.0351 [*CLN1*], p = 0.0013 [*CLN2*], two-tailed t-test). In contrast, the MBF-specific targets *CDC21* and *RNR1* remained similar (Figure 1E, p = 0.8488 [*CDC21*], p = 0.0859 [*RNR1*], two-tailed t-test). These findings indicate that upregulation of *SWI4* is sufficient to induce the expression of SBF-specific targets *CLN1* and *CLN2* in meiosis without affecting MBF-specific targets.

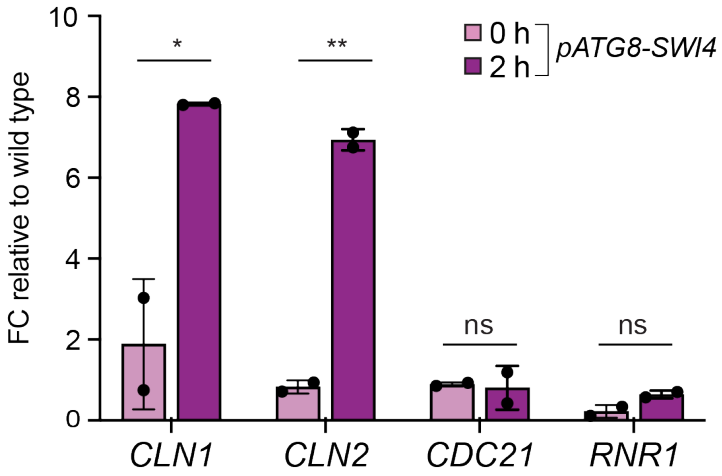

Figure 2.5. Increased expression of Swi4 during meiotic entry is sufficient to increase expression of SBF targets. Wild type (UB22199) and *pATG8-SWI4* (UB22226) cells were collected to perform RT-qPCR for *CLN1, CLN2, CDC21,* and *RNR1* transcripts. Transcript abundance was quantified using primer sets specific for each respective gene from three technical replicates for each biological replicate. Quantification was performed in reference to *PFY1* and then normalized to wild-type control. FC = fold change. Experiments were performed twice using biological replicates, mean value plotted with range.

To test whether the downregulation of *SWI4* is functionally important for meiotic progression, we used time-lapse fluorescence microscopy and visualized the kinetics of meiotic divisions in *pATG8-SWI4* cells relative to wild type. By tracking the endogenous histone H2B fused to the red fluorescent protein mCherry (Htb1-mCherry), we found that *SWI4* overexpression caused a significant delay in meiotic progression (Figure 2.6, p = 0.0045, Mann-Whitney test). We conclude that downregulation of *SWI4* is necessary for timely meiotic progression.

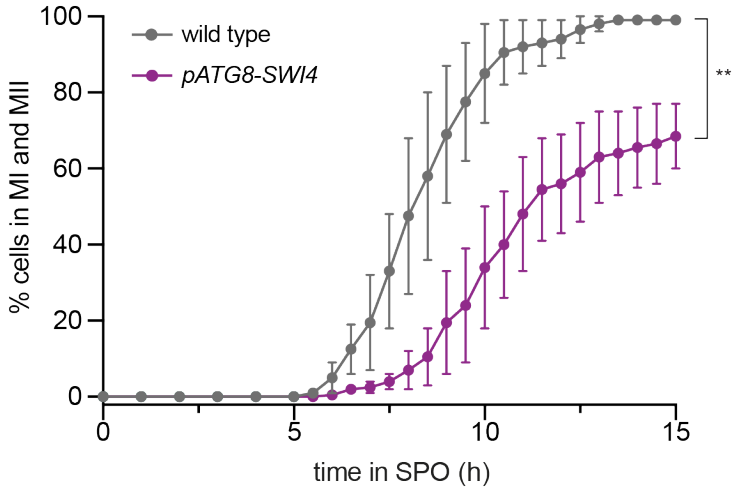

Figure 2.6. Meiotic progression is delayed when Swi4 is over expressed. Live-cell imaging of strains containing the fluorescently tagged histone Htb1-mCherry for wild type (UB32085) and pATG8-SWI4 (UB32089). Experiments were performed twice using biological replicates, mean value plotted with range.

2.2.2 Regulation of Swi4 abundance is required for timely meiotic entry

Since Swi4 abundance, and by inference SBF activity, was decreased during the mitosis-to-meiosis transition, we hypothesized that the meiotic progression delay observed in *pATG8-SWI4* cells was due to meiotic entry defects. To test this we monitored Ime1, a meiosis-specific transcription factor and a master regulator of meiotic entry (Kassir et al., 1988; Honigberg, 2003; reviewed in van Werven and Amon, 2011). To quantify the bulk levels of Ime1 protein in meiosis, we performed immunoblotting. During meiotic entry (2 h in SPO), when Swi4 abundance was elevated, there was a 50% reduction in Ime1 levels in *pATG8-SWI4* cells compared to wild type (Figure 2.4). In parallel, we monitored meiotic entry on a single-cell basis by measuring the localization of endogenous Ime1 carrying an N-terminal green fluorescent protein tag (*GFP-IME1*; Moretto 2018) and Htb1-mCherry. Compared to wild type where > 90% of the cells had nuclear Ime1 following meiotic entry (2 h in SPO), only ~50% of *pATG8-SWI4* cells had nuclear Ime1, which was significantly lower (Figure 2.7, p = 0.0169, two-tailed t-test).

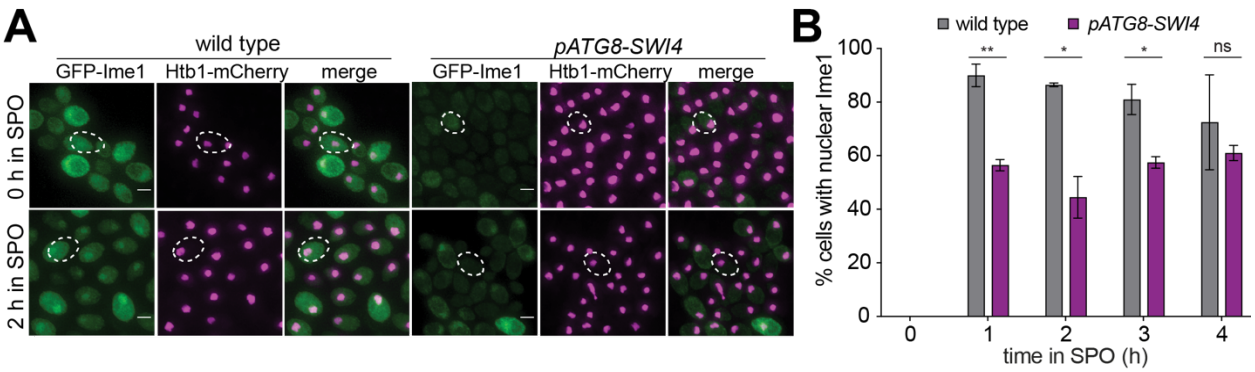

Figure 2.7 Decreased percent of cells with nuclear Ime1 during meiotic entry when Swi4 abundance is increased. Fixed imaging of cells marked with GFP-Ime1 and Htb1-mCherry. Wild type (UB22199) and *pATG8-SWI4* (UB22226) cells were collected between 0-4 h in SPO. **A.** Representative images with merge

at 0 h and 2 h in SPO. Representative cells outlined. Scale bar: 3 μm. **B.** Quantification as percent cells with nuclear Ime1. Experiments were performed twice using biological replicates, mean value plotted with range. Total of 200 cells analyzed per strain. Differences in the fraction of cells with nuclear Ime1 was compared using a two- tailed t-test (**, p = 0.0099 [1 h in SPO]; *, p = 0.0169 [2 h in SPO]; *, p = 0.0315 [3 h in SPO]; ns, two-tailed p = 0.4595 [4 h in SPO]).

Given that the increase in Swi4 levels coincided with a decrease in Ime1 protein expression and nuclear localization, this raised the possibility that Swi4 interferes with Ime1 function. To further investigate the relationship between these two transcription factors at a single-cell level, we generated strains carrying endogenous fluorescent protein tags for each transcription factor (*GFP-IME1, SWI4-mCherry*). Using DAPI as a nuclear marker, we measured the mean nuclear intensity of each transcription factor before (0 h) and after meiotic entry (4 h) (see Materials and Methods for details on image quantification). In wild type, most cells exhibited decreased nuclear Swi4 and increased nuclear Ime1 upon meiotic entry (Figure 2.8). Conversely, in the *pATG8-SWI4* mutant, there was a significant shift in the fraction of cells with higher nuclear Swi4 levels (Figure 2.2B and 2.2C, p < 0.0001, Mann-Whitney test,). Additionally, the cells with increased nuclear Swi4 had reduced levels of nuclear Ime1 (Figure 2.8C, p < 0.0001, Mann-Whitney test). This inverse relationship between Swi4 and Ime1 nuclear localization further indicates that higher levels of Swi4 are antagonistic to Ime1 function.

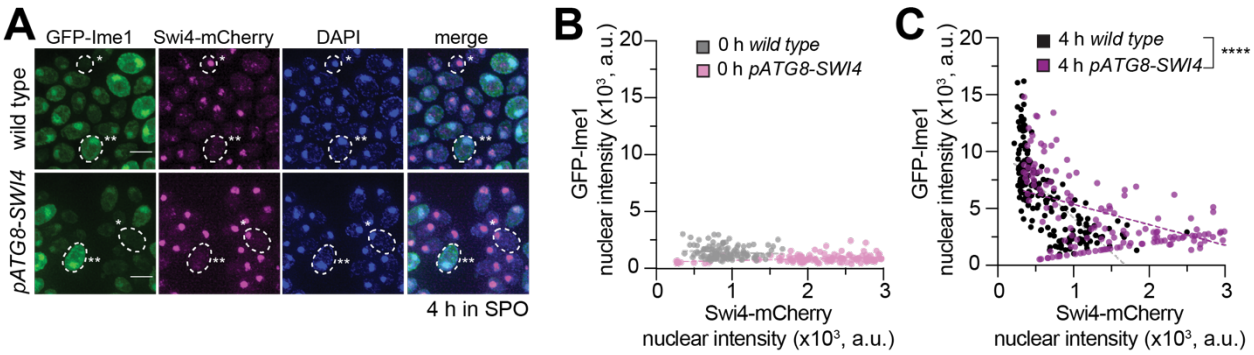

Figure 2.8. A-C. Nuclear localization of Swi4 and Ime1 are inversely correlated during meiotic entry. Fixed imaging of cells marked with GFP-Ime1 and Swi4-mCherry. Wild type (UB31378) and *pATG8-SWI4* (UB31381) cells were collected at 0 h and 4 h in SPO. **A.** Example images with merge at 4 h in SPO. Example cells outlined (*low nuclear GFP-Ime1 with high nuclear Swi4-mCherry, **high nuclear GFP-Ime1 with low nuclear Swi4-mCherry). Scale bar: 3 μm. **B.** Scatterplot of GFP-Ime1 mean nuclear intensity and Swi4-mCherry mean nuclear intensity for wild type and *pATG8-SWI4* cells at 0 h in SPO. See Materials and Methods for further details about image quantification. Dashed line is linear regression plotted for each condition and strain. A total number of 269 cells were analyzed. **C.** Same as in (D) but for wild type and. pATG8-SWI4 cells at 4 h in SPO. A total number of 341 cells were analyzed. Differences in mean nuclear GFP-Ime1 or Swi4-mCherry intensity between wild type and pATG8-SWI4 compared using a Mann-Whitney test, two-tailed (****, p < 0.0001 [wild type vs. *pATG8-SWI4* (GFP-Ime1)]; ****, p < 0.0001 [wild type vs. *pATG8-SWI4* (Swi4-mCherry)]).

Ime1 is necessary for the expression of early meiotic genes. Therefore, we next characterized the changes in the early meiotic transcriptome upon *SWI4* overexpression by mRNA-sequencing (mRNA-seq). Using DESeq2 (Love et al., 2014), we identified differentially expressed genes in *pATG8-SWI4* mutant compared to wild type during meiotic entry (2 h in SPO). To investigate general pathways being affected by increased

Swi4 levels in meiosis, we ran gene ontology analysis of statistically significant (padj < 0.05) output from DESeq2, which revealed that the genes with significantly increased expression were involved in mitosis while those with significantly decreased expression were involved in meiotic processes (Figure 2.9).

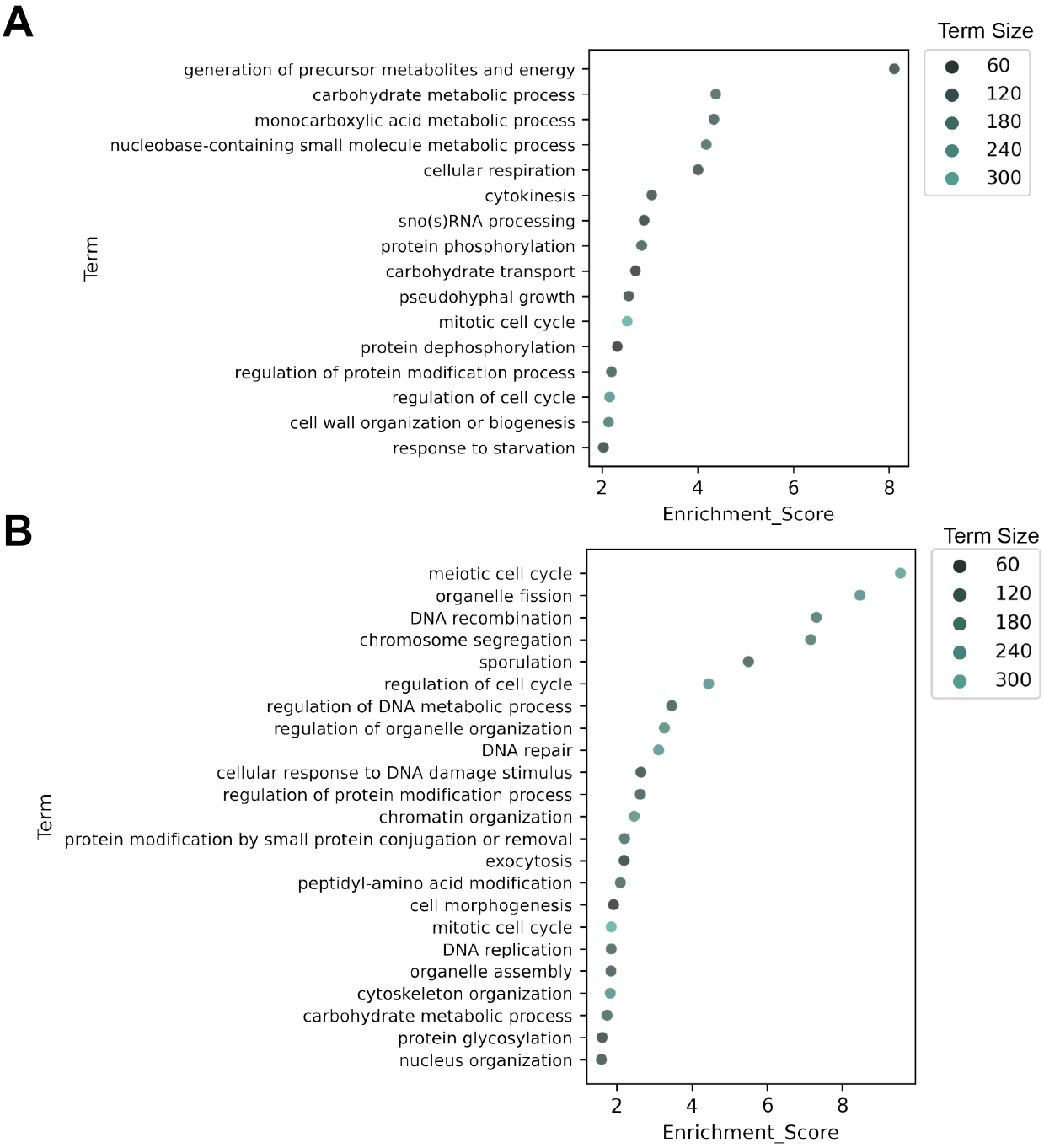

Figure 2.9. Increased Swi4 abundance result in expression of cell cycle genes and decreased expression of early meiotic genes. **A.** Gene ontology analysis for genes that have significant increased expression by DESeq2 (see Materials and Methods) in *pATG8-SWI4* (UB2226) and wild type (UB22199). Term size is the number of genes within a defined term. Enrichment score calculated for each term and plotted. **B.** same as in (A) but for genes that have significant decreased expression.

Regarding the SBF targets, we noticed increased expression of many genes, including *CLN1* and *CLN2* (Figure 2.4A). We focused on a cluster of previously identified early meiotic genes involved in DNA replication and recombination (Brar et al., 2012) and observed that more than 50% had a significant decrease in their expression upon *SWI4* overexpression (padj < 0.05, Figure 2.10A). Finally, gene set enrichment analysis was performed to test whether expression of either the early meiotic gene set or SBF target gene set is enriched in wild type or *pATG8-SWI4* mutant cells (Subramanian et al., 2005). This gene set level analysis revealed significant enrichment of SBF target gene expression (NES = 2.88, p < 0.001, Figure 2.10B), as well as significant disenrichment of early meiotic gene expression (NES = -2.88, p < 0.001, Figure 2.10B) in the *pATG8-SWI4* mutant. Altogether, these findings demonstrate that the increased levels of Swi4 during transition from mitotic to meiotic cell fate abruptly activates SBF and disrupts the early meiotic transcriptome, highlighting the importance of *SWI4* regulation.

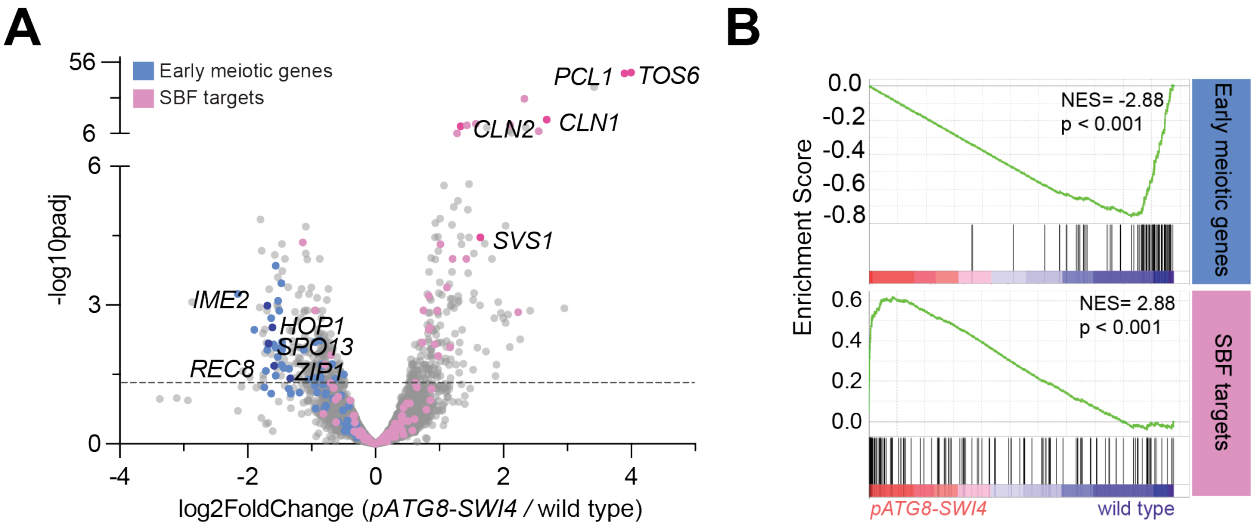

Figure 2.10. Swi4 overexpression result in increased expression of SBF targets and decreased expression of early meiotic genes. Volcano plot of DE-Seq2 analysis for pATG8-SWI4 versus wild type. **A.** Volcano plot of DE-Seq2 analysis for *pATG8-SWI4* versus wild type. Dashed line indicates padj (p value) = 0.05. Analysis was performed using mRNA-seq from two biological replicates. Wild type (UB22199) and *pATG8-SWI4* (UB22226) cells were collected at 2 h in SPO. SBF targets (pink) (Iyer et al., 2001) and early meiotic genes (blue) defined by (Brar et al., 2012). Darker pink or darker blue, labeled dots are well studied targets in either gene set list. **G.** GSEA analysis of mRNA-seq comparing wild type vs. *pATG8-SWI4* collected at 2 h in SPO. Vertical black bars represent the early meiotic cluster from (Brar et al., 2012) or SBF cluster from (Iyer et al., 2001). The heatmap indicates genes that are more enriched in *pATG8-SWI4* (red, left-side) or genes that are enriched in wild type (blue, right-side). NES = normalized enrichment score. Enrichment was determined by comparing *pATG8-SWI4* versus wild type.

As an orthogonal approach, we performed live-cell imaging of Rec8, endogenously tagged with GFP (Rec8-GFP), which is a meiosis-specific cohesin subunit and a direct transcriptional target of Ime1 (Primig et al., 2000; Klein et al., 1999). Htb1-mCherry was used as a nuclear marker. This analysis revealed a significant delay in Rec8-GFP nuclear appearance in the *pATG8-SWI4* strain compared to wild type (Figure 2.11, p = 0.0005, Mann-Whitney test). Furthermore, sporulation efficiency was decreased by ~20% in the

pATG8-SWI4 strain relative to wild type. These findings are consistent with the mRNA-seq data and further underscore the importance of SWI4 downregulation in establishing a robust meiotic cell fate.

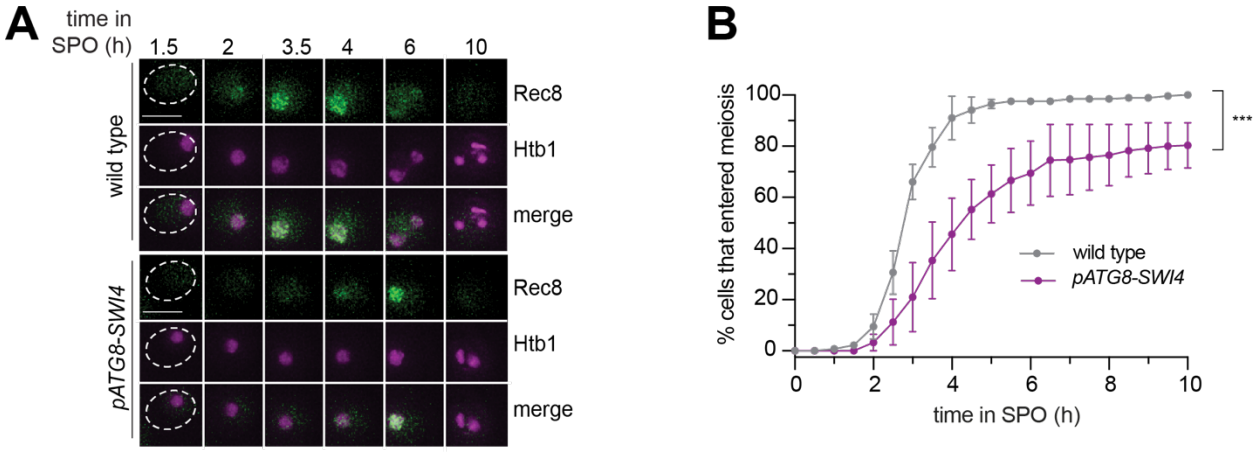

Figure 2.11. Increased Swi4 levels results in a delay in meiotic entry. **A-B.** Live-cell imaging of cells in meiosis marked by Rec8-GFP and nuclear marker Htb1-mCherry for wild type (UB32085) and pATG8-SWI4 (UB32089). **A.** Movie montage with example images throughout meiosis for Rec8-GFP and Htb1-mCherry. Scale bar: 3 μm **B.** Quantification as percent of cells that entered meiosis assayed by nuclear Rec8 appearance. Experiments were performed using two biological replicates, mean value plotted with range. A total number of 452 cells were analyzed.

2.2.3 Removal of the SBF targets Cln1 or Cln2 partially rescues the meiotic entry delay in *pATG8-SWI4* mutants

Overexpression of the G1 cyclins *CLN1*, *CLN2* and *CLN3* has been previously shown to inhibit meiotic entry (Colomina et al., 1999). Given that *CLN1* and *CLN2* are transcriptional targets of SBF, we next determined whether the meiotic progression delay in *pATG8-SWI4* cells could be due to increased G1 cyclin protein levels. We first examined Cln1 and Cln2 protein levels using epitope-tagged alleles at their endogenous loci (CLN1-3V5 or CLN2-3V5) in wild-type and *pATG8-SWI4* cells. In response to *SWI4* overexpression, we observed up to 2-fold and 10-fold increase in Cln1 and Cln2 protein levels, respectively, corroborating the mRNA-seq data (Figure 2.12).

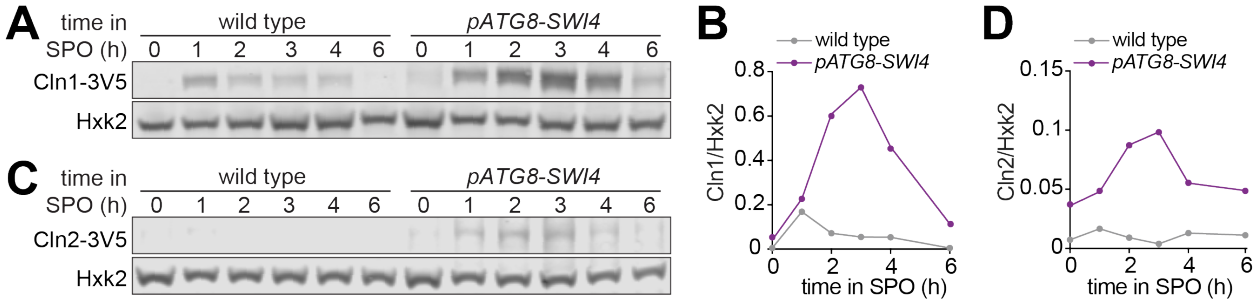

Figure 2.12. A-D Increased expression of G1 cyclins when Swi4 is overexpressed. **A.** Immunoblotting was performed on samples collected for wild type (UB29326) and *pATG8-SWI4* (UB29328) between 0-6 h in

SPO using α-V5 antibody to track Cln1-3V5. Hxk2 was used a loading control. Representative blots from one of two biological replicates are shown. **B.** Quantification of (A). **C.** Same as in (A) but for wild type (UB29330) and *pATG8-SWI4* (UB29332) cells using α-V5 antibody to track Cln2-3V5. Hxk2 was used a loading control. Representative blots from one of two biological replicates are shown. **D.** Quantification of (C).

To determine whether these two G1 cyclins are functionally responsible for the meiotic progression delay observed in response to SBF misregulation, we performed time-lapse fluorescence microscopy in cells carrying Rec8-GFP and Htb1-mCherry. We found that deletion of either *CLN1* or *CLN2* significantly rescued the meiotic progression delay in the *pATG8-SWI4* mutant ($p = 0.0111$ [cln1Δ], $p = 0.0478$ [cln2Δ], Mann-Whitney test). However, the progression was still delayed compared to wild type, suggesting redundancy (Figure 2.13). We were unable to examine meiotic progression in the cln1Δ cln2Δ double mutant due to its severe sickness in the SK1 background. Nevertheless, our analyses establish a causal link demonstrating that both *CLN1* and *CLN2* contribute to the meiotic defects arising from SBF misregulation.

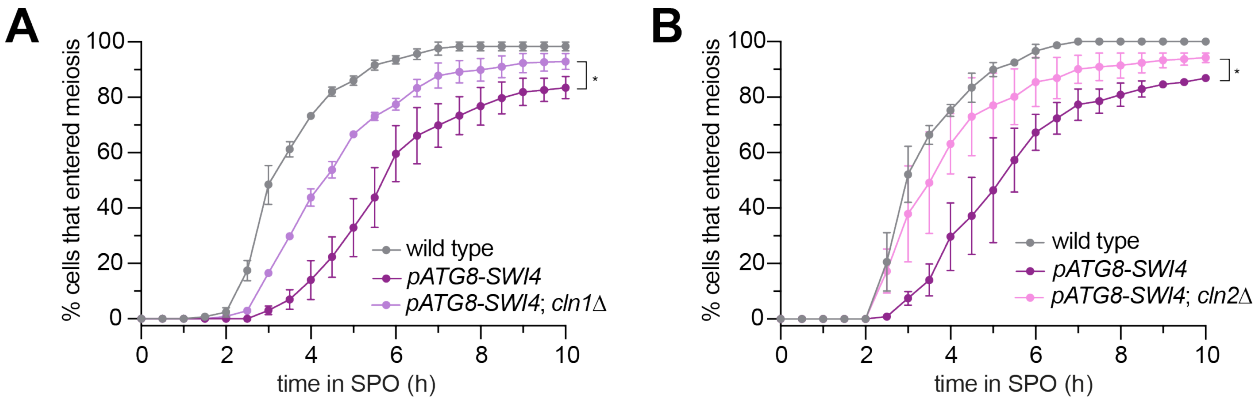

Figure 2.13. Delay in meiotic entry is partial due to increased cyclin levels. **A.** Live-cell imaging of meiotic cells marked by Rec8-GFP and nuclear marker Htb1-mCherry, with the following genotypes: wild type (UB32085), *pATG8-SWI4* (UB32089), and *pATG8-SWI4*; *cln1*Δ (UB34536). Quantification of cells that entered meiosis assayed by the initial timing of nuclear Rec8 appearance. Experiments were performed using two biological replicates, mean value plotted with range. A total number of 883 cells were analyzed. *cln1*Δ alone (not shown) has similar meiotic progression kinetics relative to wild type. **B.** Same as (A) but with the following genotypes: wild type (UB32085), *pATG8-SWI4* (UB32089), and *pATG8-SWI4; cln2*Δ (UB34165). A total number of 610 cells were analyzed. *cln2*Δ alone (not shown) has similar meiotic progression kinetics relative to wild type.

2.2.4 Tethering of Ime1 to Ume6 is sufficient to overcome the meiotic block exerted by G1 cyclin overexpression

Given the partial rescue of the meiotic delay in *pATG8-SWI4* mutants by the deletion of individual G1 cyclins, we next investigated how the G1 cyclins interfere with meiosis. To this end, we generated transgenes that expressed either *CLN1* or *CLN2* under the control of the *pATG8* promoter for meiotic overexpression. While wild-type cells successfully completed meiosis with more than 94% sporulation efficiency, *CLN2* overexpression resulted in only 8.5% of cells forming gametes. Overexpression of *CLN1* also resulted in

a meiotic defect, albeit to a lesser extent than the *pATG8-CLN2* mutant (65% sporulation efficiency, Figure 2.14).

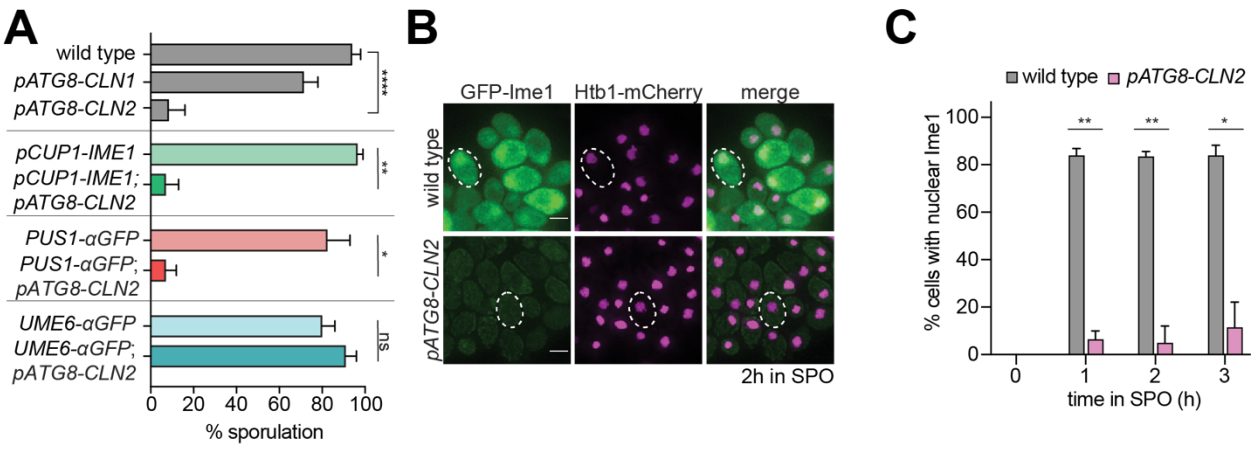

Figure 2.14. Overexpression of CLN2 blocks meiosis at the level of entry. **A.** Sporulation efficiency of cells at 24 h in SPO media wild type (UB22199), *pATG8-CLN1* (UB32820), *pATG8-CLN2* (UB25959), *pCUP-GFP-IME1* (UB34641), *pCUP1-GFP-IME1; pATG8-CLN2* (UB35057), *PUS1-αGFP* (UB35593), *PUS1-αGFP; pATG8-CLN2* (UB35982), *UME6-αGFP* (UB35300), and *UME6-αGFP; pATG8-CLN2* (UB35177). Experiments shown in this figure were performed using two biological replicates, mean value plotted with range. Total of 200 cells counted per strain. Differences in sporulation efficiency was compared by two-tailed t-test (****, $p < 0.0001$ [wild type vs *pATG8-CLN2*], **, $p = 0.0052$ [*pCUP1-IME1 vs pCUP1-IME1; pATG8-CLN2*], *, $p = 0.0229$ [*PUS1-αGFP vs PUS1-αGFP; pATG8-CLN2*], ns, $p = 0.2943$, [*UME6-αGFP vs UME6-αGFP; pATG8-CLN2*]. **B-C.** Fixed imaging of cells marked with GFP-Ime1 and Htb1-mCherry. Wild type (UB22199) and *pATG8-CLN2* (UB25959) cells were collected between 0-3 h in SPO. **B.** Representative images with merge at 2 h in SPO. Representative cells outlined. Scale bar: 3 μm. **C.** Quantification of cells with nuclear Ime1. Experiments were performed using two biological replicates, mean value plotted with range. Total of 200 cells analyzed per strain. Differences in percent of cells with nuclear Ime1 was compared by two-tailed t-test (**, $p = 0.00917$ [1 h in SPO]; **, $p = 0.0044$ [2 h in SPO]; *, $p = 0.0122$ [3 h in SPO]).

Since the meiotic defect was more pronounced in response to *CLN2* overexpression, we decided to use the *pATG8-CLN2* mutant to explore how G1 cyclins counteract meiosis. To assess meiotic entry, we performed fixed-cell imaging for GFP-Ime1 and found that when *CLN2* was overexpressed, only 5% of the *pATG8-CLN2* cells displayed nuclear GFP-Ime1 signal during early meiosis as opposed to >84% of wild-type cells (Figure 2.14B and 2.14C, 2 h in SPO). In parallel, we measured *IME1* transcript and Ime1 protein levels. In both cases, we observed ~30% decrease in abundance in the *pATG8-CLN2* mutant relative to wild type (Figure 2.15, 2 h in SPO, and Figure 2.16A). These data raise the possibility that the meiotic entry defect observed in the *pATG8-CLN2* mutant arises from downregulation of *IME1* expression.

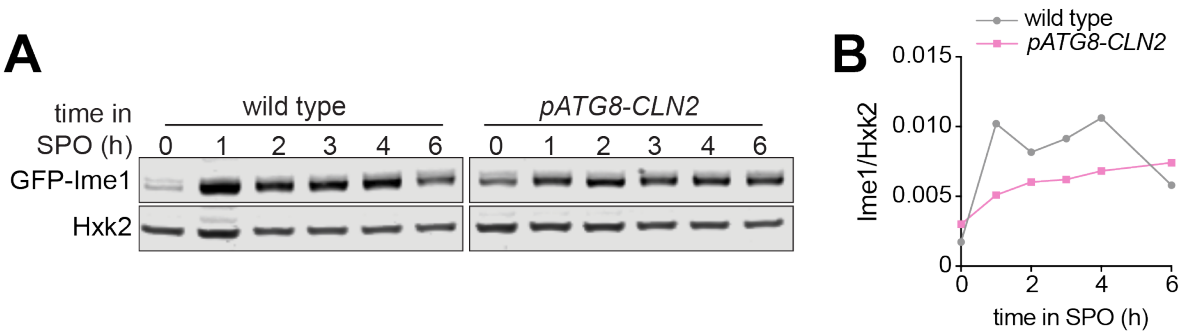

Figure 2.15. Cln2 protein levels after overexpression in meiosis. **A.** Immunoblot was performed on wild type (UB22199) and *pATG8-CLN2* (UB35106) cells collected between 0-6 h in SPO. Immunoblotted using α-GFP to quantify GFP-Ime1 abundance. Normalized to Hxk2 loading control. Representative blots from one of two biological replicates are shown. All blots in this figure were performed the same way. **B.** Quantification of the immunoblot in (A).

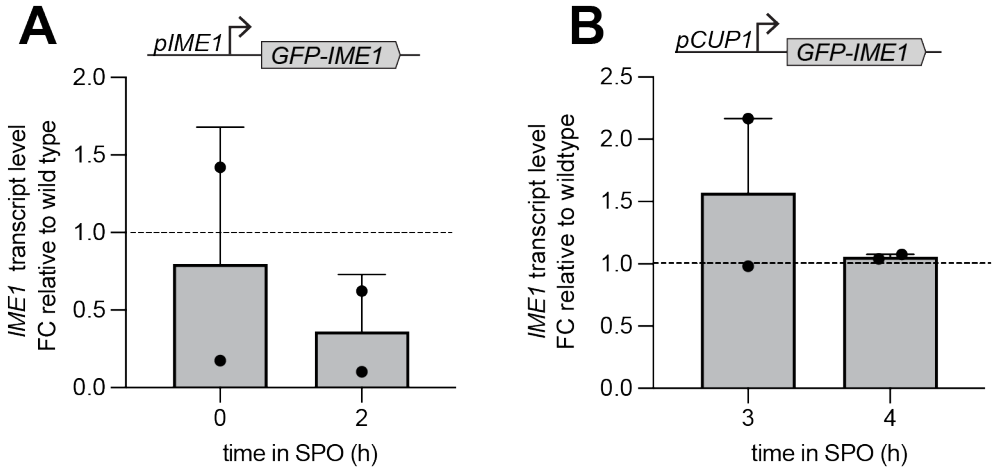

Figure 2.16. Rescue of decreased IME1 transcript levels when Cln2 is overexpressed. **A.** RT-qPCR was performed on *IME1* transcript for samples collected in (A). Quantification was performed in reference to levels of meiotic housekeeping gene *PFY1* and then normalized to wild type. FC = fold change. Experiments were performed in duplicate, mean value plotted with range. **B.** Same as in (A) but for *pCUP1-GFP-IME1* (UB34641) and *pCUP1-GFP-IME1*; *pATG8-CLN2* (UB35057).

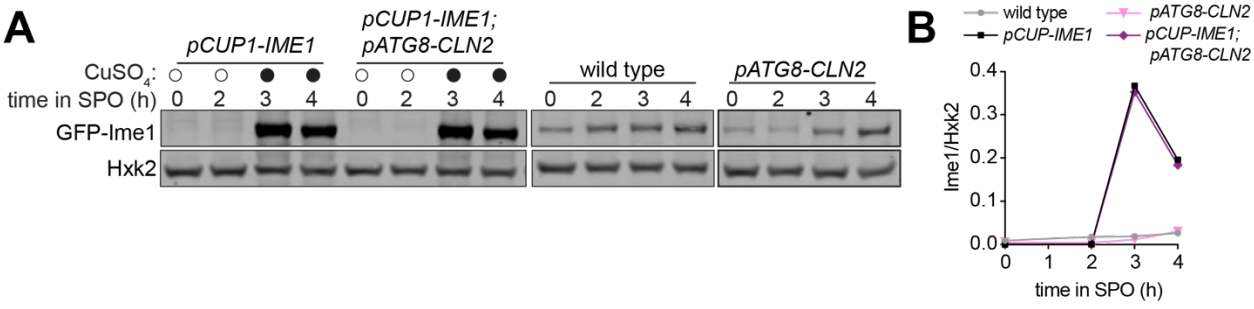

Figure 2.17. Rescue of Ime1 abundance when Cln2 is overexpressed. **A.** Immunoblot was performed on samples from wild type (UB22199), *pATG8-CLN2* (UB35106), *pCUP1-GFP-IME1* (UB34641), and *pCUP1-GFP-IME1*; *pATG8-CLN2* (UB35057) strains collected between 0-4 h in SPO. 50 μM $CuSO_4$ after 2 h in

SPO was added to all cells. Representative blots from one of two biological replicates are shown. **B.** Quantification of the immunoblot in (A).

To test whether the increased levels of Ime1 can rescue the meiotic defect of *pATG8-CLN2* mutant, we replaced the endogenous *IME1* promoter with a copper-inducible *CUP1* promoter (Figure 2.18A). We adapted a previously well-characterized overexpression allele of *IME1*, *pCUP1-IME1,* (Berchowitz et al., 2013; Chia and van Werven, 2016) and included a functional, N-terminal GFP tag to track Ime1's subcellular localization *(pCUP1-GFP-IME1*). Use of the *CUP1* promoter was successful in elevating *IME1* transcript and protein levels in the presence of *CLN2* overexpression (Figure 2.16B, Figure 2.17). Despite the rescue of *IME1* expression, gamete formation was still severely perturbed (Figure 2.14A).

Using a single z-slice to measure mean nuclear intensity, we noticed that the intensity of the nuclear Ime1 signal was significantly lower in the *pATG8-CLN2; pCUP1-GFP-IME1* cells compared to the *pCUP1-GFP-IME1* control (Figure 2.18B and 2.112, $p < 0.0001$, Mann-Whitney test). This finding indicates that rescue of *IME1* expression did not also rescue sporulation, further suggesting a defect in Ime1 nuclear localization (Figure 2.8A)

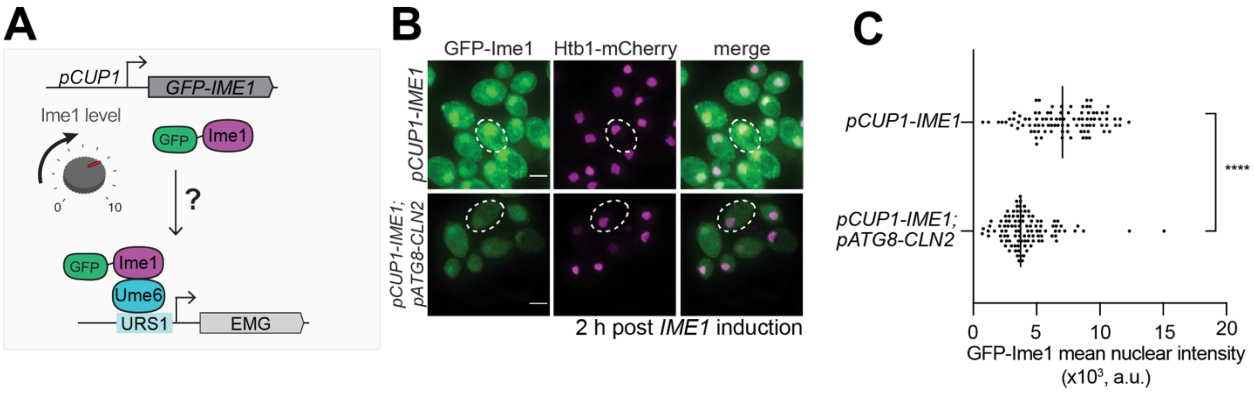

Figure 2.18. Normalization of both transcript and protein levels is not sufficient to rescue meiotic defect caused by increased Cln2 levels. **A.** Schematic depicting use of *pCUP1* promoter (*pCUP1-GFP-IME1*) to rescue Ime1 transcript and protein levels. **B-C** Fixed imaging of cells marked with GFP-Ime1 and Htb1-mCherry. Cells with the following genotypes were collected at 2 h in SPO: wild type (UB22199), *pATG8-CLN2* (UB35106), *pCUP1-GFP-IME1* (UB34641), and *pCUP1-GFP-IME1; pATG8-CLN2* (UB35057). **B.** Representative images with merge and representative cells outlined. Scale bar: 3 μm. **C.** GFP-Ime1 mean nuclear intensity measured for a single z-slice. A total number of 433 cells were analyzed. Differences in mean nuclear intensity compared by Mann-Whitney test, two tailed, (****, $p < 0.0001$ [*pCUP1-IME1* vs. *pCUP1-IME1; pATG8-CLN2*]).

To test this possibility, we utilized a nanobody trap strategy (Fridy et al., 2014) where we C-terminally fused a single-domain anti-GFP antibody to Pus1, a constitutively nuclear localized protein (*PUS1-αGFP*, Figure 2.19A). In this background, control strains carrying a *GFP-IME1* allele sporulated efficiently, demonstrating that tethering of Ime1 to Pus1 does not interfere with Ime1 function (Figure 2.14A). Furthermore, mean nuclear intensity of GFP-Ime1 was indistinguishable between *PUS1-αGFP* and *pATG8-CLN2; PUS1-αGFP*, indicating that nuclear localization was fully rescued (Figure 2.19B and 2.19C, $p = 0.6563$ [*PUS1-αGFP* vs. *pATG8-CLN2; PUS1-αGFP*], Mann-Whitney test). Surprisingly,

these cells still failed to undergo meiosis (Figure 2.14A), suggesting that G1 cyclins interfere with Ime1 function at an additional step beyond misregulating its expression and localization. Alternatively, G1 cyclins could disrupt a different meiotic factor in addition to Ime1.

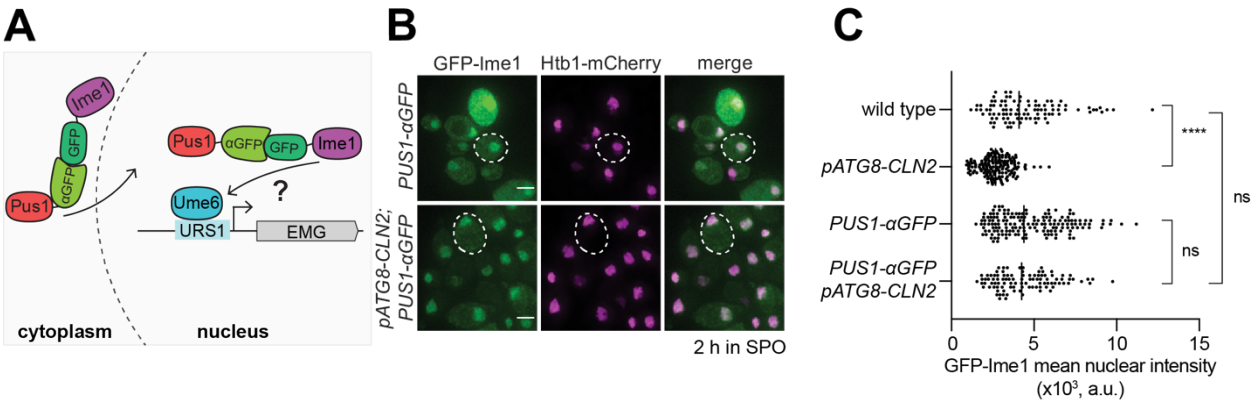

Figure 2.19. Rescue of GFP-Ime1 nuclear localization with Pus1-GFP-nanobody. **A.** Schematic of nanobody trap strategy with *PUS1-αGFP* and GFP-Ime1 to rescue Ime1 nuclear localization in meiosis. **B-C.** Fixed imaging of cells marked with GFP-Ime1 and Htb1-mCherry. Cells with the following genotypes were collected at 2 h in SPO: wild type (UB22199), *pATG8-CLN2* (UB35106), *PUS1-αGFP* (UB35593), and *PUS1-αGFP; pATG8-CLN2* (UB35982). **B.** Representative images with merge and example cells outlined. Scale bar: 3 μm. **C.** GFP-Ime1 mean nuclear intensity measured for a single z-slice. A total number of 934 cells were analyzed. Differences in mean nuclear intensity compared by Mann-Whitney test, two-tailed, (****, $p < 0.0001$ [wild type vs. *pATG8-CLN2*]; not significant (ns), $p = 0.6563$ [*PUS1-αGFP* vs. *pATG8-CLN2; PUS1-αGFP*]; not significant (ns), $p = 0.8881$ [wildtype vs. *pATG8-CLN2; PUS1-αGFP*]).

To induce early meiotic genes, Ime1 must interact with another transcription factor called Ume6 (Rubin-Bejerano et al., 1996). Since Ime1 itself does not possess a DNA-binding domain, its binding to Ume6 is essential for targeting Ime1 to early meiotic gene promoters (Smith et al., 1993; Rubin-Bejerano et al., 1996). To address whether the G1 cyclins might disrupt the interaction between Ime1 and Ume6, we fused the anti-GFP nanobody to Ume6 (*UME6-αGFP*) in the *pATG8-CLN2* strain carrying a GFP tagged Ime1 (Figure 2.20A). This nanobody trap should lead to constitutive tethering of Ime1 to Ume6, as evidenced by the rescue of Ime1 nuclear localization (Figure 2.20B and 2.20C, $p = 0.035$ [wild type vs. *pATG8-CLN2 UME6-αGFP*] Mann-Whitney test). Under these conditions, the sporulation defect of *pATG8-CLN2* mutant was rescued, reaching similar levels to wild type (Figure 2.14A). Since *IME1* is expressed from its endogenous promoter in the *pATG8-CLN2; UME6-αGFP* strain, these data suggest that overexpression of G1 cyclins results in meiotic failure due to reduced Ime1-Ume6 interaction.

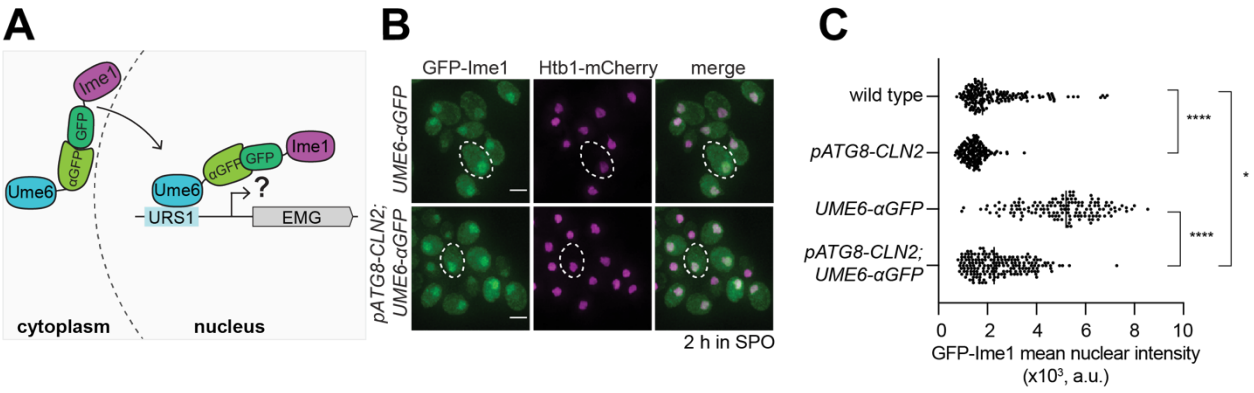

Figure 2.20. Rescue of Ime1-Ume6 interaction with Ume6-GFP-nanobody. **A.** Schematic of nanobody trap strategy with *UME6-αGFP* and GFP-Ime1 to rescue Ime1-Ume6 interaction in meiosis. **B-C** Fixed imaging of cells marked with GFP-Ime1 and Htb1-mCherry. Cells with the following genotypes were collected at 2 h in SPO: wild type (UB22199), *pATG8-SWI4* (UB35106), *UME6-αGFP* (UB35300), and *UME6-αGFP; pATG8-CLN2* (UB35177). **B.** Representative images with merge and representative cells outlined. Scale bar: 3 μm. **C.** GFP-Ime1 mean nuclear intensity measured for a single z-slice. A total number of 1220 cells were analyzed. Differences in mean nuclear intensity compared by Mann-Whitney test, two-tailed (****, $p < 0.0001$ [wild type vs. *pATG8-CLN2]*; ****, $p < 0.0001$ [*UME6-αGFP* vs. *pATG8-CLN2; UME6-αGFP*]; *, $p = 0.0354$ [wildtype vs. *pATG8-CLN2; UME6-αGFP*]).

Our findings thus far highlight the biological significance of restricting SBF activity during the transition from mitotic to meiotic cell fate. By downregulating the limiting Swi4 subunit, cells ensure that the SBF regulon is turned off under conditions that favor meiotic entry. Among the SBF targets, G1 cyclins pose a major block to meiotic entry by interfering with Ime1 function, critically at the level of Ime1-Ume6 interaction. While these findings emphasize the importance of *SWI4* regulation to ensure timely SBF activity, the question remains as to how SBF activity is downregulated during transition from mitosis to meiosis.

2.3 Discussion

In this chapter we investigate the biological significance of SBF repression in meiosis. We show that increased levels of Swi4 is sufficient to result in expression of SBF targets and that this increased expression of SBF targets correlates with a delay in meiotic progression. Further experimentation reveals that the delay in meiotic progression is occurring at the level of Ime1, the key regulator of early meiotic gene expression. Increase in Swi4 levels leads to decreased nuclear Ime1 as well as decreased expression of early meiotic genes. While SBF has hundreds of targets, the meiotic entry delay is largely caused by 2 SBF targets: *CLN1* and *CLN2*. Finally, we further elucidate the molecular mechanism by which CLNs lead to meiotic delays, which occurs through disruption of Ime1-Ume6 interaction.

We found that the meiotic entry delay due to untimely SBF activation can be partially rescued by loss of either *CLN1* or *CLN2*, demonstrating that both cyclins are responsible for the meiotic defects associated with SBF misregulation. In addition to *CLN1* and *CLN2*, improper activation of SBF also leads to upregulation of *PCL1* during meiotic entry (Figure 2.10A). *PCL1* encodes a cyclin that interacts with the Pho85 CDK and is involved in the

regulation of polarized cell growth and morphogenesis as well as progression through the cell cycle (Espinoza et al., 2016). Whether *PCL1* misexpression contributes to the SBF-associated meiotic entry defects is an interesting avenue for future studies.

We and others have demonstrated that elevated levels of G1 cyclins inhibit meiotic entry. Therefore, it is crucial to dissect the mechanisms that govern the downregulation of G1 cyclins during this process. Among the G1 cyclins that are known to inhibit meiotic entry (Colomina et al., 1999), only the mechanism of *CLN3* restriction was previously known (Parviz and Heideman, 1998; Gallego et al., 1997). In Chapter 3 we will investigate the molecular mechanisms that play a role in restricting SBF and/or *CLN1-CLN2* in meiosis.

Our findings also shed light on the mechanism by which G1 cyclins prevent meiotic entry. Previous work demonstrated that G1 cyclin overexpression leads to downregulation of *IME1* expression and inhibition of Ime1 nuclear localization (Colomina et al., 1999). Even though we observed similar defects in *IME1* in response to *CLN2* overexpression, increasing *IME1* expression or targeting Ime1 to the nucleus did not result in successful meiosis (Figure 2.18). Instead, we found that restoring the interaction between Ime1 and its cofactor Ume6 was sufficient to bypass the meiotic blockage exerted by Cln/CDK. Collectively, our analyses suggest that the primary reason why G1 cyclins cause a meiotic failure is due to a deficiency in Ime1-Ume6 interaction.

Future work could be aimed at dissecting how G1 cyclins affect the interaction between Ime1 and Ume6 and whether their impact on Ime1's subcellular localization is primarily due to G1 cyclin-dependent changes in Ime1-Ume6 interaction. Since there are no CDK consensus phosphorylation sites on Ime1 itself, other players are likely to be involved. Rim11 and Rim15 are potential candidates since these two kinases have been implicated in Ime1-Ume6 phosphorylation as well as regulation of Ime1 localization and its interaction with Ume6 (Rubin-Bejerano et al., 1996; Vidan and Mitchell, 1997; Bowdish et al., 1994). Interestingly, Rim15 contains CDK consensus phosphorylation sites (Holt et al., 2009; Moreno-Torres et al., 2017; Breitkreutz et al., 2010), Furthermore, Cln2/CDK activity has been previously shown to inhibit Rim15 nuclear localization (Talarek et al., 2010), thereby making it an attractive candidate for further investigation.

Chapter 3: Meiotic regulation of SBF

This chapter is adapted from the following publication:
Su, A.J., S.C. Yendluri, and E. Ünal. (2023). Control of meiotic entry by dual inhibition of a key mitotic transcription factor. *bioRxiv*. https://doi.org/10.1101/2023.03.17.533246

3.1 Introduction

To build on Chapter 2, where we elucidate the functional consequences of misregulating SBF in meiosis, we next wanted to characterize the molecular mechanisms that restrict SBF activity in meiosis. SBF and MBF activity has been shown to be regulated, in part, through subunit abundance (Dorsey et al., 2018). However, abundance is not the sole regulator of SBF activity as mass spectrometry in budding yeast mitotic growth revealed

Swi4 protein levels to be relatively constant instead of periodic (Kelliher et al., 2018). There are three main mechanisms regulating SBF activity in mitotic growth: 1) periodic transcription via the early cell cycle box (ECB) in the *SWI4* promoter (Mcinerny et al., 1997), 2) Whi5 repression of SBF activity (De Bruin et al., 2004; Costanzo et al., 2004), 3) Clb-Cdk (B-type cyclin) repression of SBF (Siegmund and Nasmyth, 1996). Clb2 has been the only B-type cyclin shown to directly interact with Swi4 via ankyrin repeats (Amon et al., 1993; Koch et al., 1996). During starvation, Whi5 is nuclear during G1 and is repressing SBF mediated transcription (Brush et al., 2012; Argüello-Miranda et al., 2018). Additionally, *CLB2* is not expressed throughout meiosis (Carlile and Amon, 2008) and therefore this mode of regulation is unlikely to be utilized for SBF restriction during meiotic entry.

During meiotic entry, a LUTI transcript is expressed from the *SWI4* locus, which likely downregulates Swi4 protein synthesis (Tresenrider et al., 2021). LUTI-based gene regulation repurposes gene-activating transcription factors as repressors by a two-pronged mechanism (Chen et al., 2017; Chia et al., 2017; Tresenrider and Ünal, 2017; Tresenrider et al., 2021). First, transcription factor-dependent activation of the distal LUTI promoter results in co-transcriptional silencing of the downstream canonical gene promoter. Second, the coding sequence (CDS) within the LUTI is translationally repressed due to competitive translation of the upstream open reading frames (uORFs) in the LUTI-specific 5′ leader. Consequently, upregulation of the LUTI results in downregulation of the canonical mRNA and corresponding protein. While LUTIs are conserved from yeast to humans and have been identified in different cellular contexts (Cheng et al., 2018; Van Dalfsen et al., 2018; Hollerer et al., 2019; Jorgensen et al., 2020), their biological significance remains poorly understood. In fact, only a single LUTI has been assigned a biological role so far with distinct phenotypic outcomes resulting from its loss or gain of function (Chen et al., 2017; Chia et al., 2017).

In this study we identify two parallel mechanisms that restrict SBF activity to ensure timely meiotic entry. We characterize the LUTI-based mechanism, which results in downregulation of Swi4 protein synthesis and acts in conjunction with Whi5 to restrict SBF activity during meiosis. In sum, our study reveals the functional role of a LUTI in establishing the early meiotic transcriptome, demonstrates how the LUTI-based regulation is integrated into a larger regulatory network to ensure timely downregulation of SBF activity during the mitotic to meiotic cell fate transition.

3.2 Results

3.1.1 Ime1-dependent expression of a LUTI from the *SWI4* locus leads to a reduction in Swi4 protein levels during meiotic entry

A previous study identified a long undecoded transcript isoform (LUTI) expressed from the *SWI4* locus in meiotic cells (Brar et al., 2012, Figure 3.1A). When $SWI4^{LUTI}$ is expressed, the canonical protein-coding *SWI4* transcript, $SWI4^{canon}$, is downregulated (Tresenrider et al., 2021, Figure 3.1B), suggesting that LUTI expression restricts Swi4 protein levels and thus SBF activity during meiotic entry.

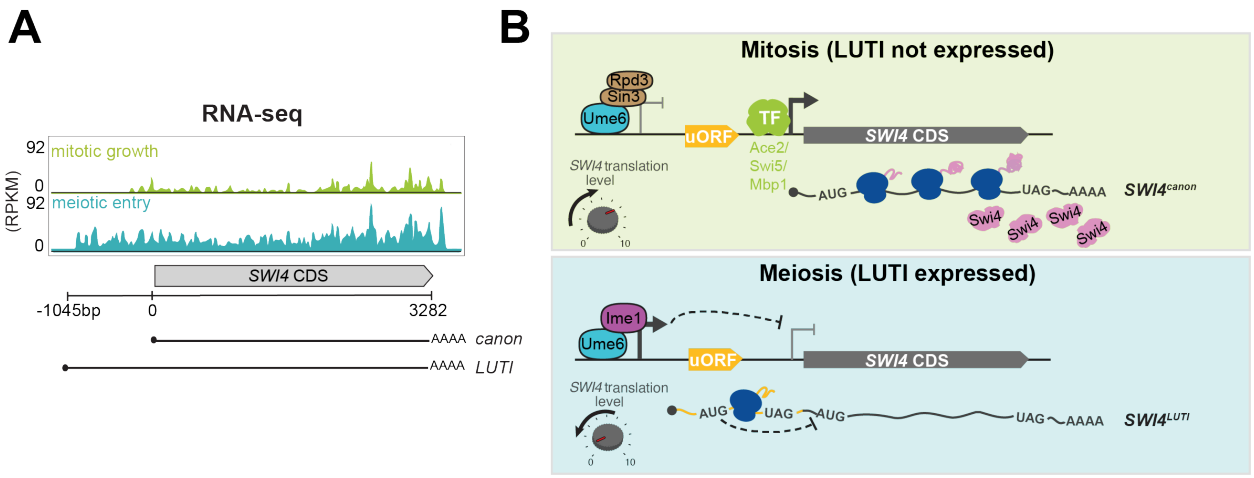

Figure 3.1. *SWI4*^{LUTI} is expressed in meiosis. **A.** Genome browser views of RNA-seq data (Brar et al., 2012) of the *SWI4* locus. *SWI4*^{LUTI} transcription start site is ~1045bp upstream of *SWI4* ORF translation start site. **B.** A schematic of LUTI-based gene regulation. Top: Mitotic growth, *SWI4*^{LUTI} is repressed due to Ume6-Rpd3-Sin3 complex and *SWI4*^{canon} is induced by one or more transcription factors including Ace2, Mbp1 and Swi5, leading to Swi4 protein production. Bottom: Meiosis-specific expression of *SWI4*^{LUTI} by Ime1-Ume6 leads to downregulation of Swi4 protein production due to combined effect of transcriptional and translation interference. *SWI4*^{LUTI} 5′ leader contains 7 AUG uORFs but only one is shown in the model for simplicity. Schematic is adapted from (Tresenrider et al., 2021).

To further investigate LUTI-based repression of *SWI4*, we examined the relationship between *SWI4*^{LUTI} and *SWI4*^{canon} transcripts using single molecule RNA fluorescence in situ hybridization (smFISH: Chen et al., 2017, 2018; Raj et al., 2008). Two distinct probes were used: one, conjugated to Quasar 670 (Q670) and complementary to the *SWI4* coding sequence (CDS) and the other, conjugated to CAL Fluor Red 590 (CF590) and unique to the 5′ extended LUTI sequence. Accordingly, a spot where the two probe sets colocalized indicated a *SWI4*^{LUTI} transcript, whereas a spot marked with Q670 probe alone highlighted a *SWI4*^{canon} transcript. We used a well-established meiotic cell synchronization system (Berchowitz et al., 2013) to investigate the precise temporal expression of these two mRNA isoforms. In comparison to premeiotic state, meiotic cells displayed a significant increase in *SWI4*^{LUTI} transcripts ($p < 0.0001$, Mann-Whitney test) as well as a significant decrease in *SWI4*^{canon} transcripts ($p = 0.0007$, Mann-Whitney test) (Figure 3.2A and 3.2B), thus confirming their inverse expression pattern.

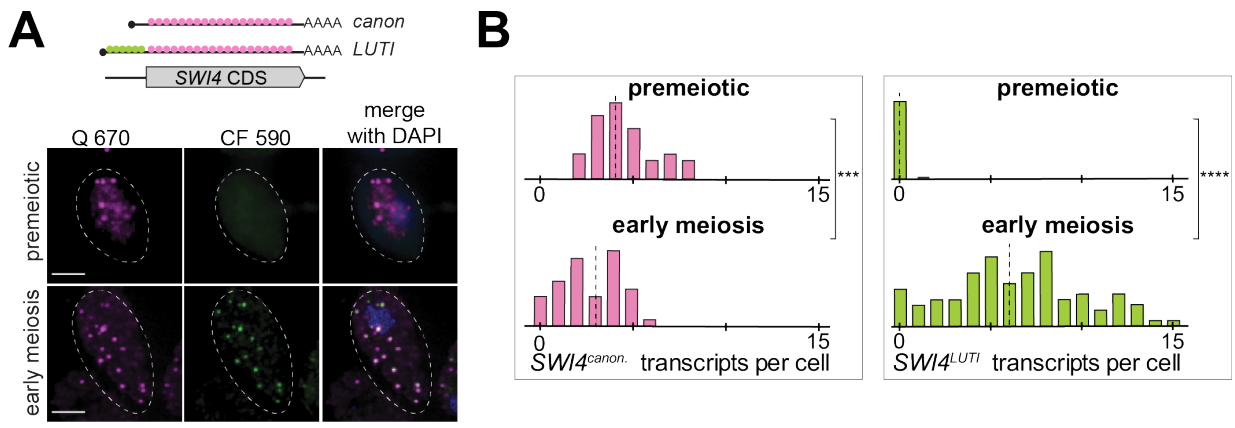

Figure 3.2. Representative smFISH images collected from premeiotic and meiotic cells for detecting *SWI4*^{canon} and *SWI4*^{LUTI}. **A.** Cells with *pCUP1-IME1/pCUP1-IME4* meiotic synchronization system were induced to enter meiosis with 50 µM $CuSO_4$ after 2 h in SPO. Premeiotic cells were collected before *IME1/4* induction and meiotic cells were collected 2 h post *IME1/4* induction from strain UB14273. Q 670 probes (green) hybridize to shared region within *SWI4* CDS. CF590 probes hybridize to the unique 5′ leader region of *SWI4*^{LUTI} (depicted on the schematic shown above the images). DNA was stained with DAPI. Scale bar: 3 µm. **B.** Quantification of smFISH shown in (A), plotted as relative frequency histograms of cells with *SWI4*^{canon} and *SWI4*^{LUTI} transcripts per cell. Data pooled from two independent biological replicates. Dashed line indicates median number of transcripts per cell. Each histogram is normalized with maximum bin height being the same across all histograms. A total number of 44 cells counted for premeiotic and 102 cells counted in meiotic prophase. Differences in premeiotic versus meiotic were compared by Mann-Whitney test, two-tailed (***, p = 0.0007 [*SWI4*^{canon}]; ****, p < 0.0001 [*SWI4*^{LUTI}]).

To characterize the functional contribution of the LUTI to *SWI4* downregulation, we eliminated *SWI4*^{LUTI} production (Δ*LUTI*) by deleting its promoter (Tresenrider et al., 2021) and used RNA blotting to visualize the *SWI4* mRNA isoforms. In wild-type cells, *SWI4*^{LUTI} was readily detectable after 1 hour in SPO, corresponding to early meiotic entry (Figure 3.3A). During the time points when *SWI4*^{LUTI} was highly expressed, *SWI4*^{canon} transcript levels were lower, consistent with the smFISH results revealing *SWI4*^{LUTI} and *SWI4*^{canon} levels are anticorrelated. In Δ*LUTI* cells, we observed an increase in the abundance of *SWI4*^{canon} mRNA (Figure 3.3A). This finding corroborates previous reports, where LUTI expression leads to co-transcriptional silencing of the canonical gene promoter, thereby silencing expression of the protein-coding transcript (Chen et al., 2017; Chia et al., 2017; Van Dalfsen et al., 2018; Tresenrider et al., 2021; Vander Wende et al., 2022). Finally, by immunoblotting, we observed an increase in Swi4 protein abundance in the Δ*LUTI* mutant compared to wild type (Figure 3.3A and 3.3B), further indicating that *SWI4*^{LUTI} expression downregulates Swi4 protein levels in meiosis.

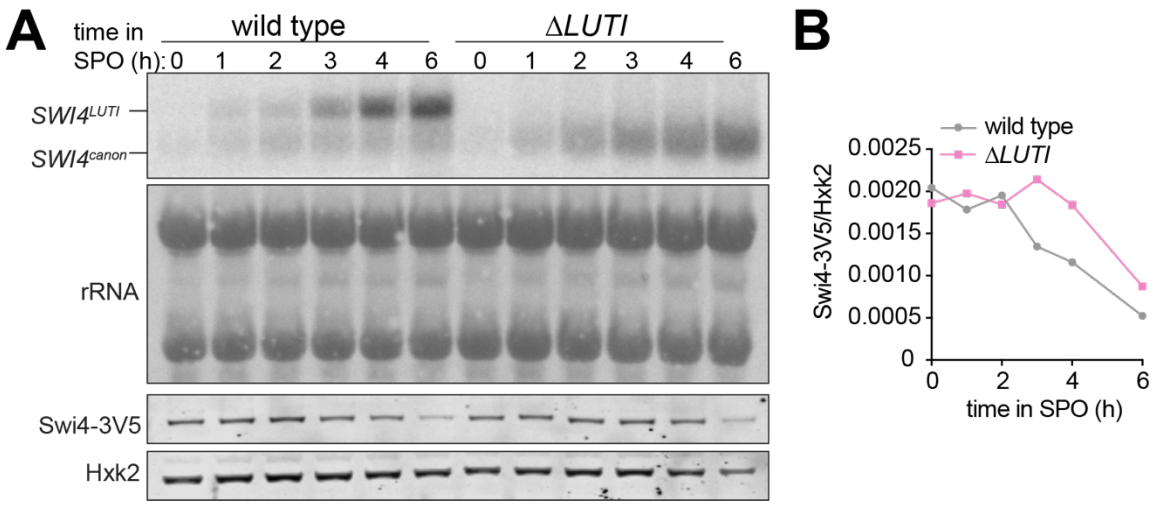

Figure 3.3. *SWI4*^{LUTI} and *SWI4*^{canon} levels in meiosis with protein abundance in Δ*LUTI*. **A.** RNA blot performed on cells collected between 0-6 h in SPO. All strains carry a SWI4-3V5 tagged allele. Probe was specific for 3V5. Methylene blue staining of rRNA bands was used as a loading control. Matched immunoblotting was performed against Swi4-3V5 using α-V5 and normalized to Hxk2 loading control for each sample. Cells collected are wild type (UB22199) and ΔLUTI (UB23012). Representative blots from one of two biological replicates are shown. **B.** Quantification of immunoblot in (A)

SWI4^{LUTI} translation occurs within the upstream ORFs (uORFs) of its 5′ leader sequence (Brar et al., 2012). If the uORFs repress productive translation of the *SWI4* CDS contained within the LUTI, then their removal should result in increased Swi4 protein levels. To determine whether the uORFs inhibit translation of the *SWI4* CDS, we mutated the start codon of all seven uORFs within *SWI4*^{LUTI} from ATG to ATC (Δ*uORF*) and measured Swi4 protein levels using immunoblotting. Compared to wild type, the Δ*uORF* mutant had higher levels of Swi4 protein (Figure 5G and 5H). RNA blotting confirmed that *SWI4*^{canon} transcript levels remained similar between wild type and Δ*uORF* mutant, whereas *SWI4*^{LUTI} levels were higher in the Δ*uORF* mutant compared to wild type (Figure 3.4A), likely resulting from increased transcript stability due to bypass of nonsense mediated decay (Tresenrider et al., 2021). Our findings indicate that the uORFs within the LUTI are translated at the expense of *SWI4* CDS, thus halting Swi4 synthesis during early meiosis.

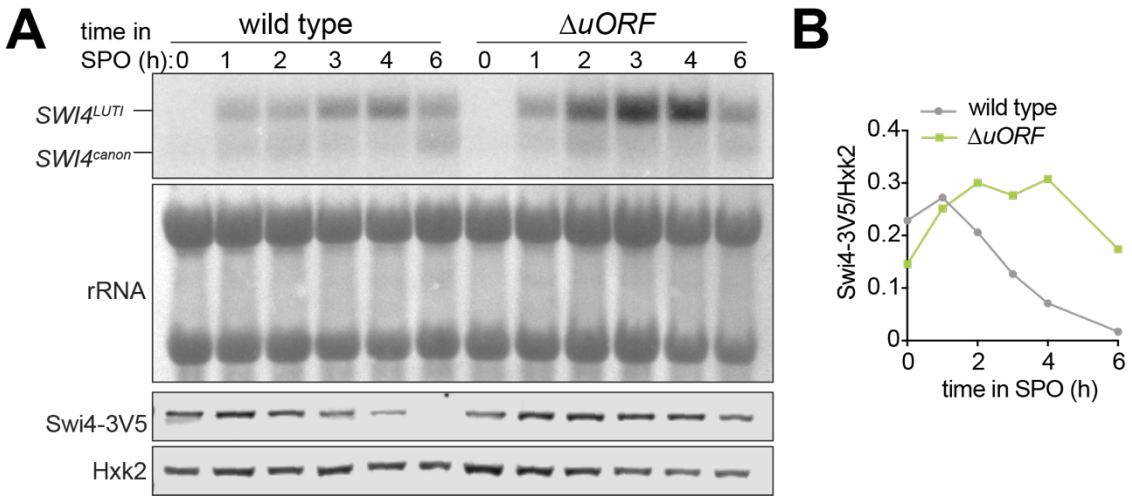

Figure 3.4. *SWI4*^{LUTI} and *SWI4*^{canon} levels in meiosis with protein abundance in Δ*uORF.* **A.** Performed as described in (Figure 3.3A) for wild type (UB21386) and ΔuORF (UB23636) strains. Representative blots from one of two biological replicates are shown. **B.** Quantification of immunoblot in (A).

Our previous findings highlight an antagonistic relationship between Swi4 and Ime1 nuclear localization, whereby overexpression of *SWI4* leads to a decrease in Ime1 nuclear localization (Figure 2.2C). Given the previous finding that Ime1 activates transcription of LUTIs in early meiosis (Tresenrider et al., 2021), we were curious whether the reverse regulation could also occur, where Ime1 causes downregulation of Swi4 through activating *SWI4*^{LUTI} transcription. To test this possibility, we used an inducible allele of *IME1* (*pCUP1-IME1*) (Chia and van Werven, 2016) and measured Swi4 protein abundance. In the absence of *IME1* induction, Swi4 levels remained constant. However, after 1 hour of *IME1* induction, Swi4 levels started to decrease dramatically (Figure 3.5). Therefore, reduction in Swi4 levels is dependent on Ime1 rather than being driven by nutrient deprivation in sporulation media, a condition that is known to trigger autophagy (Abeliovich and Klionsky, 2001).

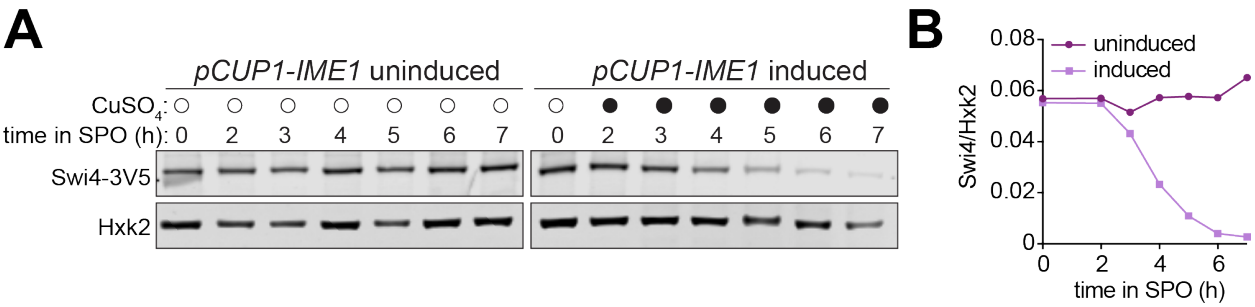

Figure 3.5. Decrease in Swi4 levels is dependent on Ime1 expression. **A.** Immunoblot using α-V5 performed on cells collected between 0-7 h in SPO from a strain carrying *pCUP1-IME1* and *SWI4-3V5* alleles (UB34641). Swi4-3V5 abundance was normalized to Hxk2 loading control. Cells were induced to enter meiosis with 50 μM $CuSO_4$ after 2 h preincubation in SPO. Representative blots from one of two biological replicates are shown. **B.** Quantification of immunoblot in (A).

To further assess whether *SWI4*^{LUTI} is regulated by the Ime-Ume6 transcription factor complex, we analyzed a published Ume6 ChIP-seq dataset (Tresenrider et al., 2021) and found evidence for Ume6 binding at the *SWI4*^{LUTI} promoter (Figure 3.6A). Additionally, analysis of an mRNA-seq dataset from *UME6-T99N* (Tresenrider et al., 2021), an allele of *UME6* that can no longer interact with Ime1, revealed a dramatic reduction in *SWI4*^{LUTI} expression in meiotic conditions (Figure 3.6B). Together, these data support the notion that Ime1-Ume6 complex induces the expression of *SWI4*^{LUTI}, which in turn inhibits Swi4 protein synthesis through the combined act of transcriptional and translational interference.

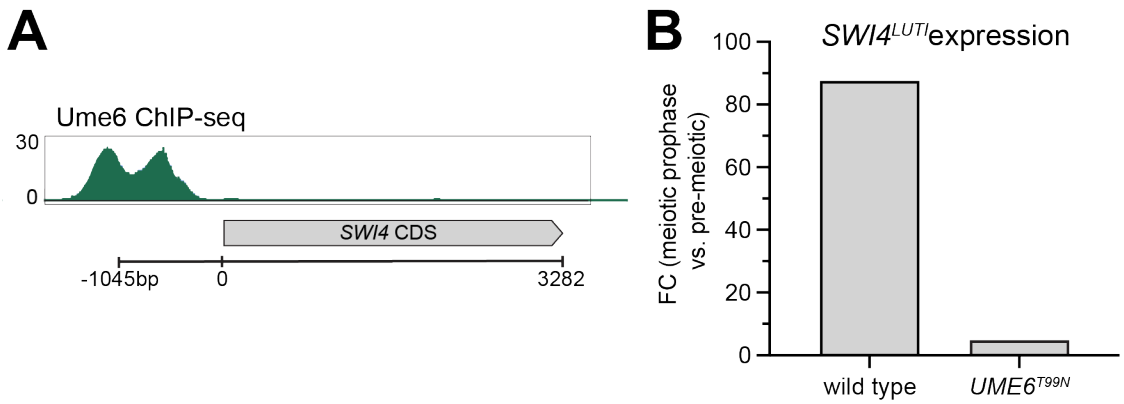

Figure 3.6. *SWI4*^{LUTI} is regulated by Ime1. **A.** Genome browser view of Ume6-ChIP at the *SWI4* locus (adapted from Tresenrider et al., 2021). Fold change expression in wild type or Ume6(T99N) mutant between pre meiotic conditions and meiotic prophase (Tresenrider et al., 2021).

3.1.2 *SWI4*^{LUTI} is integrated into a larger regulatory network to regulate SBF activity during meiotic entry

Since the removal of *SWI4*^{LUTI} resulted in an increase in Swi4 levels, we next wanted to investigate how the loss of LUTI-based regulation affects meiotic entry. We performed mRNA-seq in Δ*LUTI* mutant or wild-type cells during meiotic entry (2 h in SPO) and used DESeq2 to identify differentially expressed genes. To our surprise, there was no obvious increase in the expression of many SBF targets (Figure 3.7). Namely, *CLN1* and *CLN2* were both expressed at similar levels to wild type upon loss of *SWI4*^{LUTI}. Therefore, it appears that disruption of the LUTI-based regulation alone is not sufficient to reactivate SBF targets.

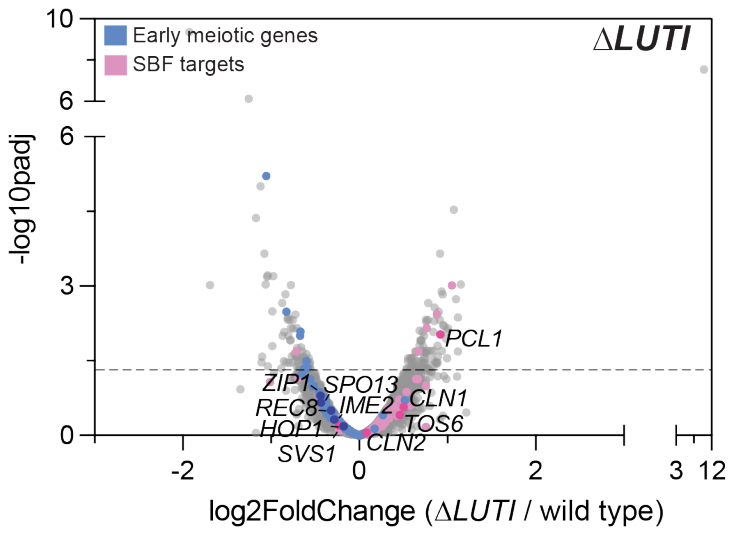

Figure 3.7. Δ*LUTI* has no significant changes in SBF targets or early meiotic genes. Volcano plot of DESeq2 analysis for Δ*LUTI* versus wild type. Dashed line indicates padj (p-value) = 0.05. Analysis was performed with mRNA-seq in duplicate. Wild type (UB27083) and Δ*LUTI* (UB26874) collected at 2 h in SPO. SBF targets (pink) and early meiotic genes (blue) defined by (Iyer et al., 2001 and; Brar et al., 2012). Darker pink or darker blue, labeled dots are well studied targets in either gene set list.

Since transition from the mitotic to meiotic program is a critical cell fate decision, it is likely that additional players are in place to restrict SBF activity. In this case, even when the LUTI-based regulation fails, SBF would remain largely inactive due to a backup mechanism. In support of this notion and consistent with a previous report (Argüello-Miranda et al., 2018), the SBF inhibitor Whi5 was expressed during early meiosis (0 h in SPO) and localized to the nucleus (Figure 3.8A). During the mitotic G1 phase, Whi5 associates with promoter-bound SBF, thereby preventing the transcription of SBF target genes (De Bruin et al., 2004; Costanzo et al., 2004). Shortly before the G1/S transition, phosphorylation of Whi5 via the Cln3/CDK pathway activates SBF by promoting nuclear export of Whi5 (De Bruin et al., 2004; Costanzo et al., 2004). However, in nutrient-deprived conditions that favor meiosis such as nitrogen limitation, *CLN3* is translationally repressed and any Cln3 protein that is expressed is also unstable (Parviz and Heideman, 1998; Gallego et al., 1997). Without Cln3/CDK, Whi5 is expected to inhibit SBF in a constitutive manner.

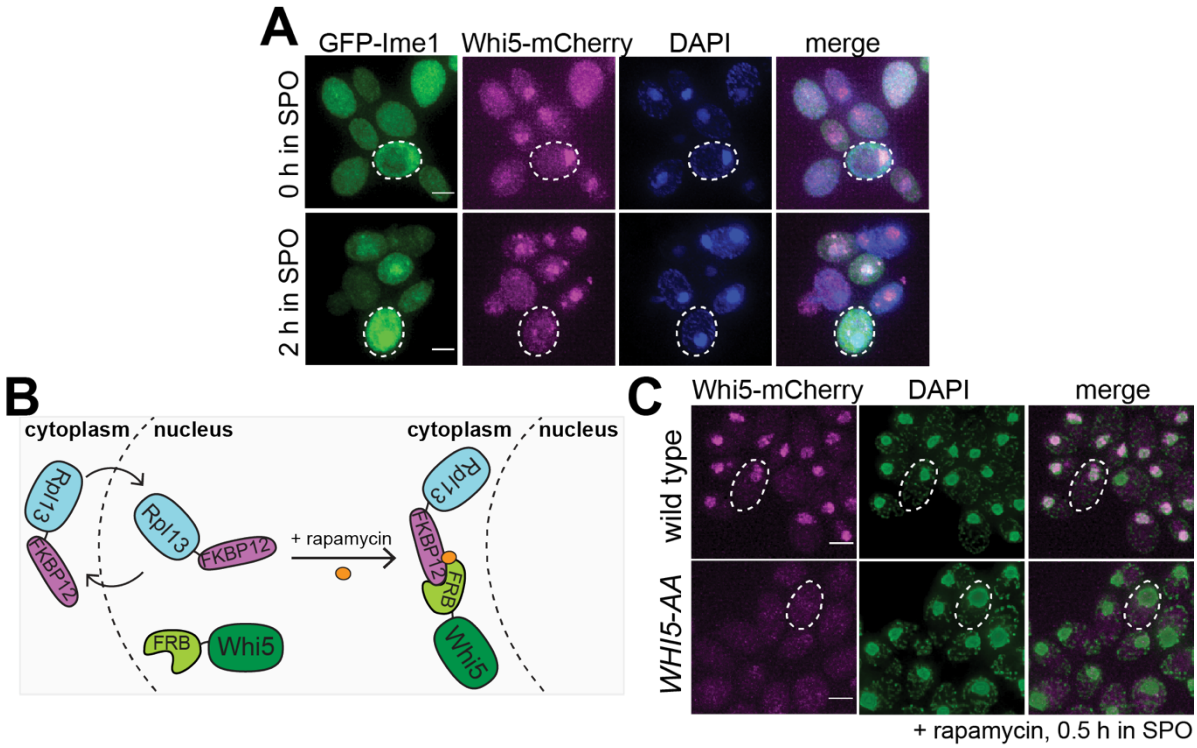

Figure 3.8. Nuclear depletion of Whi5 during meiotic entry using anchor-away. **A.** Fixed imaging of cells marked with GFP-Ime1 and Whi5-mCherry with DNA stained with DAPI. Representative images with merge at 0 h and 2 h in SPO. Representative cells outlined. **B.** Schematic of the anchor-away system using *WHI5-mCherry-FRB* (*WHI5-AA*) and *RPL13a-FKBP12* alleles. **C.** Fixed imaging of cells marked with *WHI5-mCherry-FRB* (*WHI5-AA*) with DNA stained with DAPI. 1 μM rapamycin added at 0 h in SPO to induce nuclear exclusion of Whi5 (UB25431) strain collected at 0.5 h in SPO. Scale bar: 3 μm. Cells are rapamycin resistant due to mutated *TOR1* (*tor1-1*) and frp1Δ (yeast FKBP12 homolog) to reduce competition between for binding of Frb and Fkbp12.

To determine whether Whi5 and *SWI4*^{LUTI} act in parallel to restrict SBF activity, we removed Whi5 from the nucleus using the anchor-away method, which enables compartment-specific depletion of a target protein via inducible dimerization (Haruki et al., 2008). Whi5 was tagged with FRB and ribosomal protein Rpl13a was tagged with FKBP12. Upon addition of rapamycin, Rpl13a-FKBP12 and Whi5-FRB formed a heterodimer, leading to successful nuclear exclusion of Whi5 (Figure 3.8B and 3.8C). Using Whi5 anchor away (*WHI5-AA)* alone or in combination with removal of LUTI-based *SWI4* regulation (Δ*LUTI)*, we performed mRNA-seq to measure expression of SBF targets and early meiotic genes. Similar to the Δ*LUTI* single mutant, *WHI5-AA* alone did not significantly change the expression of SBF targets or early meiotic genes relative to wild type (Figure 3.9A). However, loss of both modes of regulation resulted in increased expression of SBF targets as well as a concomitant decrease in early meiotic transcripts compared to wild type (Figure 3.9B).

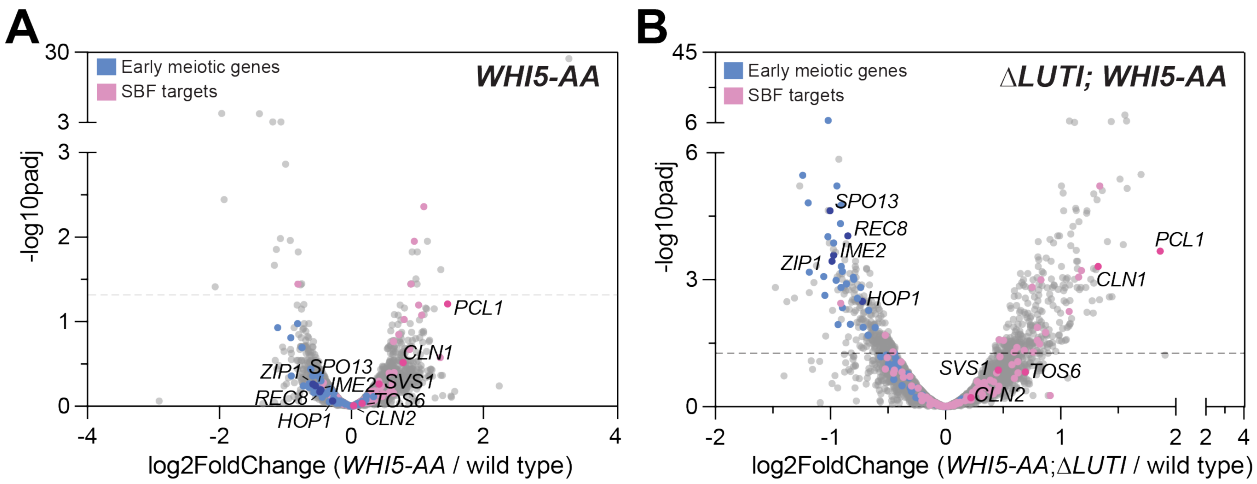

Figure 3.9. Whi5-AA and ΔLUTI double mutant have increased expression of SBF targets and decreased expression of early meiotic genes. **A** Same as in (Figure 3.7) but for wild type (UB27083) and *WHI5-AA* (UB25431) collected at 2 h in SPO. **D.** Same as in (Figure 3.7) but for wild type (UB27083) and Δ*LUTI; WHI5-AA* (UB25428) collected at 2 h in SPO.

As expected, Swi4 levels were similar to wild type in *WHI5-AA* but were elevated in Δ*LUTI* and Δ*LUTI*; *WHI5-AA* mutants (Figure 3.10A-C). Gene set enrichment analysis revealed a significant enrichment of the SBF regulon (NES = 1.95, p < 0.001) as well as significant disenrichment of the early meiotic genes (NES = -3.39, p < 0.001) in the Δ*LUTI*; *WHI5-AA* double mutant (3.10D).

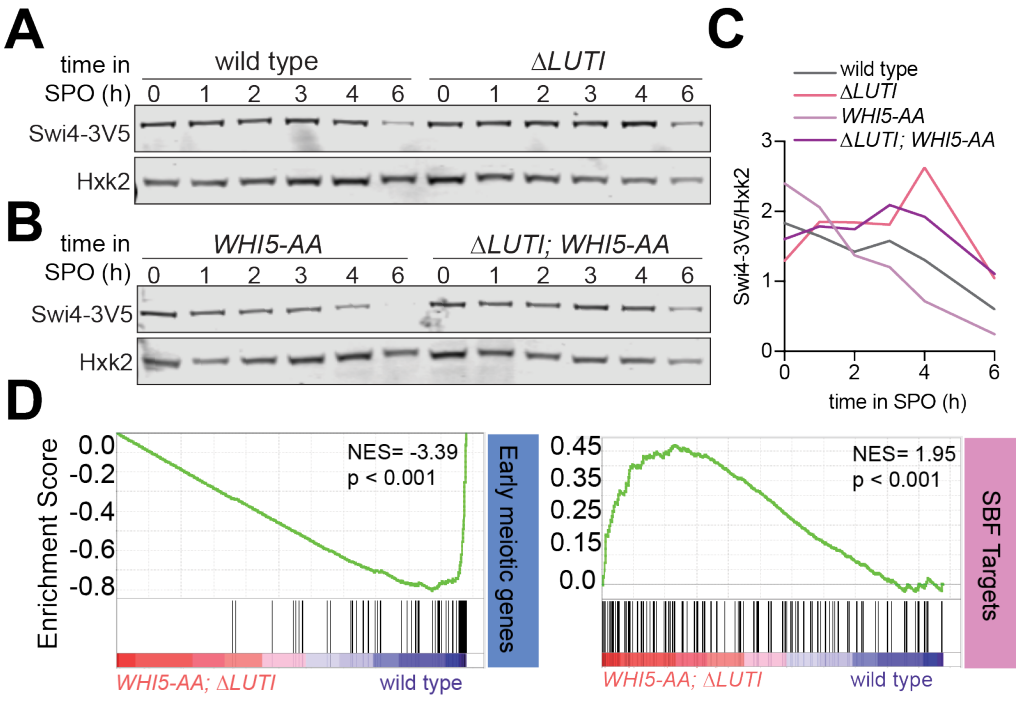

Figure 3.10. Swi4 levels do not change in Whi5-AA system. **A-B.** Cells with the following genotypes were collected between 0-6 h in SPO: wild type (UB27083), Δ*LUTI* (UB26874), *WHI5-AA* (UB25431), Δ*LUTI; WHI5-AA* (UB25428). Immunoblotted using α-V5 to quantify Swi4-3V5 abundance. Normalized to Hxk2

loading control. Representative blots from one of two biological replicates are shown. **C.** Quantification of blots (A and B). **D.** GSEA analysis of mRNA-seq comparing wildtype vs. Δ*LUTI; WHI5-AA (UB25428)* cells collected at 2 h in SPO. Vertical black bars represent early meiotic gene cluster from (Brar et al., 2012) or SBF cluster from (Iyer et al., 2001). The heatmap indicates genes that are more enriched in Δ*LUTI; WHI5-AA* (red, left-side) or genes that are enriched with wild type (blue, right-side). NES = normalized enrichment score. Enrichment was determined comparing wild type to Δ*LUTI; WHI5-AA.*

Finally, we monitored meiotic entry using time-lapse fluorescence microscopy in strains carrying endogenously tagged Rec8-GFP in conjunction with Htb1-mCherry. In agreement with our mRNA-seq data, loss of either LUTI- or Whi5-based repression of SBF alone was not sufficient to cause a delay in meiotic entry (Figure 6E). However, simultaneous perturbation of both pathways led to a significant delay in meiotic entry (Figure 6E, p = 0.0112, Mann-Whitney test). These data further support the notion that *SWI4*^{LUTI} is integrated into a larger regulatory network to regulate SBF activity during meiotic entry, which includes Whi5-mediated repression of SBF.

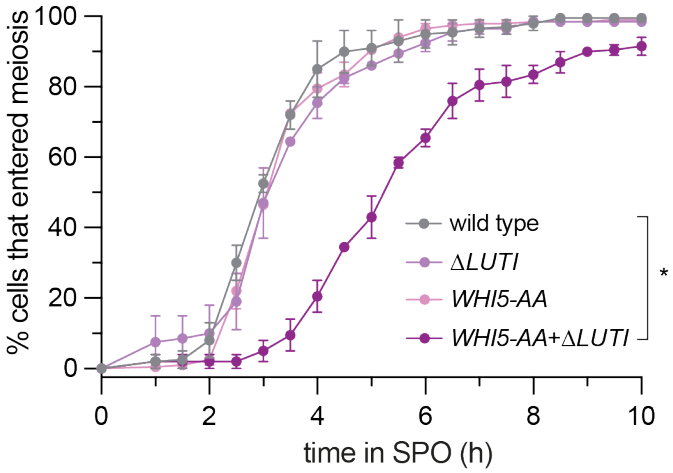

Figure 3.11. Live-cell imaging of cells in meiosis marked by Rec8-GFP and nuclear marker Htb1-mCherry. The following genotypes were imaged: wild type (UB35987), Δ*LUTI* (UB35989), *WHI5-AA* (UB35991), Δ*LUTI; WHI5-AA* (UB35989)**.** Quantification as percent of cells that entered meiosis assayed by nuclear Rec8 appearance. Experiments were performed using two biological replicates, mean value plotted with range. Differences in meiotic progression compared by Mann-Whitney test, two-tailed (*, p = 0.0112 [wild type vs. Δ*LUTI*; *WHI5-AA*]).

3.3 Discussion

In this chapter we identified and characterized the biological mechanisms in place that repress SBF activity for timely meiotic entry. We validated the Ime1 regulated, meiotic LUTI expressed at the *SWI4* locus (*SWI4*^{LUTI}) by demonstrating (1) expression of *SWI4*^{LUTI} suppresses downstream expression of *SWI4*^{canon} and (2) the uORFs within the LUTI leader sequence are repressive. Surprisingly, in contrast to Swi4 overexpression loss of LUTI-mediated repression was not sufficient to cause a delay in meiotic entry. However, when combined nuclear depletion of Whi5 (*Whi5-AA*), this double mutant (*Whi5-AA;* Δ*LUTI*) resulted in a meiotic delay. A previous study characterized Whi5's function in meiosis via constitutive deletion and observed a delay in meiotic S phase via

flow cytometry (Brush et al., 2012). This is inconsistent with our result of nuclear depletion of Whi5 (*Whi5-AA*) not being sufficient to cause a delay in meiosis. The *Whi5-AA* allele was functionally tested via cell coulter counter to measure cell size in mitotically dividing cells and found Whi5-AA reduced cell size comparable to a *whi5*Δ indicating successful Whi5 loss of function. Our data is not consistent with previous observations of loss of Whi5 function in meiosis, however this could be due to secondary effects from constitutive deletions. Additionally, our finding that nuclear depletion of Whi5 was not sufficient to de-repress SBF activity in meiosis further highlights the biological function of LUTI mediated repression of Swi4 abundance. This study elucidates the biological function a LUTI at the *SWI4* locus working in parallel with Whi5 to suppress SBF during meiotic entry.

While LUTI-based regulation is both necessary and sufficient to downregulate Swi4 levels, disrupting it alone is not enough to activate the SBF regulon. We found that the LUTI-based mechanism works together with the Whi5 pathway to inhibit SBF activity (Figure 7). As a result, only when both mechanisms are simultaneously disrupted, do cells exhibit abrupt activation of SBF targets and subsequent meiotic entry defects. This two-pronged inhibition of SBF activity is reminiscent of how meiotic cells prevent microtubule-kinetochore interactions during prophase I (Miller et al., 2012). Specifically, LUTI-based regulation represses the expression of a limiting outer kinetochore subunit, Ndc80 (Chen et al., 2017). Even when the outer kinetochore assembles upon disruption of $NDC80^{LUTI}$, microtubules are still unable to engage with the kinetochores due to restriction of CLB/CDK activity. The loss of both regulations results in meiotic chromosome segregation defects (Chen et al., 2017). Integrating LUTI-based repression into larger regulatory networks likely ensures robustness in cellular decision-making, providing a fail-safe system. However, combinatorial use of the LUTI-based mechanism with other regulatory pathways poses a challenge to uncover their functional importance. Despite their widespread expression during the meiotic program and impact on at least 8% of the proteome(Cheng et al., 2018), the biological significance of only two LUTIs, $NDC80^{LUTI}$ and $SWI4^{LUTI}$, have been uncovered thus far. Therefore, systematic studies aiming to dissect the functional impact of LUTIs in meiosis and beyond would benefit from simultaneous perturbation approaches, including synthetic genetic interactions.

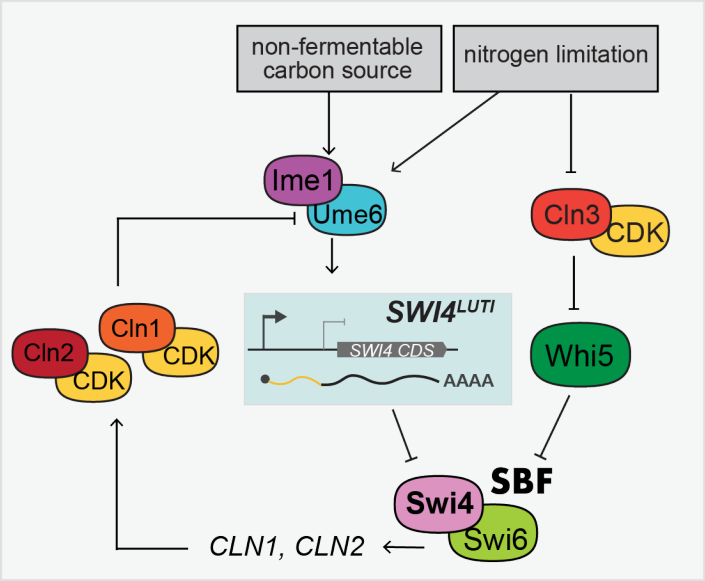

Figure 3.12. Model of SBF regulation during meiotic entry. Ime1 downregulates Swi4 protein expression via induction of *SWI4*^{LUTI} while Whi5 represses SBF activity in parallel to LUTI-based mechanism to prevent expression of SBF targets, including G1 cyclins, which perturb meiotic entry via blocking interaction between Ime1 and its cofactor Ume6.

Chapter 4: Conclusions and Future Directions

In this thesis we characterized the biological significance of SBF repression in meiosis. To do so, we overexpressed the limiting subunit of SBF, Swi4, at meiotic entry. We found that *SWI4* overexpression resulted in the abrupt activation of SBF transcriptional targets and a concomitant decline in the expression of early meiotic genes. Consequently, cells overexpressing *SWI4* exhibited meiotic progression delays. Additionally, we show that the SBF targets *CLN1* and *CLN2* are the major drivers of the meiotic entry defect resulting from SBF misregulation. The *CLN*-dependent phenotypes can be largely rescued by tethering of the central meiotic regulator Ime1 to its cofactor Ume6, suggesting that the primary reason for meiotic failure caused by these G1 cyclins is due to a defect in Ime1-Ume6 interaction (Chapter 2).

Since repression of SBF is crucial for timely meiotic entry we also set out to identify mechanisms of SBF regulation in meiosis. We elucidated two distinct mechanisms by which meiotic cells inhibit the activity of SBF. The dual inhibition of SBF converges on its unique subunit Swi4 and occurs through: (1) meiosis-specific expression of a LUTI from the *SWI4* locus, *SWI4*^{LUTI}, which downregulates Swi4 protein levels, and (2) repression of Swi4 activity by the Rb homolog Whi5, which restricts SBF even when the LUTI-based regulation is disrupted (Chapter 3).

Our findings reveal the functional role of a LUTI in establishing the meiotic transcriptional program and demonstrate how the LUTI-based regulation is integrated into a larger

regulatory network to ensure timely SBF activity. Our study additionally provides mechanistic insights into how SBF misregulation impedes transition from the mitotic to meiotic cell fate (Figure 3.10).

4.1 Mutually exclusive programs via the antagonistic relationship between Swi4 and Ime1

Swi4 and Ime1 regulate each other in an antagonistic manner (Figure 3.12), as supported by several observations. First, overexpression of *SWI4* leads to a reduction in Ime1 nuclear localization (Figure 2.7). Second, premature activation of SBF through *SWI4* overexpression or simultaneous disruption of *SWI4*^{LUTI} and Whi5 pathways results in a significant delay in the chromosomal localization of Rec8, a direct transcriptional target of Ime1 (Figure 2.11, Figure 3.10). Additionally, many early meiotic genes that are also transcriptional targets of Ime1 are downregulated under the same conditions (Figure 2.10A and Figure 3.9). Third, entry is inhibited by the G1 cyclins, which are themselves targets of Swi4/SBF, by perturbing the Ime1-Ume6 interaction (Figure 2.20). An open question from this thesis work is what is the target of Cln-CDK phosphorylation? While Ime1 does not contain the CDK motif -S/TPxR/K (Moses et al., 2007) Ume6 contain a few consensus sites. Future work could determine the sites of phosphorylation on Ume6 or potentially a more degenerate CDK consensus is phosphorylated on Ime1 itself (Verma et al., 1997, communication with JT). Alternatively, the Cln-CDK activity could also be indirectly regulating Ime1 localization through Rim11 and/or Rim15, two kinases that regulate Ime1-Ume6 phosphorylation (Rubin-Bejerano et al., 1996; Vidan and Mitchell, 1997; Bowdish et al, 1994). There are CDK consensus phosphorylation sites on Rim15 kinase which has been shown to be phosphorylated by Cln2-CDK (Holt et al., 2009; Moreno-Torres et al., 2017; Breitkreutz et al., 2010; Talarek et al., 2010).

The reverse regulation, where Ime1 inhibits Swi4, is also in place. This occurs through the Ime1-dependent expression of *SWI4* ^{LUTI}, which is necessary to downregulate Swi4 levels (Figure 3.5 and Figure 3.6, also reported in Tresenrider et al., 2021). Via *SWI4* ^{LUTI} induction, Ime1 ensures downregulation of the G1 cyclins, which negatively regulate Ime1-Ume6 interaction and thus the propensity to enter meiosis. The antagonistic relationship between Swi4 and Ime1 is further evidenced by their mutually exclusive pattern of nuclear localization at the single-cell level (Figure 2.8). This antagonistic relationship between two key transcription factors one necessary for mitotic entry and the other meiotic entry could serve to keep these two programs mutually exclusive. In summary, our study highlights the multiple ways in which Swi4 and Ime1 regulate each other, which likely plays a crucial role in cellular decision making between the mitotic and meiotic transcriptional programs.

4.2 Inhibition of SBF in meiosis

Chapter 2 establishes a strong case for the functional importance of downregulating meiotic SBF activity. We next wanted to elucidate the mechanisms regulating SBF in meiosis. We first characterized a meiosis specific LUTI expressed at the *SWI4* locus

(*SWI4*^{LUTI}) (Figure 3.1 and 3.2) and found upon removal of *SWI4*^{LUTI} expression (∆*LUTI*) there was subsequent derepression of *SWI4*^{canon} and increased Swi4 protein abundance (Figure 3.3). This result supports the first hallmark of LUTI based repression which is transcriptional interference. Previous single locus studies of *NDC80*^{LUTI} as well as genome wide characterization of LUTIs have shown this transcriptional interference is due to repressive chromatin marks H3K4me2 and H3K36me3 which are enriched over the canonical promoter as the LUTI mRNA is transcribed (Chia et al., 2017; Tresenrider et al., 2021). These marks are deposited by Set1/Set3C and Set2/Rpd3S pathways respectively which have been both characterized to play roles in suppressing cryptic transcription and mediating repressive lncRNA transcription (Carrozza et al., 2005; Keogh et al., 2005; Li et al., 2007; van Werven et al., 2012). These repressive marks correlate with increased nucleosome occupancy over the canonical promoter resulting in decreased expression of the canonical mRNA. Additionally, we found removal of the seven AUG uORFs (∆*uORF*) within the 5′ leader sequence lead to increased Swi4 protein (Figure 3.4), thus indicating that translation of these uORFs represses translation of the downstream ORF (Johnstone et al., 2016). Finally, expression of *SWI4*^{LUTI} is developmentally regulated as a target of TF Ime1. The decrease in Swi4 protein (Figure 2.2) is not due to nutrient deprivation, but is specific to meiotic entry and dependent on Ime1. The decrease in Swi4 abundance during meiosis but not starvation highlights an important difference in the regulation of these two processes and supports the idea that *SWI4* downregulation is functionally important for meiosis rather than just due to G1 arrest. Together these data support our model that the cells express *SWI4*^{LUTI} during the onset of meiotic entry to decrease Swi4 protein abundance in order to curb SBF activity.

Whi5 is nuclear during starvation (Argüello-Miranda et al., 2018) and represses cell cycle start by repressing activation of SBF. Dilution of Whi5 as cells grow, phosphorylation by Cln-CDK, and activation of SBF-regulated transcription via Cln3 are all mechanisms of relieving Whi5-mediated suppression of SBF (Schmoller et al., 2015; Costanzo et al., 2004; De Bruin et al., 2004; Wagner et al., 2009; Kõivomägi et al., 2021). Cln3 is the most upstream cyclin in this pathway (Figure 3.12) as it relieves Whi5 repression of SBF. Cln3 is translationally repressed during nitrogen limiting conditions in order to maintain nuclear Whi5 and suppression of SBF during meiosis. Interestingly, as cells enter meiosis indicated by nuclear Ime1 we observed these same cells without nuclear Whi5 (Figure 3.8A). We observed a similar relationship between nuclear Swi4 and Ime1 during entry (Figure 2.8). Whi5 is expressed and translated during meiosis (Brar et al., 2012) and since Whi5 has no other known binding partners aside from SBF, loss of nuclear Whi5 is most likely due decreased Swi4 abundance as *SWI4*^{LUTI} expression is turned on. Previous studies used constitutive deletions of Whi5 (Brush et al., 2012) to define its role in meiosis as a repressor of SBF. We instead used the anchor away technique (Haruki et al., 2008) to constitutively deplete it from the nucleus right before meiotic entry (Figure 3.8B and 3.8C). Our observation that loss of either LUTI-based repression or Whi5 alone was not sufficient to elevate SBF activity (Figure 3.9 and Figure 3.10) further supports the functional contribution of *SWI4*^{LUTI} which in this case is masking any phenotype with the single Whi5-AA mutant. This leads us to conclude that *SWI4*^{LUTI} and Whi5 repression of SBF act in parallel – a fail-safe mechanism to suppress SBF in meiosis. This type of dual regulation is consistent with how important SBF repression is for meiotic entry.

Our observation of Whi5-AA not being sufficient to cause a meiotic entry delay highlights the functional significance of *SWI4*^{LUTI}. Up until this point there has only been one other LUTI that when removed (∆*LUTI*) has biological consequence. *NDC80*^{LUTI} is the first characterized LUTI (Chen et al., 2017; Chia et al., 2017) and functional studies revealed that it works in parallel with tight temporal regulation of bipolar spindle assembly via B-type cyclin Clb3. Ndc80 is the limiting subunit of the kinetochore complex and downregulation of Ndc80 levels via expression of *NDC80*^{LUTI} regulates kinetochore functionality in meiosis. Only Clb3 overexpression combined with removal of LUTI-based regulation of Ndc80 abundance result in premature spindle attachments and meiotic chromosome segregation errors. With this thesis work there are now two cases in which the limiting subunit of either a TF or kinetochore complex are regulated via expression of a LUTI mRNA. This thesis work adds to the new and growing field of LUTI regulation demonstrating its biological relevance to establish the meiotic transcriptome. The utilization of LUTI-based gene repression in combination with other regulatory pathways makes the regulatory network more robust during cellular decision making. Future studies on the function of LUTIs should be sure to study loss of LUTI regulation in conjunction with other regulatory pathways.

Given how important SBF repression is for meiosis, are there other modes of regulation? During mitotic growth SBF controls its own inactivation. The protein products from SBF's gene targets *CLN1* and *CLN2* result in Cln-CDK activity which degrade repressor Sic to then activate B-type cyclins (Verma et al., 1997). Clb-CDK activity results in dissociation of SBF from promoters and exit from mitotic G1 via a negative feedback loop (Koch et al., 1996; Amon et al., 1993). The logic of this feedback loop is conserved in mammalian cells (reviewed in Bertoli et al., 2013). SBF regulating its own activity through a negative feedback loop allows the cell to restrict activity and expression of the SBF regulon to a short window during G1. Since this mode of SBF regulation requires activation of targets that repress meiotic entry, it is unlikely to serve a function during meiosis. Finally, Msa1, Msa2, and Xbp1 are all known transcriptional repressors of G1/S targets during starvation (Miles and Breeden, 2017; Mai and Breeden, 2002) that are expressed during meiotic entry (Brar et al., 2012). During glucose replete conditions, Msa1 and Msa2 have been shown to bind SBF and MBF and are required to suppress expression of many of their gene targets to arrest cells in G1 (Ashe et al., 2008; Miles et al., 2016). Xbp1 is also expressed during low glucose conditions and is a transcriptional repressor that binds DNA directly. Xpb1 has homology to Swi4 and Mbp1, the DNA binding domains of SBF and MBF respectively, and also binds similar consensus sequence but distinct sites (Mai and Breeden, 2002). Future work could investigate whether these transcriptional repressors of SBF are important for meiotic entry.

4.3 Rewiring of the G1/S regulon

It has long been known that entry into the mitotic cell cycle and meiotic differentiation are regulated differently. During the mitotic cell cycle, budding yeast cells must reach a critical size before commitment to division in late G1 phase, an event termed the "Start" (Hartwell et al., 1974; Johnston et al., 1977). Start depends on the activation of the G1/S regulon

by SBF and MBF, which regulate ~200 genes that function in polarized growth, macromolecular biosynthesis, DNA replication, and repair among other critical processes (reviewed in Jorgensen and Tyers, 2004). In contrast, entry into meiosis requires the transcriptional activator, Ime1, which is exclusively induced in diploid cells through the integration of several extrinsic cues including nitrogen levels, carbon source and extracellular pH (reviewed in van Werven and Amon, 2011). Ime1 initiates the first transcriptional wave of early meiotic genes required for DNA replication, recombination, and chromosome morphogenesis.

Before our study, it was unclear whether and how SBF-MBF activity is regulated during the transition from mitosis to meiosis, despite the transcriptome-wide differences between these two developmental programs. We found that during meiotic entry, the SBF-specific Swi4 subunit is downregulated, which indicates that the activity of SBF, but not MBF, is constrained. Consistently, SBF-specific targets display either low or no expression during early meiosis, while MBF targets are upregulated upon meiotic entry (Figure 2.3). MBF targets are involved in processes shared between mitosis and meiosis including DNA replication and repair, whereas SBF targets are predominantly involved in processes unique to mitosis such as budding and cell wall biosynthesis. The only known functional example of this specialization is during DNA replication stress where MBF but not SBF targets are turned on via check-point kinase Rad53 though phosphorylation of MBF repressor Nrm1 (Travesa et al., 2013). Therefore, the functional specialization might have enabled adaptations to accommodate specific cell fates or stresses.

Absolute measurements of the concentrations of SBF and MBF in single cells during mitotic G1 demonstrated that these transcription factors are sub-saturating with respect to their target promoters in small cells, but that SBF and MBF levels increase as cells grow, suggesting that their abundance is a limiting factor in activating the G1/S regulon (Dorsey et al., 2018). Corroborating these findings, we show that overexpression of *SWI4* as well as the simultaneous disruption of the two pathways that normally restrict SBF activity at meiotic entry – namely LUTI and Whi5 – result in abrupt activation of the SBF regulon and a concomitant decrease in early meiotic gene expression. While increased Swi4 abundance results in expression of SBF regulated genes, MBF targets do not seem to be affected. This is surprising given that SBF and MBF share a common subunit, Swi6, and that an upsurge in Swi4 abundance might be expected to titrate Swi6 away from MBF. It is possible that meiosis-specific regulators like Ime1 and Ime2 compensate to maintain MBF target expression (Brush et al., 2012). Future studies are necessary to dissect the meiotic roles of MBF and potential compensatory mechanisms.

Our discovery of a LUTI and Whi5 regulating SBF bring to light the molecular mechanisms behind how and why the G1/S regulon is modulated for meiotic entry. Additionally, the divergence of the G1/S transcription factors has been also observed in mammalian cells. Functional homologs of SBF and MBF in mammalian cells are known as E2Fs, nine of which regulate the G1/S transition (reviewed in Attwooll et al., 2004; reviewed in Bertoli et al., 2013). Each E2F regulates a distinct sets of genes (Gaubatz et al., 2000). Furthermore, some members of the E2F family are involved in tissue-specific regulation of cell fate (Julian et al., 2016). However, the molecular mechanisms driving the rewiring

of these complex gene networks are not well understood. Given the conservation of LUTI-based gene regulation and Whi5 in mammalian cells, our studies may shed light into cell type specific regulations of Rb and E2Fs.

4.5 Concluding Remarks

Altogether, this work reveals how transition from mitotic to meiotic cell fate is ensured by inhibition of the G1/S transcription factor SBF. The SBF regulon includes G1 cyclins, whose untimely expression blocks meiotic entry by interfering with Ime1, a master transcriptional regulator of meiosis. SBF and Ime1 antagonize each another, thereby helping establish a mutually exclusive state between the mitotic and meiotic transcriptional programs. Finally, the regulatory mechanisms identified in our study, including the utilization of a LUTI-based mechanism, are essential for achieving successful meiotic entry. This thesis work demonstrates the biological function of a LUTI at the transition from mitosis to meiosis. Our discovery of another functionally significant LUTI holds wider implications for the numerous functionally uncharacterized LUTIs, emphasizing the substantial gaps in our understanding of the intricate gene regulation in meiosis.

Appendix A: Unpublished findings

5.1 Additional modes of SBF regulation in meiosis

Introduction

In conditions with high SBF activity in meiosis (i.e. *pATG8-SWI4* or the ∆*LUTI; Whi5AA* mutants) we consistently observed a meiotic entry defect or delay. However, after 24 hours in sporulation media cells eventually do complete sporulation and form tetrads. Additionally, we did not observe defects in spore viability. Therefore, once cells enter meiosis, despite increased Swi4 abundance, the spores produced were healthy. We next posed the question: how do cells overcome SBF target expression to enter meiosis?

Results

To investigate additional modes of SBF regulation we decided to track Swi4 localization during and after meiotic entry. We used pCUP1-GFP-IME1 to synchronize cells in meiotic entry to observe Swi4-mCherry and GFP-Ime1 localization. At 2 h in SPO cells were treated with $CuSO_4$ to induce *IME1* expression. Protein samples were collected in parallel and immunoblotted to quantify both Swi4 and Ime1 abundance. In wild type cells after *IME1* induction, we observed a decrease in nuclear Swi4 as Ime1 became nuclear indicating meiotic entry (Figure 5.1B). Additionally, in wild type cells we also observed that the percentage of cells with nuclear Swi4 decreased from 0 to 2 h in SPO (Figure 5.1A) prior to *IME1* induction. Interestingly, Swi4 protein levels did not decrease between 0h and 2h in SPO. However, following *IME1* induction, Swi4 levels decreased (Figure 5.2A and 5.2B). Altogether, these data suggest that Swi4 localization out of the nucleus is not driven by decreasing Swi4 protein levels and is Ime1 independent.

In the *pATG8-SWI4* mutant, we observed increased Swi4 levels at 3 h in SPO (1 h after *IME1* induction). However, at 4 h in SPO we noticed a precipitous loss of nuclear Swi4. This decrease in nuclear Swi4 does not appear to be due to decreasing Swi4 protein levels (Figure 5.2A and 5.2B). Finally, at 3 h in SPO fewer cells have nuclear Ime1 in the *pATG8-SWI4* mutant.

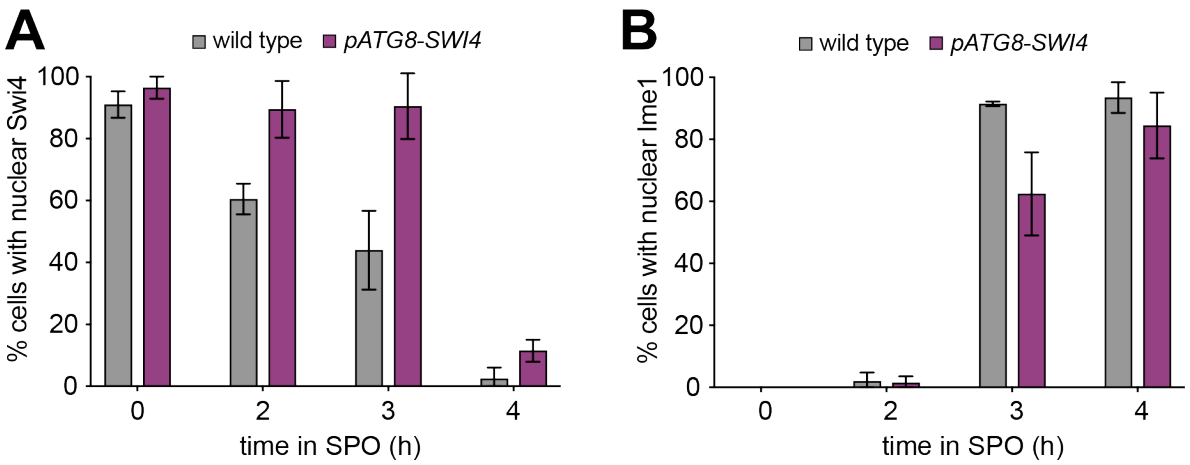

Figure 5.1. Swi4-mcherry is no longer nuclear two hours after Ime1 induction. **A.** Quantification as percent cells with nuclear Swi4-mCherry for wild type (UB30989) and *pATG8-SWI4* (UB31093) cells collected in between 0-4 h in SPO. 50 μM $CuSO_4$ after 2 h in SPO was added to all cells for *pCUP1-GFP-IME1* synchronization. Experiments were performed twice using biological replicates, mean value plotted with range. Total of 200 cells analyzed per strain. **B.** Same as (A) but for GFP-Ime1.

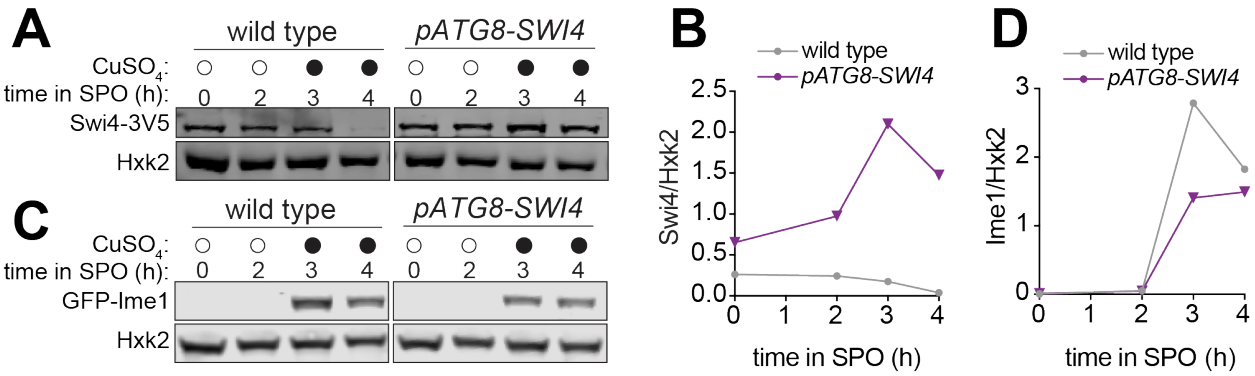

Figure 5.2. Swi4-mcherry levels do not decrease upon Ime1 induction. **A.** Same collection as Figure 5.1. Immunoblot performed using α-Swi4 to quantify Swi4 abundance. Normalized to Hxk2 loading control. **B.** Quantification of immunoblot in (A). **C.** Immunoblot performed using α-GFP to quantify GFP-Ime1 abundance. Normalized to Hxk2 loading control. **D.** Quantification of immunoblot in (C).

Discussion

Swi4 is lost from the nucleus prior to *IME1* induction suggesting that Swi4's localization is regulated during starvation or G1 arrest. Upon Swi4 overexpression, we observe nuclear Swi4-mCherry for longer than in wild type cells. This is most likely due to increased abundance outcompeting whatever mechanism is depleting Swi4 from the nucleus. However, in the *pATG8-SWI4* mutant Swi4 is suddenly depleted out of the

nucleus at 2 h following *IME1* induction (4 h in SPO), suggesting additional modes of regulation in meiosis. There is very little known about the control of Swi4's subcellular localization. Kap95-Srp1 has been identified as the karyopherin necessary for nuclear import of Swi4 (Taberner and Igual, 2010). Analysis of previous datasets shows KAP95 and SRP1 expressed throughout meiosis, so its low abundance or absence from meiosis is not likely to be the cause for sudden loss of nuclear Swi4. The identified NLS in Swi4 between amino acids 372 and 377 KKRRKK contains a serine at amino acid sites 371 and 381 which are within a reasonable range to potentially regulate import of Swi4 (Nardozzi et al., 2010). Our data support a model that depletion of Swi4 from the nucleus is not dependent on Ime1 but occurs during starvation conditions. Further experimentation would be needed to test this hypothesis as well as if the serine sites by the NLS are regulating Swi4 localization in low nutrient conditions. The work in this thesis has demonstrated the cell 1) needs to regulate SBF target expression for timely meiotic entry 2) has evolved parallel and redundant mechanisms to ensure SBF activity is repressed during meiotic entry. Therefore, it does not surprise us there are additional modes of SBF regulation in meiosis that remain to be investigated.

5.2 Mitotic expression of *SWI4^{LUTI}* is sufficient to downregulate SBF activity

Introduction

SBF is an important transcription factor for mitosis that needs to be repressed in meiosis. Our work shows that this regulation is achieved via two parallel acting mechanisms *SWI4^{LUTI}* and Whi5 repression and is important for timely meiotic entry. We next wanted to ask the question is the reverse true – does mitotic G1/S require repression of *SWI4^{LUTI}*? During meiotic G1/S, Ime1 binds Ume6 to regulate the EMG during meiotic entry one of which is *SWI4^{LUTI}*. During mitotic growth however, *IME1* is not expressed and therefore Ume6 acts as a transcriptional repressor of EMGs as it binds histone deacetylase complex Sin3/Rpd3 (Kadosh and Struhl, 1997; Williams et al., 2002). We hypothesize that Ume6 repression of *SWI4^{LUTI}* is important for mitotic growth.

Results

Given that *SWI4^{LUTI}* is necessary for downregulating Swi4 protein synthesis during meiotic entry, we wondered how its ectopic expression might affect mitotically dividing cells. During mitotic growth, transcription of *SWI4^{LUTI}* is repressed by Ume6 through its binding to Sin3/Rpd3. To determine how loss of this regulation impacts mitotic growth, we ectopically expressed *SWI4^{LUTI}* by replacing its endogenous promoter with that of 8x-lexO, which can be activated by the ß-estradiol-responsive LexA-ER-B112 transcription factor (Figure 5.3A and 5.3B, Ottoz et al., 2014). We found that increased expression of *SWI4^{LUTI}* in mitotically dividing cells was sufficient to downregulate Swi4 protein levels (Figure 5.3C and 5.3D).

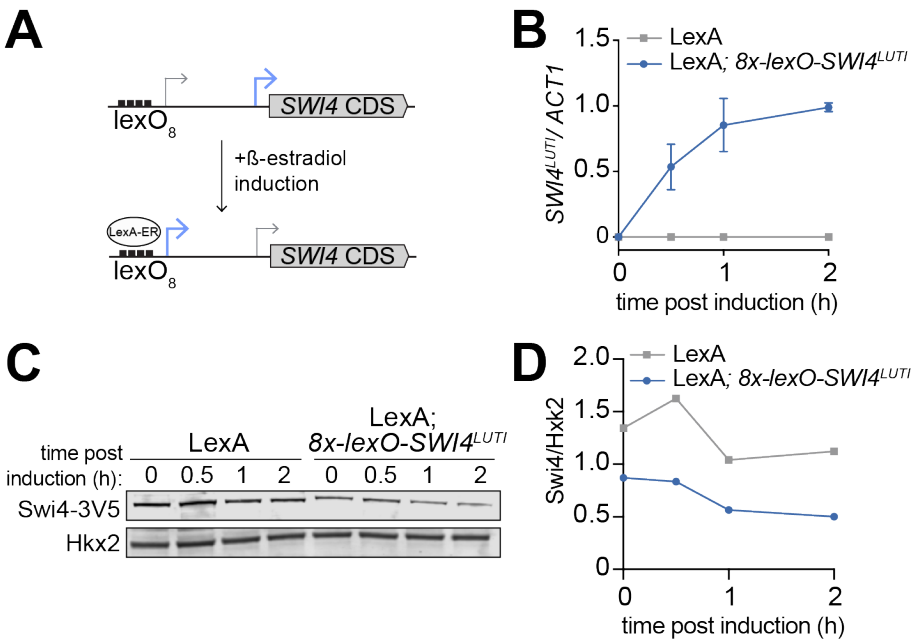

Figure 5.3. Miotic expression of *SWI4*^{LUTI} is sufficient to downregulate Swi4 protein. **A-D.** Mitotically growing cells treated with 40 nM β-estradiol induction to induce *SWI4*^{LUTI} expression. Control strain carrying *LexA-ER-B112* (UB36535) and experimental strain *LexA-ER-B112; 8x-lexO-SWI4*^{LUTI} (UB29211) collected between 0-2 h post β-estradiol induction. **A.** Schematic of *lexO-SWI4*^{LUTI} induction. **B.** RT-qPCR was performed on *SWI4*^{LUTI} transcript. Quantification was performed in reference to *ACT1* and then normalized to wild-type control. FC=fold change. Transcript abundance was quantified using primer sets specific for *SWI4*^{LUTI} from three technical replicates for each biological replicate. Experiments were performed using two biological replicates, mean value plotted with range. **C.** Immunoblot using α-V5 to quantify Swi4-3V5 abundance. Hxk2 used as a loading control. Representative blots from one of two biological replicates are shown. **D.** Quantification of immunoblot in (C).

To assess whether the reduction of Swi4 levels had a functional impact on SBF, we used RT-qPCR and observed a noticeable decrease in the expression of *CLN1* and *CLN2* (Figure 5.4A). Finally, we tracked cell growth continuously using a plate reader and found that increased expression of *SWI4*^{LUTI} led to a significant decrease in growth rate (Figure 5.4B, $P < 0.0001$, Mann-Whitney test). We conclude that ectopic expression of *SWI4*^{LUTI} is sufficient to downregulate Swi4 protein levels, restrict SBF activity and cause growth defects, possibly due to delays in cell cycle progression.

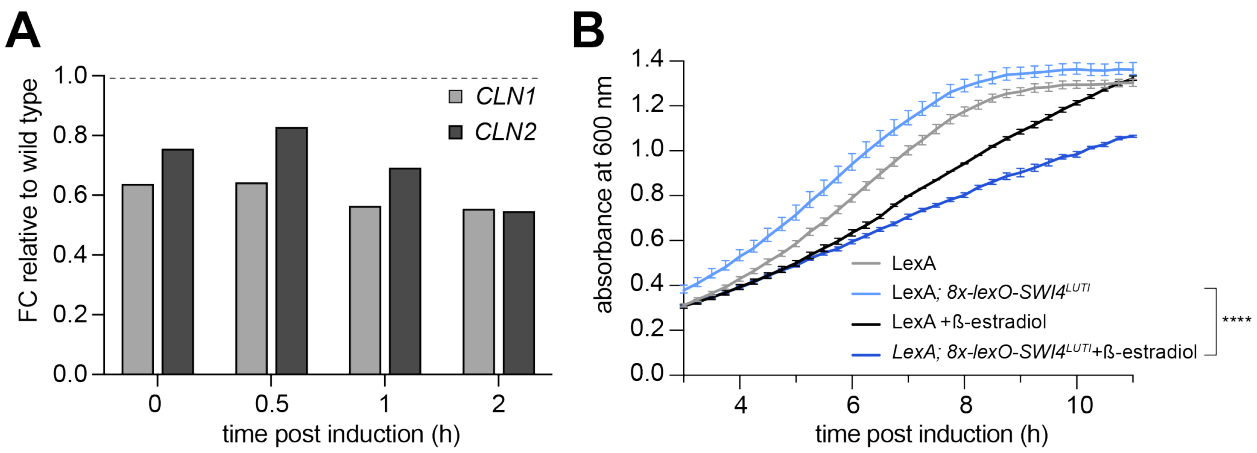

Figure 5.4. Functional consequence of mitotic expression of *SWI4*^{LUTI} in vegetative growth. **A.** Same as in Figure 5.3B but RT-qPCR performed on *CLN1* and *CLN2* transcripts. Transcript abundance was quantified using primer sets specific for each respective gene from three technical replicates for each biological replicate. FC=fold change. **B.** Vegetative growth monitored with a plate reader over 24 h. *LexA-ER-B112 (UB33062)*, and *LexA-ER-B112*; *8x-lexO-SWI4*^{LUTI} (UB33066) strains were grown in YPD or YPD+ 40 nM β-estradiol. Representative growth curve from one of two biological replicates is shown. Mean value plotted with standard deviation across three technical replicates. Difference in growth between LexA-ER-B112; 8x *lexO-SWI4*^{LUTI} with ß-estradiol vs. without was compared using a Mann-Whitney test (****, two-tailed P< 0.0001)

Discussion

Ectopic expression of *SWI4*^{LUTI} appears to be sufficient to not only decrease Swi4 protein levels in mitosis but also repress SBF activity and slow vegetative growth. This is consistent with previous data (Chia et al., 2017) showing that the molecular mechanisms of LUTI mediated repression of Swi4 are not dependent on meiotic conditions. This data also highlights the importance of repression of meiosis specific genes by Ume6 that interfere with mitotic G1/S namely in this case *SWI4*^{LUTI}. This gives further emphasis to the function of this *SWI4*^{LUTI} function as when expressed during the incorrect conditions like nutrient rich conditions will repress SBF activity and perturb vegetative growth. This data along with the greater thesis work highlights *SWI4*^{LUTI} at the intersection of the decision between mitosis and meiosis.

Appendix B: Materials and Methods

6.1 Yeast strain and plasmid construction

All strains used in this study were derived from the SK1 background. Detailed information about the strain genotypes can be found in Table 6.1.

For *SWI4* (pUB1587) 1200 bases upstream of the ORF, *SWI4* ORF, C-terminal 3V5 epitope tag, and *SWI4* 3'UTR (1000 bases downstream of ORF) were cloned into a *LEU2* single integration vector by Gibson assembly (NEB) (Gibson et al., 2009). LUTI promoter deletion (Δ*LUTI*) strain (pUB1588) was similarly constructed with -1200 to -934 bases upstream from ORF deleted. For the uORF mutant (Δ*uORF*) strain (pUB1734) all seven ATG uORFs were mutated using gBlocks with the ATG>ATC mutations and cloned by Gibson assembly into 3V5-tagged *LEU2* single integration vector. In all strains described

above, the endogenous *SWI4* gene is deleted using Pringle-based insertion of KanMX6 marker (Bähler et al., 1998).

For overexpression of *SWI4 (pUB1585)*, *CLN1 (pUB2144)*, and *CLN2 (pUB1899)*, the relevant gene carrying a 3V5 epitope tag was cloned downstream of the *ATG8* promoter, which is highly expressed during meiosis (Brar et al., 2012). A *LEU2* single integration vector was used for cloning the fragments by Gibson assembly (*NEB*). In the strains carrying overexpression transgenes, the wild-type alleles at the endogenous loci remained intact. *pCUP1-GFP-IME1* allele was made with Pringle-based insertion of the *pCUP1* promoter upstream of *GFP-IME1*. *PUS1*-αGFP and *UME6*-αGFP were made by Pringle-based insertion using a plasmid (pUB1707) gifted by the Lackner Lab. For *WHI5-AA* the *WHI5-mCherry-FRB* allele was made by Pringle-based insertion using a plasmid (pUB595) gifted by the Nasmyth lab. All plasmid sequences were confirmed by sequencing.

All single integration plasmids were digested with Pme1 before transformation. Proper integration was confirmed by PCR. The plasmids constructed in this study are listed in Table 6.2.

6.2 Sporulation Conditions

For meiotic experiments using *pCUP1-IME1/pCUP1-IME4* or *pCUP-IME1* system, cells were synchronized as described in (Chia and van Werven, 2016). Briefly, after 24 h of growth in YPD at room temperature, saturated cultures (OD_{600} > 10) were diluted to an OD_{600} of 0.25 in BYTA (1% yeast extract, 2% bacto tryptone, 1% potassium acetate, and 1.02% potassium phthalate) for 16-18 h of growth at 30°C (OD_{600} of > 5). Cells were washed with water twice before final resuspension in SPO with 0.5% potassium acetate to an OD_{600} of 1.85. After 2 h in SPO, *IME1* and *IME4* were induced with 50 µM $CuSO_4$. Sporulation efficiency was measured after 24 h in SPO. Anchor away meiotic experiments was performed as described above with final 1 µM rapamycin (Millipore) added to BYTA 30 minutes before transfer to SPO and again 1 µM rapamycin added to SPO media.

In all other meiotic experiments, cells were prepared as in (Carlile and Amon, 2008). Briefly, after 24 h of growth in YPD at room temperature, saturated cultures (OD_{600} > 10) were diluted to an OD_{600} of 0.25 and inoculated in BYTA (1% yeast extract, 2% bacto tryptone, 1% potassium acetate, and 1.02% potassium phthalate) for 16-18 h at 30°C (OD_{600} of > 5). Cells were washed with water twice before final resuspension in SPO with 0.5% potassium acetate to an OD_{600} of 1.85. Sporulation efficiency was counted after 24 h in SPO.

UME6-αGFP meiotic experiments were prepared as in (Chia and van Werven, 2016). Briefly, after 18 h of growth in YPD at room temperature, saturated cultures (OD_{600} > 10) were diluted to an OD_{600} of 0.2 in reduced YPD (1% yeast extract, 2% peptone, 2% dextrose, uracil [24 mg/L]). Reduced YPD was used instead of BYTA to prevent cells from prematurely entering meiosis in BYTA due to the Ime1-Ume6 interaction from the GFP nanobody. Cells were grown for ~6 h at 30°C until they reached an OD_{600} between 0.5 and 1.0. Cultures were then back diluted to OD_{600} of 0.1 and grown for 18 h at 30°C. Cells

were washed with water twice before final resuspension in SPO with 0.5% potassium acetate to an OD_{600} of 1.85. Sporulation efficiency was counted after 24 h in SPO.

6.3 RNA Extraction for mRNA-seq, RT-qPCR, and RNA Blotting

RNA extraction was performed as described in (Tresenrider et al., 2021). Briefly, ~4 OD unit of cells were pelleted by centrifugation for 1 minute at 20,000 rcf and snap frozen in liquid nitrogen. Cells were thawed on ice and resuspended in TES buffer (10 mM Tris pH 7.5, 10 mM EDTA, 0.5% SDS). An equal volume of Acid Phenol:Chloroform:Isoamyl alcohol (125:24:1; pH 4.7) was added to cells and incubated at 65°C for 45 min shaking at 1400 rpm. Aqueous phase was transferred to a new tube with chloroform, vortexed for 30 sec, separated by centrifugation, and precipitated in isopropanol and sodium acetate overnight at -20°C. Pellets were washed with 80% ethanol and resuspended in DEPC water for 10 min at 37°C. Total RNA was quantified using a nanodrop.

6.4 mRNA Sequencing (mRNA-seq) and Analysis

RNA-seq libraries were generated with the NEXTflex™ Rapid Directional mRNA-Seq Kit (NOVA-5138, Perkin Elmer). 10 µg of total RNA was used as input for all libraries. AMPure XP beads (A63881, Beckman Coulter) were used to select fragments between 200-500 bp. Libraries were quantified using the Agilent 4200 TapeStation (Agilent Technologies, Inc). Samples were submitted for 100 bp SE sequencing by the Vincent J. Coates Genomics Sequencing Laboratory with a NovaSeq SP 100SR.

Hisat2 (Kim et al., 2019) was used to align reads to map sequences to SK1 PacBio genome. Quantification of RNA as transcripts per million was done StringTie (Pertea et al., 2015). Fold-change quantification was performed by DESeq2 using default options (version 1.34.0, (Love et al., 2014)).

For Gene Set Enrichment Analysis (GSEA**)** v4.3.2 was used to compare TPM values for different gene sets. The early meiotic gene set was created from Figure 2 of (Brar et al., 2012). The SBF regulon was from Figure 3 of (Iyer et al., 2001). GSEA was performed on the desktop app with default settings expect “Collapse/Remap to gene symbols” was set to “No_Collapse” and “Permutation type" was set to "gene_set”.

For Gene Ontology (GO) Analysis, SGD Gene Ontology Slim Term Mapper was used for GO analysis using Yeast Go-Slim: process GO Set. Used output from DE-Seq2 analysis with a cutoff of padj (P value) < 0.05.

The two overlapping targets (*SWE1* and *TOS4*) between the early meiotic gene set and SBF targets are not plotted on volcano plot or used for GSEA analysis.

6.5 Reverse Transcription-Quantitative Polymerase Chain Reaction (RT-qPCR)

5 µg of isolated total RNA was treated with DNase (TURBO DNA-free™ Kit). cDNA was reverse transcribed following the Superscript III kit (ThermoFisher Scientific).

Quantification was performed with Absolute Blue qPCR Mix (ThermoFisher Scientific). Meiotic samples were normalized to *PFY1,* and mitotic samples were normalized to *ACT1.* Oligonucleotides are listed in Table 6.3.

6.6 Protein Extraction and Immunoblotting

~4 OD_{600} of cells were collected and pelleted by centrifugation for 1 min at 20,000 rcf. Pellet was resuspended in 5% (w/v) TCA for at least 15 min at 4°C. Cells were washed with TE50 (50 mM Tris-HCl [pH 7.5], 1 mM EDTA) and then with 100% acetone. The cell pellet was dried overnight and then lysed with glass beads in lysis buffer (Tris-HCl [pH 7.5], 1 mM EDTA, 2.75 mM DTT, protease inhibitor cocktail (cOmplete EDTA-free [Roche]). Next 3x SDS sample buffer (187.5 mM Tris [pH 6.8], 6% β-mercaptoethanol, 30% glycerol, 9% SDS, 0.05% bromophenol blue) was added and the cell lysate was boiled for 5 min at 95°C. Protein was separated by PAGE using 4-12% Bis-Tris Bolt gels (Thermo Fisher) and transferred onto 0.45 µm nitrocellulose membranes.

Cln1-3V5, Cln2-3V5 and GFP-GFP tagged proteins were all transferred onto 0.45 µm nitrocellulose membranes using a semi-dry transfer apparatus (Trans-Blot Turbo System (Bio-rad)). Swi4-3V5 or untagged Swi4, Swi6, and Mbp1 proteins were all transferred onto 0.45 µm nitrocellulose membranes using a PROTEAN Tetra tank (BioRAD) filled with 25 mM Tris, 192 mM glycine, and 7.5% methanol. All blots were incubated at room temperature with Odyssey Blocking Buffer (PBS) (LI-COR Biosciences).

Immunoblotting for Cln1-3V5, Cln2-3V5, and GFP-Ime1 was performed as previously described in (Tresenrider et al., 2021). Briefly, mouse α-V5 antibody (R960-25, Thermo Fisher) or mouse α-GFP antibody (632381, Takara) were diluted 1:2000 in Odyssey Blocking Buffer (PBS) (LI-COR Biosciences) with 0.01% Tween. Rabbit α-hexokinase (α-Hxk2) antibody (H2035, US Biological) was diluted to 1:20,000. Secondary antibodies used were α-mouse antibody conjugated to IRDye 800CW (926-32212, LI-COR Biosciences) and α-rabbit antibody conjugated to IRDye 680RD (926-68071, LI-COR Biosciences). Secondary antibodies were diluted to 1:20,000 in Odyssey Blocking Buffer (PBS) with 0.01% Tween.

For immunoblotting of Swi4, Swi6, and Mbp1. antibodies specific to each subunit were a generous gift from the Andrews and deBruin labs (Andrews and Herskowitz, 1989; Harris et al., 2013). α-Swi4, α-Swi6, α-Mbp1 antibodies were each diluted to 1:2000 in Odyssey Blocking Buffer (PBS) (LI-COR Biosciences) with 0.01% Tween. Secondary antibodies included a α-rabbit antibody conjugated to IRDye 800CW (926-32213, LI-COR Biosciences) and a α-rabbit antibody conjugated to IRDye 680RD (926-68071, LI-COR Biosciences).

Odyssey system (LI-COR Biosciences) was used to image the blots, and Image Studio Lite (LI-COR Biosciences) was used for image quantification.

6.7 Northern (RNA) Blotting

For each blot, 10 µg of total RNA was dried in a Savant Speed Vac (SPD111V). RNA was then resuspended and denatured in glyoxal/DMSO mix (1M deionized glyoxal, 50% v/v

DMSO, 10 mM sodium phosphate (NaPi) buffer [pH 6.8]) at 70°C for 10 min. RNA sample was loaded into an agarose gel (1.1% [w/v] agarose in 0.01 M NaPi buffer) with loading dye (10% v/v glycerol, 2 mM NaPi buffer [pH 6.8], ~0.25% w/v xylene cyanol, and orange G) and ran for 3 h at 100 V with a Variable Speed Pump (BioRad) to circulate buffer during the entire gel run.

RNA was transferred overnight to nylon membrane (Hybond-N+ [GE]) in SSC. Membrane was crosslinked using a Stratalinker UV Crosslinker (Stratagene). Ribosomal RNA (rRNA) bands were visualized with methylene blue staining and imaged on a Gel Doc XR+ Molecular Imager with Image Lab software (BioRad).

Probe templates containing the T7 promoter were amplified using PCR. PCR product was concentrated with MinElute Spin Columns (Qiagen) and then used for *in vitro* transcription to generate a strand-specific RNA probe using a MaxiScript T7 Kit (Invitrogen) according to the manufacturer's instructions, except cold UTP was replaced with α-P32 labeled UTP (PerkinElmer). Excess nucleotides were removed with NucAway Spin Columns (Invitrogen). Blots were blocked in ULTRAhyb Ultrasensitive Hybridization Buffer (Invitrogen) for 1 h and then incubated with the α-P32 labeled probe overnight at 68°C. Blots were then washed twice with low stringency wash buffer (2X SSC, 0.1% SDS) for 10 min and then washed twice with high stringency wash buffer (0.1X SSC, 0.1% SDS) for 15 min. Blots were then exposed overnight on a storage phosphor screen (Molecular Dynamics) and then imaged on a Typhoon phosphor-imaging system.

6.8 Fluorescence Microscopy

For time course imaging of cells expressing *GFP-IME1*, *SWI4-mCherry*, or *WHI5-mCherry*, 500 µL of meiotic culture was fixed with a final concentration of 3.7% formaldehyde (v/v) at room temperature for 15 min. Cells were then washed in 1 ml of 100 mM potassium phosphate [pH 6.4] and stored at 4°C in 20 µl of KPi Sorbitol solution overnight (100 mM potassium phosphate [pH 7.5], 1.2M sorbitol). Cells were mounted on a slide and imaged using DeltaVision Elite wide-field fluorescence microscope (GE Healthcare) with a 60x/1.516 oil immersion objective. Deconvolution of images was done with softWoRx imaging software (GE Life Sciences).

For live-cell imaging, cells at OD_{600} of 1.85 in conditioned SPO (filter-sterilized SPO culture after ~5 h in 30°C) were sonicated and transferred to a concanavalin A (Sigma) treated 96-well clear, flat bottom plate (Corning). Four z positions (2 µm step size) were acquired per XY position. Acquisition was performed in a temperature-controlled chamber at 30°C. Please refer to Table 6.4 for acquisition settings.

6.9 Image Quantification

All image analysis was performed with FIJI (Schindelin et al., 2012). Maximum z-projection are shown in figures and were modified using linear brightness and contrast adjustments in FIJI.

To quantify localization of GFP-Ime1 and Rec8-GFP, z-slices containing the nucleus were selected using the Htb1-mCherry signal. Max projection was created from these slices and GFP-Ime1 was scored double-blinded as nuclear or not nuclear.

For mean nuclear intensity of GFP-Ime1 and Swi4-mCherry, an individual z-slice containing the nucleus was selected and nuclear mask was generated using the Htb1-mCherry signal. The nuclear mask was then used to quantify the mean nuclear intensity of GFP-Ime1 signal.

6.10 Single molecule RNA FISH

smFISH was performed and quantified as previously described in (Chen et al., 2018). All probes were ordered from (Biosearch Technologies). Unique region of *SWI4*^{LUTI} was visualized by twenty-eight 20-mer oligonucleotide probes coupled to CAL fluor Red 590. Thirty-eight 20-mer probes coupled to Quasar 670 dye targeted to *SWI4*^{canon}. ~ 4 OD unit of cells were fixed in final 3% formaldehyde (v/v) and incubated at room temperature for 20 minutes. Fixed samples were moved to 4°C to continue fixing overnight. Cells were washed three times in cold Buffer B (0.1 M potassium phosphate [pH 7.5], 1.2 M sorbitol) and resuspended in digestion buffer (Buffer B, 200 mM Vanadyl ribonucleoside complex [VRC from NEB], zymolyse [zymolase 100T, MP Biomedicals]). Cells were digested at 30°C for 20 min and then gently washed with 1 mL of cold Buffer B and resuspended in 1 mL of 70% ethanol for 3.5-5 h.

Cells were then incubated in 1mL of 10% formamide wash buffer (10% formamide, 2X SSC) at room temperature for 15 minutes. For hybridization, each probe set was added (final concentration of 500 nM) to 20mM VRC and hybridization buffer (1% Dextran sulfate [EMD Millipore], 1 mg/mL E. coli tRNA [Sigma], 2 mM VRC, 0.2 mg/mL BSA, 1X SSC, 10% formamide in nuclease-free water). Hybridization was done overnight at 30°C. Samples were incubated in the dark for 30 min at 30°C in 1 mL of 10% formamide wash buffer. Buffer was then removed, and cells were stained with DAPI and resuspended in glucose-oxygen-scavenging buffer or GLOX buffer (10 mM Tris [pH 8.0], 2x SSC, 0.4% glucose) without enzymes. Before imaging, GLOX solution with enzyme (1% v/v catalase, 1% v/v glucose oxidase (Sigma), 2 mM Trolox (Sigma)) was added to sample.

Images were acquired with the DeltaVision microscope as described in previous section with filters: TRITC (EX542/27, EM597/45) for CAL Fluor Red 590 and CY5 (EX632/22, EM679/34) for Quasar 670. Series of z-stacks (15–25 slices) were acquired with a step size of 0.2 μm.

Matlab script (Chen et al., 2017, 2018) was run to quantify FISH spots with max intensity projection of z-stacks. The same "signal" and "SNR" thresholds were applied to all the images within a replicate.

6.11 Plate Reader

Strains were grown in YPD overnight at 30 °C. Cells were diluted to 0.2 OD_{600} in YPD or YPD with 40nM β-estradiol and grown for ~4 h, until they reached log phase. Cells were then diluted to 0.1 OD_{600} (in YPD or YPD with 40nM β-estradiol) and transferred to a 96-

well plate in triplicate. The plate was sealed with a “Breathe-Easy” cover (Sigma-Aldrich). The plate was placed in a plate reader set to read the absorbance at OD_{600} every 15 min for 24 h. The plate was also shaken for 5 seconds and the beginning and for at least 3 sec between reads.

Table 6.1 Strains

Strain	Genotype
SK1 wild-type	*ho::LYS2 lys2 ura3 leu2::hisG his3::hisG trp1::hisG*
14273	*MAT**a**/alpha SWI4-3V5::KanMX/SWI4-3V5::KanMX pCUP-IME1::NAT/pCUP-IME1::NAT pCUP-IME4::NAT/pCUP-IME4::NAT*
15411	*MAT**a**/alpha irt1:cup1::Hphmx/irt1:cup1::Hphmx ime4::cup1::NAT/ime4::cup1::NAT HisMX::Δ(-1000 to -800)-SWI4-3V5::KanMX/HisMX::Δ(-1000 to -800)-SWI4-3V5::KanMX*
21386	*MAT**a**/alpha swi4::KanMX/swi4::KanMX leu2::LEU2::pSWI4(-1200 to -1)-SWI4-3V5-3'UTR/leu2::LEU2::pSWI4(-1200 to -1)-SWI4-3V5-3'UTR ura3::CA-URA3/ura3::CA-URA3 trp1::TRP1/trp1::TRP1*
22199	*MAT**a**/alpha HTB1-mCherry-HISMX6/HTB1-mCherry-HISMX6 ime1-N-sfGFP/ime1-N-sfGFP swi4::KanMX/swi4::KanMX leu2::LEU2::pSWI4(-1200 to -1)-SWI4-3V5-3'UTR/leu2::LEU2::pSWI4(-1200 to -1)-SWI4-3V5-3'UTR ura3::CA-URA3/ura3::CA-URA3 trp1::TRP1/ trp1::TRP1*
22226	*MAT**a**/alpha HTB1-mCherry-HISMX6/HTB1-mCherry-HISMX6 ime1-N-sfGFP/ime1-N-sfGFP leu2::pATG8-SWI4-3V5::LEU2/leu2::pATG8-SWI4-3V5::LEU2 ura3::CA-URA3/ura3::CA-URA3 trp1::TRP1/trp1::TRP1*
23012	*MAT**a**/alpha HTB1-mCherry-HISMX6/HTB1-mCherry-HISMX6 ime1-N-sfGFP/ime1-N-sfGFP swi4::KanMX/swi4::KanMX leu2::LEU2::pSWI4LUTI(-1200 to -934)Δ-SWI4-3V5-SWI4_3'UTR/leu2::LEU2::pSWI4LUTI(-1200 to -934)Δ-SWI4-3V5-SWI4_3'UTR ura3::CA-URA3/ura3::CA-URA3 trp1::TRP1/trp1::TRP1*
23636	*MAT**a**/alpha* leu2::LEU2::pSWI4(-1200 to -1)∆7AUG-uORF-SWI4-3V5-3'UTR/leu2::LEU2::pSWI4(-1200 to -1)∆7AUG-uORF-SWI4-3V5-3'UTR swi4::KanMX/swi4::KanMX ura3::CA-URA3/ura3::CA-URA3 trp1::TRP1/trp1::TRP1
25428	*MAT**a**/alpha* whi5::WHI5-mcherry-linker-FRB::KanMX/whi5::WHI5-mcherry-linker-FRB::KanMX RPL13a-2xFKBP12::TRP1/RPL13a-2xFKBP12::TRP1 fpr1::KanMX/fpr1::KanMX tor1-1::HIS3/tor1-1::HIS3 swi4::KanMX/swi4::KanMX leu2::LEU2::pSWI4LUTI(-1200 to -934)Δ-SWI4-3V5-SWI4_3'UTR/leu2::LEU2::pSWI4LUTI(-1200 to -934)Δ-SWI4-3V5-SWI4_3'UTR ura3::CA-URA3/ura3::CA-URA3
25431	*MAT**a**/alpha* whi5::WHI5-mcherry-linker-FRB::KanMX/whi5::WHI5-mcherry-linker-FRB::KanMX RPL13a-2xFKBP12::TRP1/RPL13a-2xFKBP12::TRP1 fpr1::KanMX/fpr1::KanMX tor1-1::HIS3/tor1-1::HIS3 swi4::KanMX/swi4::KanMX leu2::LEU2::pSWI4(-1200 to -1)-SWI4-3V5-3'UTR/leu2::LEU2::pSWI4(-1200 to -1)-SWI4-3V5-3'UTR ura3::CA-URA3/ura3::CA-URA3
25959	*MAT**a**/alpha his3::HIS3::pATG8-CLN2-3V5/his3::HIS3::pATG8-CLN2-3V5 HTB1-mCherry-HISMX6/HTB1-mCherry-HISMX6 ime1-N-sfGFP/ime1-N-sfGFP ura3::CA-URA3/ura3::CA-URA3 trp1::TRP1/trp1::TRP1*

25982	*MAT**a**/alpha his3::HIS3::pATG8-CLN2-3V5/his3::HIS3::pATG8-CLN2-3V5 Pus1-VH16::URA3/Pus1-VH16::URA3 HTB1-mCherry-HISMX6/HTB1-mCherry-HISMX6 ime1-N-sfGFP/ime1-N-sfGFP swi4::KanMX/swi4::KanMX leu2::LEU2::pSWI4(-1200 to -1)-SWI4-3V5-3'UTR/leu2::LEU2::pSWI4(-1200 to -1)-SWI4-3V5-3'UTR trp1::TRP1/trp1::TRP1*
26874	*MAT**a**/alpha* whi5::WHI5-mcherry-linker-FRB::KanMX/whi5::WHI5-mcherry-linker-FRB::KanMX fpr1::KanMX/fpr1::KanMX tor1-1::HIS3/tor1-1::HIS3 swi4::KanMX/swi4::KanMX leu2::LEU2::pSWI4LUTI(-1200 to -934)Δ-SWI4-3V5-SWI4_3'UTR/leu2::LEU2::pSWI4LUTI(-1200 to -934)Δ-SWI4-3V5-SWI4_3'UTR ura3::CA-URA3/ura3::CA-URA3 trp1::TRP1/trp1::TRP1
27083	*MAT**a**/alpha* whi5::WHI5-mcherry-linker-FRB::KanMX/whi5::WHI5-mcherry-linker-FRB::KanMX fpr1::KanMX/fpr1::KanMX tor1-1::HIS3/tor1-1::HIS3 swi4::KanMX/swi4::KanMX leu2::LEU2::pSWI4(-1200 to -1)-SWI4-3V5-3'UTR/leu2::LEU2::pSWI4(-1200 to -1)-SWI4-3V5-3'UTR ura3::CA-URA3/ura3::CA-URA3 trp1::TRP1/trp1::TRP1
29211	*MATa swi4::KanMX leu2::LEU2::pSWI4LUTI(-1200 to -934)Δ-pCYC1-8xLexO-SWI4-3V5-SWI4_3'UTR trp1::pGPD1-LexA-ER-HA-B112::TRP1*
29326	*MAT**a**/alpha CLN1-3V5::HYG/CLN1-3V5::HYG HTB1-mCherry-HISMX6/HTB1-mCherry-HISMX6 ime1-N-sfGFP/ime1-N-sfGFP swi4::KanMX/swi4::KanMX leu2::LEU2::pSWI4(-1200 to -1)-SWI4-3V5-3'UTR/leu2::LEU2::pSWI4(-1200 to -1)-SWI4-3V5-3'UTR ura3::CA-URA3/ura3::CA-URA3 trp1::TRP1/trp1::TRP1*
29328	*MAT**a**/alpha CLN1-3V5::HYG/CLN1-3V5::HYG HTB1-mCherry-HISMX6/HTB1-mCherry-HISMX6 ime1-N-sfGFP/ime1-N-sfGFP leu2::pATG8-SWI4-3V5::LEU2/leu2::pATG8-SWI4-3V5::LEU2 ura3::CA-URA3/ura3::CA-URA3 trp1::TRP1/trp1::TRP1*
29330	*MAT**a**/alpha CLN2-3v5::KAN/CLN2-3v5::KAN HTB1-mCherry-HISMX6/HTB1-mCherry-HISMX6 ime1-N-sfGFP/ime1-N-sfGFP swi4::KanMX/swi4::KanMX leu2::LEU2::pSWI4(-1200 to -1)-SWI4-3V5-3'UTR/leu2::LEU2::pSWI4(-1200 to -1)-SWI4-3V5-3'UTR ura3::CA-URA3/ura3::CA-URA3 trp1::TRP1/trp1::TRP1*
29332	*MAT**a**/alpha CLN2-3v5::KAN/CLN2-3v5::KAN HTB1-mCherry-HISMX6/HTB1-mCherry-HISMX6 ime1-N-sfGFP/ime1-N-sfGFP leu2::pATG8-SWI4-3V5::LEU2/leu2::pATG8-SWI4-3V5::LEU2 ura3::CA-URA3/ura3::CA-URA3 trp1::TRP1/trp1::TRP1*
30989	*MAT**a**/alpha KanMX:pCUP-ime1-N-sfGFP/KanMX:pCUP-ime1-N-sfGFP swi4::KanMX/swi4::KanMX leu2::LEU2::pSWI4(-1200 to -1)-SWI4-mCherry::HIS3/leu2::LEU2::pSWI4(-1200 to -1)-SWI4-mCherry::HIS3*
31093	*MAT**a**/alpha KanMX:pCUP-ime1-N-sfGFP/KanMX:pCUP-ime1-N-sfGFP leu2::LEU2::pATG8-SWI4-mCherry::HIS3/leu2::LEU2::pATG8-SWI4-mCherry::HIS3*
31378	*MAT**a**/alpha swi4::KanMX/swi4::KanMX leu2::LEU2::pSWI4(-1200 to -1)-SWI4-mCherry::HIS3/leu2::LEU2::pSWI4(-1200 to -1)-SWI4-mCherry::HIS3 ime1-N-sfGFP/ime1-N-sfGFP ura3::CA-URA3/ura3::CA-URA3 trp1::TRP1/trp1::TRP1*
31381	*MAT**a**/alpha leu2::LEU2::pATG8-SWI4-mCherry::HIS3/leu2::LEU2::pATG8-SWI4-mCherry::HIS3 ime1-N-sfGFP/ime1-N-sfGFP ura3::CA-URA3/ura3::CA-URA3 trp1::TRP1/trp1::TRP1*
32820	*MAT**a**/alpha trp1::TRP1::pATG8-CLN1-3V5/trp1::TRP1::pATG8-CLN1-3V5*

	HTB1-mCherry-HISMX6/HTB1-mCherry-HISMX6 ime1-N-sfGFP/ime1-N-sfGFP ura3::CA-URA3/ura3::CA-URA3
32085	*MAT**a**/alpha swi4::KanMX/swi4::KanMX leu2::LEU2::pSWI4(-1200 to -1)-SWI4-3V5-3'UTR/leu2::LEU2::pSWI4(-1200 to -1)-SWI4-3V5-3'UTR HTB1-mCherry-HISMX6/HTB1-mCherry-HISMX6 REC8-GFP-URA3/REC8-GFP-URA3 trp1::TRP1/trp1::TRP1*
32089	*MAT**a**/alpha leu2::LEU2::pATG8-SWI4-3V5/leu2::LEU2::pATG8-SWI4-3V5 HTB1-mCherry-HISMX6/HTB1-mCherry-HISMX6 REC8-GFP-URA3/REC8-GFP-URA3 trp1::TRP1/trp1::TRP1*
33062	*MAT**a**/alpha leu2::LEU2/leu2::LEU2 trp1::pGPD1-LexA-ER-HA-B112::TRP1/trp1::pGPD1-LexA-ER-HA-B112::TRP1*
33066	*MAT**a**/alpha swi4::KanMX/swi4::KanMX leu2::LEU2::pSWI4LUTI(-1200 to -934)Δ-pCYC1-8xLexO-SWI4-3V5-SWI4_3'UTR/leu2::LEU2::pSWI4LUTI(-1200 to -934)Δ-pCYC1-8xLexO-SWI4-3V5-SWI4_3'UTR trp1::pGPD1-LexA-ER-HA-B112::TRP1/trp1::pGPD1-LexA-ER-HA-B112::TRP1*
34165	*MAT**a**/alpha cln2Δ::NatMX/cln2Δ::NatMX leu2::pATG8-SWI4-3V5::LEU2/leu2::pATG8-SWI4-3V5::LEU2 REC8-GFP-URA3/REC8-GFP-URA3 HTB1-mCherry-HISMX6/HTB1-mCherry-HISMX6 trp1::TRP1/trp1::TRP1*
34536	*MAT**a**/alpha cln1Δ::hyg/cln1Δ::hyg leu2::LEU2::pATG8-SWI4-3V5/leu2::LEU2::pATG8-SWI4-3V5 HTB1-mCherry-HISMX6/HTB1-mCherry-HISMX6 REC8-GFP-URA3 /REC8-GFP-URA3 trp1::TRP1/trp1::TRP1*
34641	*MAT**a**/alpha HTB1-mCherry-HISMX6/HTB1-mCherry-HISMX6 KanMX:pCUP-ime1-N-sfGFP/KanMX:pCUP-ime1-N-sfGFP swi4::KanMX/swi4::KanMX leu2::LEU2::pSWI4(-1200 to -1)-SWI4-3V5-3'UTR/leu2::LEU2::pSWI4(-1200 to -1)-SWI4-3V5-3'UTR ura3::CA-URA3/ura3::CA-URA3 trp1::TRP1/trp1::TRP1*
35057	*MAT**a**/alpha HTB1-mCherry-HISMX6/HTB1-mCherry-HISMX6 KanMX:pCUP-ime1-N-sfGFP/KanMX:pCUP-ime1-N-sfGFP swi4::KanMX/swi4::KanMX leu2::LEU2::pSWI4(-1200 to -1)-SWI4-3V5-3'UTR/leu2::LEU2::pSWI4(-1200 to -1)-SWI4-3V5-3'UTR his3::HIS3::pATG8-CLN2-3V5/his3::HIS3::pATG8-CLN2-3V5 ura3::CA-URA3/ura3::CA-URA3 trp1::TRP1/trp1::TRP1*
35106	*MAT**a**/alpha his3::HIS3::pATG8-CLN2-3V5/his3::HIS3::pATG8-CLN2-3V5 HTB1-mCherry-HISMX6/HTB1-mCherry-HISMX6 ime1-N-sfGFP/ime1-N-sfGFP swi4::KanMX/swi4::KanMX leu2::LEU2::pSWI4(-1200 to -1)-SWI4-3V5-3'UTR/leu2::LEU2::pSWI4(-1200 to -1)-SWI4-3V5-3'UTR ura3::CA-URA3/ura3::CA-URA3 trp1::TRP1/trp1::TRP1*
35177	*MAT**a**/alpha his3::HIS3::pATG8-CLN2-3V5/his3::HIS3::pATG8-CLN2-3V5 HTB1-mCherry-HISMX6/HTB1-mCherry-HISMX6 ime1-N-sfGFP/ime1-N-sfGFP swi4::KanMX/swi4::KanMX leu2::LEU2::pSWI4(-1200 to -1)-SWI4-3V5-3'UTR/leu2::LEU2::pSWI4(-1200 to -1)-SWI4-3V5-3'UTR UME6-VH16::URA3/UME6-VH16::URA3 trp1::TRP1/trp1::TRP1*
35246	*MAT**a**/alpha ura3::CA-URA3/ura3::CA-URA3 trp1::TRP1/trp1::TRP1*
35300	*MAT**a**/alpha HTB1-mCherry-HISMX6/HTB1-mCherry-HISMX6 ime1-N-sfGFP/ime1-N-sfGFP swi4::KanMX/swi4::KanMX leu2::LEU2::pSWI4(-1200 to -1)-SWI4-3V5-3'UTR/leu2::LEU2::pSWI4(-1200 to -1)-SWI4-3V5-3'UTR UME6-VH16::URA3/UME6-VH16::URA3 trp1::TRP1/trp1::TRP1*
35593	*MAT**a**/alpha Pus1-VH16::URA3/Pus1-VH16::URA3 HTB1-mCherry-HISMX6/HTB1-mCherry-HISMX6 ime1-N-sfGFP/ime1-N-sfGFP swi4::KanMX/swi4::KanMX leu2::LEU2::pSWI4(-1200 to -1)-SWI4-3V5-*

	3'UTR/leu2::LEU2::pSWI4(-1200 to -1)-SWI4-3V5-3'UTR trp1::TRP1/trp1::TRP1
35985	*MAT**a**/alpha whi5::WHI5-mcherry-linker-FRB::KanMX/whi5::WHI5-mcherry-linker-FRB::KanMX RPL13a-2xFKBP12::TRP1/RPL13a-2xFKBP12::TRP1 fpr1::KanMX/fpr1::KanMX tor1-1::HIS3/tor1-1::HIS3 HTB1-mCherry-HISMX6/HTB1-mCherry-HISMX6 REC8-GFP-URA3/REC8-GFP-URA3 swi4::KanMX/swi4::KanMX leu2::LEU2::pSWI4L UTI(-1200 to -934)Δ-SWI4-3V5-SWI4_3'UTR/leu2::LEU2::pSWI4L UTI(-1200 to -934)Δ-SWI4-3V5-SWI4_3'UTR trp1::TRP1/trp1::TRP1*
35987	*MAT**a**/alpha whi5::WHI5-mcherry-linker-FRB::KanMX/whi5::WHI5-mcherry-linker-FRB::KanMX tor1-1::HIS3/tor1-1::HIS3 fpr1::KanMX/fpr1::KanMX HTB1-mCherry-HISMX6/HTB1-mCherry-HISMX6 REC8-GFP-URA3/REC8-GFP-URA3 swi4::KanMX/swi4::KanMX leu2::LEU2::pSWI4(-1200 to -1)-SWI4-3V5-3'UTR/leu2::LEU2::pSWI4(-1200 to -1)-SWI4-3V5-3'UTR trp1::TRP1/trp1::TRP1*
35989	*MAT**a**/alpha swi4::KanMX/swi4::KanMX leu2::LEU2::pSWI4LUTI(-1200 to -934)Δ-SWI4-3V5-SWI4_3'UTR/leu2::LEU2::pSWI4LUTI(-1200 to -934)Δ-SWI4-3V5-SWI4_3'UTR whi5::WHI5-mcherry-linker-FRB::KanMX/whi5::WHI5-mcherry-linker-FRB::KanMX fpr1::KanMX/fpr1::KanMX tor1-1::HIS3/tor1-1::HIS3 HTB1-mCherry-HISMX6/HTB1-mCherry-HISMX6 REC8-GFP-URA3 /REC8-GFP-URA3 trp1::TRP1/trp1::TRP1*
35991	*MAT**a**/alpha whi5::WHI5-mcherry-linker-FRB::KanMX whi5::WHI5-mcherry-linker-FRB::KanMX RPL13a-2xFKBP12::TRP1/RPL13a-2xFKBP12::TRP1 fpr1::KanMX/fpr1::KanMX tor1-1::HIS3/tor1-1::HIS3 HTB1-mCherry-HISMX6/HTB1-mCherry-HISMX6 REC8-GFP-URA3/REC8-GFP-URA3 swi4::KanMX/swi4::KanMX leu2::LEU2::pSWI4(-1200 to -1)-SWI4-3V5-3'UTR/leu2::LEU2::pSWI4(-1200 to -1)-SWI4-3V5-3'UTR*
36535	*MATa trp1::pGPD1-LexA-ER-HA-B112::TRP1 swi4::KanMX leu2::LEU2::pSWI4(-1200 to -1)-SWI4-3V5-3'UTR*

Table 6.2 Plasmids

Plasmid Number	Plasmid Info
pUB595	pFA6a-FRB-KanMX6
pUB1585	LEU2-pATG8-SWI4-linker-3V5
pUB1587	LEU2-pSWI4(-1200 to -1)-SWI4-3V5-3′UTR
pUB1588	LEU2-pSWI4(-1200 to -934)Δ-SWI4-3V5-3′UTR (LUTIΔ)
pUB1734	LEU2-pSWI4(ATG>ATC mutant)-SWI4-3V5-3'UTR (uORFΔ)
pUB1899	HIS3-pATG8-CLN2-linker-3V5
pUB2144	TRP1-pATG8-CLN1-linker-3V5

Table 6.3 Primers

Primer Name	Sequence from 5′ to 3′
6852_CLN2_F	TCGTGTTACGGGACCAAGCC
6853_CLN2_R	TACGTGCCCTTGGGTTGGGA
6887_CLN1_F	ACGTCTCCATCCCCACAGGT
6888_CLN1_R	CGGACCCGCCGCAATAATGA
3301_PFY1_F	ACGGTAGACATGATGCTGAGG
3302_PFY1_R	ACGGTTGGTGGATAATGAGC

2081_IME1_F	TCACCACCGCCATCACTACA
2082_IME1_R	TGAAGGAGTAAGCCGCAGCA
6854_CDC21_F	TTGGCCGGTGATACAGACGC
6855_CDC21_R	ACGGGCCCCAGATCTCCTAC
6858_RNR1_F	ACCCTAGCGGCCAGAATTGC
6859_RNR1_R	CATGGGAGCGGGCTTACCAG
2598_ACT1_F	GTACCACCATGTTCCCAGGTATT
2599_ACT1_R	AGATGGACCACTTTCGTCGT
5429_SWI4LUTI_F	ACAAGGACTAAGAAGCACGTCA
5430_SWI4LUTI_R	ACCAATGCTAAAGGATGGCA
5918_3V5_probe_F	CTAGTGGATCCAGGTAAACCTAT
2921_3V5_probe_R	TAATACGACTCACTATAGGCCAGTCCTAATAGAGGATTAGG

Table 6.4 Image acquisition settings

Genotype	GFP	RFP	DAPI	POL
GFP-Ime1; Htb1-mCherry	50% T, 0.1s EX: 475/28 EM: 523/36	32% T, 0.05s EX: 575/25 EM: 632/60	N/A	32% T, 0.1s
GFP-Ime1; Swi4-mCherry	50% T, 0.1s EX: 475/28 EM: 523/36	50% T, 0.05s EX: 575/25 EM: 632/60	32% T, 0.05s EX: 390/18 EM: 435/48	32% t, 0.1s
GFP-Ime1; Whi5-mCherry	50% T, 0.1s EX: 475/28 EM: 523/36	100% T, 0.08s EX: 575/25 EM: 632/60	32% T, 0.05s EX: 390/18 EM: 435/48	32% T, 0.1s
Rec8-GFP; Htb1-mCherry	10% T, 0.025s EX: 475/28 EM: 523/36	10% T, 0.025s EX: 575/25 EM: 632/60	N/A	32% t, 0.1s

References

Abeliovich, H., and D.J. Klionsky. 2001. Autophagy in Yeast: Mechanistic Insights and Physiological Function. *Microbiol. Mol. Biol. Rev.* 65:463–479. doi:10.1128/mmbr.65.3.463-479.2001.

Amon, A., M. Tyers, B. Futcher, and K. Nasmyth. 1993. Mechanisms that help the yeast cell cycle clock tick: G2 cyclins transcriptionally activate G2 cyclins and repress G1 cyclins. *Cell*. 74:993–1007. doi:10.1016/0092-8674(93)90722-3.

Andrews, B.J., and I. Herskowitz. 1989. The yeast SWI4 protein contains a motif present in developmental regulators and is part of a complex involved in cell-cycle-dependent transcription. *Nature*. 342:830–833. doi:10.1038/342830a0.

Andrews, S.J., and J.A. Rothnagel. 2014. Emerging evidence for functional peptides encoded by short open reading frames. *Nat. Rev. Genet.* 15:193–204. doi:10.1038/nrg3520.

Argüello-Miranda, O., Y. Liu, N.E. Wood, P. Kositangool, and A. Doncic. 2018. Integration of Multiple Metabolic Signals Determines Cell Fate Prior to Commitment. *Mol. Cell*. 71:733-744.e11. doi:10.1016/j.molcel.2018.07.041.

Ashe, M., R.A.M. De Bruin, T. Kalashnikova, W.H. McDonald, J.R. Yates, and C. Wittenberg. 2008. The SBF- and MBF-associated protein Msa1 is required for proper timing of G1-specific transcription in Saccharomyces cerevisiae. *J. Biol. Chem.* 283:6040–6049. doi:10.1074/jbc.M708248200.

Attwooll, C., E.L. Denchi, and K. Helin. 2004. The E2F family: Specific functions and overlapping interests. *EMBO J.* 23:4709–4716. doi:10.1038/sj.emboj.7600481.

Bähler, J., J.Q. Wu, M.S. Longtine, N.G. Shah, A. McKenzie, A.B. Steever, A. Wach, P. Philippsen, and J.R. Pringle. 1998. Heterologous modules for efficient and versatile PCR-based gene targeting in Schizosaccharomyces pombe. *Yeast*. 14:943–951. doi:10.1002/(SICI)1097-0061(199807)14:10<943::AID-YEA292>3.0.CO;2-Y.

Bean, J.M., E.D. Siggia, and F.R. Cross. 2005. High functional overlap between MluI cell-cycle box binding factor and Swi4/6 cell-cycle box binding factor in the G1/S transcriptional program in Saccharomyces cerevisiae. *Genetics*. 171:49–61. doi:10.1534/genetics.105.044560.

Berchowitz, L.E., A.S. Gajadhar, F.J. van Werven, A.A. De Rosa, M.L. Samoylova, G.A. Brar, Y. Xu, C. Xiao, B. Futcher, J.S. Weissman, F.M. White, and A. Amon. 2013. A developmentally regulated translational control pathway establishes the meiotic chromosome segregation pattern. *Genes Dev.* 27:2147–2163. doi:10.1101/gad.224253.113.

Bertoli, C., J.M. Skotheim, and R.A.M. De Bruin. 2013. Control of cell cycle transcription during G1 and S phases. *Nat. Rev. Mol. Cell Biol.* 14:518–528. doi:10.1038/nrm3629.

Bloom, J., and F.R. Cross. 2007. Multiple levels of cyclin specificity in cell-cycle control. *Nat. Rev. Mol. Cell Biol.* 8:149–160. doi:10.1038/nrm2105.

Bowdish, K.S., H.E. Yuan, and A.P. Mitchell. 1994. Analysis of RIM11, a yeast protein kinase that phosphorylates the meiotic activator IME1. *Mol. Cell. Biol.* 14:7909–7919. doi:10.1128/mcb.14.12.7909-7919.1994.

Bowdish, K.S., H.E. Yuan, and A.P. Mitchell. 1995. Positive control of yeast meiotic genes by the negative regulator UME6. *Mol. Cell. Biol.* 15:2955–2961.

doi:10.1128/mcb.15.6.2955.
Brar, G.A., M. Yassour, N. Friedman, A. Regev, N.T. Ingolia, and J.S. Weissman. 2012. High-Resolution View of the Yeast Meiotic Program Revealed by Ribosome Profiling. *Science (80-.).* 335:552–558. doi:10.1126/science.1215110.
Breitkreutz, A., H. Choi, J.R. Sharom, L. Boucher, V. Neduva, B. Larsen, Z.Y. Lin, B.J. Breitkreutz, C. Stark, G. Liu, J. Ahn, D. Dewar-Darch, T. Reguly, X. Tang, R. Almeida, Z.S. Qin, T. Pawson, A.C. Gingras, A.I. Nesvizhskii, and M. Tyers. 2010. A global protein kinase and phosphatase interaction network in yeast. *Science (80-.).* 328:1043–1046. doi:10.1126/science.1176495.
De Bruin, R.A.M., W.H. McDonald, T.I. Kalashnikova, J. Yates, and C. Wittenberg. 2004. Cln3 activates G1-specific transcription via phosphorylation of the SBF bound repressor Whi5. *Cell*. 117:887–898. doi:10.1016/j.cell.2004.05.025.
Brush, G.S., N.A. Najor, A.A. Dombkowski, D. Cukovic, and K.E. Sawarynski. 2012. Yeast ime2 functions early in meiosis upstream of cell cycle-regulated sbf and mbf targets. *PLoS One*. 7:1–12. doi:10.1371/journal.pone.0031575.
Carlile, T.M., and A. Amon. 2008. Meiosis I Is Established through Division-Specific Translational Control of a Cyclin. *Cell*. 133:280–291. doi:10.1016/j.cell.2008.02.032.
Carrozza, M.J., B. Li, L. Florens, T. Suganuma, S.K. Swanson, K.K. Lee, W.J. Shia, S. Anderson, J. Yates, M.P. Washburn, and J.L. Workman. 2005. Histone H3 methylation by Set2 directs deacetylation of coding regions by Rpd3S to suppress spurious intragenic transcription. *Cell*. 123:581–592. doi:10.1016/j.cell.2005.10.023.
Chen, J., D. Mcswiggen, and E. Ünal. 2018. Single Molecule Fluorescence In Situ Hybridization (smFISH) Analysis in Budding Yeast Vegetative Growth and Meiosis. 1–14. doi:10.3791/57774.
Chen, J., A. Tresenrider, M. Chia, D.T. McSwiggen, G. Spedale, V. Jorgensen, H. Liao, F.J. Van Werven, and E. Ünal. 2017. Kinetochore inactivation by expression of a repressive mRNA. *Elife*. 6:1–31. doi:10.7554/eLife.27417.
Cheng, Z., G.M. Otto, E.N. Powers, A. Keskin, P. Mertins, S.A. Carr, M. Jovanovic, and G.A. Brar. 2018. Pervasive, Coordinated Protein-Level Changes Driven by Transcript Isoform Switching during Meiosis. *Cell*. 172:910-923.e16. doi:10.1016/j.cell.2018.01.035.
Chia, M., C. Li, S. Marques, V. Pelechano, N.M. Luscombe, and F.J. van Werven. 2021. Author Correction: High-resolution analysis of cell-state transitions in yeast suggests widespread transcriptional tuning by alternative starts (Genome Biology, (2021), 22, 1, (34), 10.1186/s13059-020-02245-3). *Genome Biol.* 22:1–37. doi:10.1186/s13059-021-02274-6.
Chia, M., A. Tresenrider, J. Chen, G. Spedale, V. Jorgensen, E. Ünal, and F.J. van Werven. 2017. Transcription of a 5' extended mRNA isoform directs dynamic chromatin changes and interference of a downstream promoter. *Elife*. 6:1–23. doi:10.7554/eLife.27420.
Chia, M., and F.J. van Werven. 2016. Temporal Expression of a Master Regulator Drives Synchronous Sporulation in Budding Yeast. *G3: Genes|Genomes|Genetics*. 6:3553–3560. doi:10.1534/g3.116.034983.
Chu, S., J. DeRisi, M. Eisen, J. Mulholland, D. Botstein, P.O. Brown, and I. Herskowitz. 1998. The transcriptional program of sporulation in budding yeast. *Science (80-.).*

282:699–705. doi:10.1126/science.282.5389.699.
Colomina, N., E. Garí, C. Gallego, E. Herrero, and M. Aldea. 1999. G1cyclins block the Ime1 pathway to make mitosis and meiosis incompatible in budding yeast. *EMBO J.* 18:320–329. doi:10.1093/emboj/18.2.320.
Colomina, N., Y. Liu, M. Aldea, and E. Garí. 2003. TOR Regulates the Subcellular Localization of Ime1, a Transcriptional Activator of Meiotic Development in Budding Yeast. *Mol. Cell. Biol.* 23:7415–7424. doi:10.1128/mcb.23.20.7415-7424.2003.
Costanzo, M., J.L. Nishikawa, X. Tang, J.S. Millman, O. Schub, K. Breitkreuz, D. Dewar, I. Rupes, B. Andrews, and M. Tyers. 2004. CDK activity antagonizes Whi5, an inhibitor of G1/S transcription in yeast. *Cell*. 117:899–913. doi:10.1016/j.cell.2004.05.024.
Covitz, P.A., I. Herskowitz, and A.P. Mitchell. 1991. The yeast RME1 gene encodes a putative zinc finger protein that is directly repressed by a1-α2. *Genes Dev.* 5:1982–1989. doi:10.1101/gad.5.11.1982.
Van Dalfsen, K.M., S. Hodapp, A. Keskin, G.M. Otto, C.A. Berdan, A. Higdon, T. Cheunkarndee, D.K. Nomura, M. Jovanovic, and G.A. Brar. 2018. Global Proteome Remodeling during ER Stress Involves Hac1-Driven Expression of Long Undecoded Transcript Isoforms. *Dev. Cell*. 46:219-235.e8. doi:10.1016/j.devcel.2018.06.016.
Dirick, L., L. Goetsch, G. Ammerer, and B. Byers. 1998. Regulation of Meiotic S Phase by Ime2 and a Clb5 , 6-Associated Kinase in Saccharomyces cerevisiae. 281:1854–1858.
Doncic, A., M. Falleur-Fettig, and J.M. Skotheim. 2011. Distinct Interactions Select and Maintain a Specific Cell Fate. *Mol. Cell*. 43:528–539. doi:10.1016/j.molcel.2011.06.025.
Dorsey, S., S. Tollis, J. Cheng, L. Black, S. Notley, M. Tyers, and C.A. Royer. 2018. G1/S Transcription Factor Copy Number Is a Growth-Dependent Determinant of Cell Cycle Commitment in Yeast. *Cell Syst.* 6:539-554.e11. doi:10.1016/j.cels.2018.04.012.
Eisenberg, A.R., A.L. Higdon, I. Hollerer, A.P. Fields, I. Jungreis, P.D. Diamond, M. Kellis, M. Jovanovic, and G.A. Brar. 2020. Translation Initiation Site Profiling Reveals Widespread Synthesis of Non-AUG-Initiated Protein Isoforms in Yeast. *Cell Syst.* 11:145-160.e5. doi:10.1016/j.cels.2020.06.011.
Eser, U., M. Falleur-Fettig, A. Johnson, and J.M. Skotheim. 2011. Commitment to a Cellular Transition Precedes Genome-wide Transcriptional Change. *Mol. Cell*. 43:515–527. doi:10.1016/j.molcel.2011.06.024.
Espinoza, F.H., J. Ogas, I. Herskowitz, and D. Morgant. 2016. Cell Cycle Control by a Complex of the Cyclin HCS26 (PCL1) and the Kinase PHO85 Author (s): F . Hernan Espinoza , Joseph Ogas , Ira Herskowitz and David O . Morgan Published by : American Association for the Advancement of Science Stable URL : http://. 266:1388–1391.
Ferrezuelo, F., N. Colomina, B. Futcher, and M. Aldea. 2010. The transcriptional network activated by Cln3 cyclin at the G1-to-S transition of the yeast cell cycle. *Genome Biol.* 11. doi:10.1186/gb-2010-11-6-r67.
Fridy, P.C., Y. Li, S. Keegan, M.K. Thompson, I. Nudelman, J.F. Scheid, M. Oeffinger, M.C. Nussenzweig, D. Fenyö, B.T. Chait, and M.P. Rout. 2014. A robust pipeline

for rapid production of versatile nanobody repertoires. *Nat. Methods*. 11:1253–1260. doi:10.1038/nmeth.3170.
Gallego, C., E. Garí, N. Colomina, E. Herrero, and M. Aldea. 1997. The Cln3 cyclin is down-regulated by translational repression and degradation during the G1 arrest caused by nitrogen deprivation in budding yeast. *EMBO J.* 16:7196–7206. doi:10.1093/emboj/16.23.7196.
Gaubatz, S., G.J. Lindeman, S. Ishida, L. Jakoi, J.R. Nevins, D.M. Livingston, and R.E. Rempel. 2000. E2F4 and E2F5 play an essential role in pocket protein-mediated G1 control. *Mol. Cell*. 6:729–735. doi:10.1016/S1097-2765(00)00071-X.
Gibson, D.G., L. Young, R.Y. Chuang, J.C. Venter, C.A. Hutchison, and H.O. Smith. 2009. Enzymatic assembly of DNA molecules up to several hundred kilobases. *Nat. Methods*. 6:343–345. doi:10.1038/nmeth.1318.
Goldmark, J.P., T.G. Fazzio, P.W. Estep, G.M. Church, and T. Tsukiyama. 2000. The Isw2 chromatin remodeling complex represses early meiotic genes upon recruitment by Ume6p. *Cell*. 103:423–433. doi:10.1016/S0092-8674(00)00134-3.
Görner, W., E. Durchschlag, M.T. Martinez-Pastor, F. Estruch, G. Ammerer, B. Hamilton, H. Ruis, and C. Schüller. 1998. Nuclear localization of the C2H2 zinc finger protein Msn2p is regulated by stress and protein kinase A activity. *Genes Dev.* 12:586–597. doi:10.1101/gad.12.4.586.
Gullerova, M., and N.J. Proudfoot. 2010. Transcriptional interference and gene orientation in yeast: Noncoding RNA connections. *Cold Spring Harb. Symp. Quant. Biol.* 75:299–311. doi:10.1101/sqb.2010.75.048.
Guttmann-Raviv, N., S. Martin, and Y. Kassir. 2002. Ime2, a Meiosis-Specific Kinase in Yeast, Is Required for Destabilization of Its Transcriptional Activator, Ime1. *Mol. Cell. Biol.* 22:2047–2056. doi:10.1128/mcb.22.7.2047-2056.2002.
Handel, M.A., and J.C. Schimenti. 2010. Genetics of mammalian meiosis: Regulation, dynamics and impact on fertility. *Nat. Rev. Genet.* 11:124–136. doi:10.1038/nrg2723.
Harris, M.R., D. Lee, S. Farmer, N.F. Lowndes, and R.A.M. de Bruin. 2013. Binding Specificity of the G1/S Transcriptional Regulators in Budding Yeast. *PLoS One*. 8:1–7. doi:10.1371/journal.pone.0061059.
Hartwell, L.H., J. Culotti, J.R. Pringle, and B.J. Reid. 1974. Genetic control of the cell division cycle in yeast. *Science*. 183:46–51. doi:10.1126/SCIENCE.183.4120.46.
Haruki, H., J. Nishikawa, and U.K. Laemmli. 2008. The Anchor-Away Technique: Rapid, Conditional Establishment of Yeast Mutant Phenotypes. *Mol. Cell*. 31:925–932. doi:10.1016/j.molcel.2008.07.020.
Hasan, M., S. Brocca, E. Sacco, M. Spinelli, P. Elena, L. Matteo, A. Lilia, and M. Vanoni. 2014. A comparative study of Whi5 and retinoblastoma proteins : from sequence and structure analysis to intracellular networks. 4:1–24. doi:10.3389/fphys.2013.00315.
Hassold T, and Hunt P. 2001. To err (meiotically) is human: the genesis of human aneuploidy. *Nat. Rev. Genet.* 2:280–91.
Van Den Heuvel, S., and N.J. Dyson. 2008. Conserved functions of the pRB and E2F families. *Nat. Rev. Mol. Cell Biol.* 9:713–724. doi:10.1038/nrm2469.
Higdon, A.L., and G.A. Brar. 2021. Rules are made to be broken: a “simple” model organism reveals the complexity of gene regulation. *Curr. Genet.* 67:49–56.

doi:https://doi.org/10.1007/s00294-020-01121-8.
Hollerer, I., J.C. Barker, V. Jorgensen, A. Tresenrider, C. Dugast-Darzacq, L.Y. Chan, X. Darzacq, R. Tjian, E. Ünal, and G.A. Brar. 2019. Evidence for an integrated gene repression mechanism based on mRNA isoform toggling in human cells. *G3 Genes, Genomes, Genet.* 9:1045–1053. doi:10.1534/g3.118.200802.
Holt, L., B. Tuch, J. Villén, A. Johnson, S. Gygi, and D. Morgan. 2009. Global analysis of Cdk1 substrate phosphorylation sites provides insights into evolution. *Science (80-.).* 325:1682–1686.
Hongay, C.F., P.L. Grisafi, T. Galitski, and G.R. Fink. 2006. Antisense Transcription Controls Cell Fate in Saccharomyces cerevisiae. *Cell*. 127:735–745. doi:10.1016/j.cell.2006.09.038.
Honigberg, S.M. 2003. Signal pathway integration in the switch from the mitotic cell cycle to meiosis in yeast. *J. Cell Sci.* 116:2137–2147. doi:10.1242/jcs.00460.
Honigberg, S.M. 2004. Ime2p and Cdc28p: Co-pilots driving meiotic development. *J. Cell. Biochem.* 92:1025–1033. doi:10.1002/jcb.20131.
Iyer, V.R., C.E. Horak, P.O. Brown, D. Botstein, V.R. Iyer, M. Snyder, and C.S. Scafe. 2001. Genomic binding sites of the yeast cell-cycle transcription factors SBF and MBF. *Nature*. 409:533–538. doi:10.1038/35054095.
Johnston, G.C., J.R. Pringle, and L.H. Hartwell. 1977. Coordination of Growth With Cell Division. *Exp. Cell Res.* 105:79–98.
Johnstone, T.G., A.A. Bazzini, and A.J. Giraldez. 2016. Upstream ORF s are prevalent translational repressors in vertebrates . *EMBO J.* 35:706–723. doi:10.15252/embj.201592759.
Jorgensen, P., and M. Tyers. 2004. How cells coordinate growth and division. *Curr. Biol.* 14:1014–1027. doi:10.1016/j.cub.2004.11.027.
Jorgensen, V., J. Chen, H. Vander Wende, D.E. Harris, A. McCarthy, S. Breznak, S.W. Wong-Deyrup, Y. Chen, P. Rangan, G.A. Brar, E.M. Sawyer, L.Y. Chan, and E. Ünal. 2020. Tunable transcriptional interference at the endogenous alcohol dehydrogenase gene locus in Drosophila melanogaster. *G3 Genes, Genomes, Genet.* 10:1575–1583. doi:10.1534/g3.119.400937.
Julian, L.M., Y. Liu, C.A. Pakenham, D. Dugal-Tessier, V. Ruzhynsky, S. Bae, S.Y. Tsai, G. Leone, R.S. Slack, and A. Blais. 2016. Tissue-specific targeting of cell fate regulatory genes by E2f factors. *Cell Death Differ.* 23:565–575. doi:10.1038/cdd.2015.36.
Kadosh, D., and K. Struhl. 1997. Repression by Ume6 involves recruitment of a complex containing Sin3 corepressor and Rpd3 histone deacetylase to target promoters. *Cell*. 89:365–371. doi:10.1016/S0092-8674(00)80217-2.
Kassir, Y., D. Granot, and G. Simchen. 1988a. IME1, a positive regulator gene of meiosis in S. cerevisiae. *Cell*. 52:853–862. doi:10.1016/0092-8674(88)90427-8.
Kassir, Y., D. Granot, and G. Simchen. 1988b. IME1, a positive regulator gene of meiosis in S. cerevisiae. *Cell*. 52:853–862. doi:10.1016/0092-8674(88)90427-8.
Kearse, M.G., and J.E. Wilusz. 2017. Non-AUG translation: A new start for protein synthesis in eukaryotes. *Genes Dev.* 31:1717–1731. doi:10.1101/gad.305250.117.
Keeney, S., J. Lange, and N. Mohibullah. 2014. Self-organization of meiotic recombination initiation: General principles and molecular pathways. *Annu. Rev. Genet.* 48:187–214. doi:10.1146/annurev-genet-120213-092304.

Kelliher, C.M., M.W. Foster, F.C. Motta, A. Deckard, E.J. Soderblom, M.A. Moseley, and S.B. Haase. 2018. Layers of regulation on cell-cycle gene expression in the budding yeast *Saccharomyces cerevisiae*. *Mol. Biol. Cell*. mbc.E18-04-0255. doi:10.1091/mbc.E18-04-0255.

Keogh, M.C., S.K. Kurdistani, S.A. Morris, S.H. Ahn, V. Podolny, S.R. Collins, M. Schuldiner, K. Chin, T. Punna, N.J. Thompson, C. Boone, A. Emili, J.S. Weissman, T.R. Hughes, B.D. Strahl, M. Grunstein, J.F. Greenblatt, S. Buratowski, and N.J. Krogan. 2005. Cotranscriptional set2 methylation of histone H3 lysine 36 recruits a repressive Rpd3 complex. *Cell*. 123:593–605. doi:10.1016/j.cell.2005.10.025.

Kim, D., J.M. Paggi, C. Park, C. Bennett, and S.L. Salzberg. 2019. Graph-based genome alignment and genotyping with HISAT2 and HISAT-genotype. *Nat. Biotechnol.* 37:907–915. doi:10.1038/s41587-019-0201-4.

Kim Guisbert, K.S., Y. Zhang, J. Flatow, S. Hurtado, J.P. Staley, S. Lin, and E.J. Sontheimer. 2012. Meiosis-induced alterations in transcript architecture and noncoding RNA expression in S. cerevisiae. *Rna*. 18:1142–1153. doi:10.1261/rna.030510.111.

Koch, C., A. Schleiffer, A. Gustav, and K. Nasmyth. 1996. Switching transcription on and off during the yeast cell cycle : Cln / Cdc28 kmases activate bound transcription factor SBF (Swi4 / Swi6) at Start , whereas Clb / Cdc28 kinases displace it from the promoter in G 2. *Genes Dev*. 10:129–141. doi:10.1101/gad.10.2.129.

Kõivomägi, M., M.P. Swaffer, J.J. Turner, G. Marinov, and J.M. Skotheim. 2021. G1 cyclin-Cdk promotes cell cycle entry through localized phosphorylation of RNA polymerase II. *Science (80-.).* 374:347–351. doi:10.1126/science.aba5186.

Lardenois, A., Y. Liu, T. Walther, F. Chalmel, B. Evrard, M. Granovskaia, A. Chu, R.W. Davis, L.M. Steinmetz, and M. Primig. 2011. Execution of the meiotic noncoding RNA expression program and the onset of gametogenesis in yeast require the conserved exosome subunit Rrp6. *Proc. Natl. Acad. Sci. USA*. 108:1058–1063. doi:10.1073/pnas.1016459108.

Li, B., M. Carey, and J.L. Workman. 2007. The Role of Chromatin during Transcription. *Cell*. 128:707–719. doi:10.1016/j.cell.2007.01.015.

Love, M.I., W. Huber, and S. Anders. 2014. Moderated estimation of fold change and dispersion for RNA-seq data with DESeq2. *Genome Biol.* 15:1–21. doi:10.1186/s13059-014-0550-8.

Mai, B., and L. Breeden. 2002. CLN1 and Its Repression by Xbp1 Are Important for Efficient Sporulation in Budding Yeast. *Mol. Cell. Biol.* 20:478–487. doi:10.1128/mcb.20.2.478-487.2000.

Malathi, K., Y. Xiao, and A.P. Mitchell. 1997. Interaction of yeast repressor-activator protein Ume6p with glycogen synthase kinase 3 homolog Rim11p. *Mol. Cell. Biol.* 17:7230–7236. doi:10.1128/mcb.17.12.7230.

Malathi, K., Y. Xiao, and A.P. Mitchell. 1999. Catalytic roles of yeast GSK3β/shaggy homolog Rim11p in meiotic activation. *Genetics*. 153:1145–1152. doi:10.1093/genetics/153.3.1145.

Martínez-Pastor, M.T., G. Marchler, C. Schüller, A. Marchler-Bauer, H. Ruis, and F. Estruch. 1996. The Saccharomyces cerevisiae zinc finger proteins Msn2p and Msn4p are required for transcriptional induction through the stress-response element (STRE). *EMBO J.* 15:2227–2235. doi:10.1002/j.1460-

2075.1996.tb00576.x.
McCord, R., M. Pierce, J. Xie, S. Wonkatal, C. Mickel, and A.K. Vershon. 2003. Rfm1, a Novel Tethering Factor Required To Recruit the Hst1 Histone Deacetylase for Repression of Middle Sporulation Genes. *Mol. Cell. Biol.* 23:2009–2016. doi:10.1128/mcb.23.6.2009-2016.2003.
Mcinerny, C.J., J.F. Partridge, G.E. Mikesell, D.P. Creemer, and L.L. Breeden. 1997. A novel Mcml-dependent element in the WI4 , CLN3 , CDC6 , and CDC4S7 promoters activates M / Gi-specific transcription. *Genes Dev.* 1277–1288. doi:10.1101/gad.11.10.1277.
Miles, S., and L. Breeden. 2017. A common strategy for initiating the transition from proliferation to quiescence. *Curr. Genet.* 63:179–186. doi:10.1007/s00294-016-0640-0.
Miles, S., M.W. Croxford, A.P. Abeysinghe, and L.L. Breeden. 2016. Msa1 and Msa2 Modulate G1-Specific Transcription to Promote G1 Arrest and the Transition to Quiescence in Budding Yeast. *PLoS Genet.* 12:1–27. doi:10.1371/journal.pgen.1006088.
Miller, M.P., E. Ünal, G.A. Brar, and A. Amon. 2012. Meiosis I chromosome segregation is established through regulation of microtubule-kinetochore interactions. *Elife*. 2012:1–30. doi:10.7554/eLife.00117.
Mizuno, T., N. Nakazawa, P. Remgsamrarn, T. Kunoh, Y. Oshima, and S. Harashima. 1998. The Tup1-Ssn6 general repressor is involved in repression of IME1 encoding a transcriptional activator of meiosis in Saccharomyces cerevisiae. *Curr. Genet.* 33:239–247. doi:10.1007/s002940050332.
Moreno-Torres, M., M. Jaquenoud, M.P. Péli-Gulli, R. Nicastro, and C. De Virgilio. 2017. TORC1 coordinates the conversion of Sic1 from a target to an inhibitor of cyclin-CDK-Cks1. *Cell Discov.* 3:1–12. doi:10.1038/celldisc.2017.12.
Moretto, F., N.E. Wood, G. Kelly, A. Doncic, and F.J. Van Werven. 2018. A regulatory circuit of two lncRNAs and a master regulator directs cell fate in yeast. *Nat. Commun.* 9. doi:10.1038/s41467-018-03213-z.
Moses, A.M., J.K. Hériché, and R. Durbin. 2007. Clustering of phosphorylation site recognition motifs can be exploited to predict the targets of cyclin-dependent kinase. *Genome Biol.* 8. doi:10.1186/gb-2007-8-2-r23.
Nardozzi, J.D., K. Lott, and G. Cingolani. 2010. Phosphorylation meets nuclear import: A review. *Cell Commun. Signal.* 8:32. doi:10.1186/1478-811X-8-32.
Neiman, A.M. 2011. Sporulation in the budding yeast Saccharomyces cerevisiae. *Genetics*. 189:737–765. doi:10.1534/genetics.111.127126.
Ottoz, D.S.M., F. Rudolf, and J. Stelling. 2014. Inducible, tightly regulated and growth condition-independent transcription factor in Saccharomyces cerevisiae. *Nucleic Acids Res.* 42. doi:10.1093/nar/gku616.
Pak, J., and J. Segall. 2002. Regulation of the Premiddle and Middle Phases of Expression of the. *Society*. 22:6417–6429. doi:10.1128/MCB.22.18.6417.
Parviz, F., and W. Heideman. 1998. Growth-independent regulation of CLN3 mRNA levels by nutrients in Saccharomyces cerevisiae. *J. Bacteriol.* 180:225–230. doi:10.1128/jb.180.2.225-230.1998.
Pedruzzi, I., F. Dubouloz, E. Cameroni, V. Wanke, J. Roosen, J. Winderickx, and C. De Virgilio. 2003. TOR and PKA Signaling Pathways Converge on the Protein Kinase

Rim15 to Control Entry into G0. *Mol. Cell*. 12:1607–1613. doi:10.1016/S1097-2765(03)00485-4.
Pertea, M., G.M. Pertea, C.M. Antonescu, T.C. Chang, J.T. Mendell, and S.L. Salzberg. 2015. StringTie enables improved reconstruction of a transcriptome from RNA-seq reads. *Nat. Biotechnol.* 33:290–295. doi:10.1038/nbt.3122.
Pnueli, L., I. Edry, M. Cohen, and Y. Kassir. 2004. Glucose and Nitrogen Regulate the Switch from Histone Deacetylation to Acetylation for Expression of Early Meiosis-Specific Genes in Budding Yeast. *Mol. Cell. Biol.* 24:5197–5208. doi:10.1128/mcb.24.12.5197-5208.2004.
Raj, A., P. van den Bogaard, S.A. Rifkin, A. van Oudenaarden, and S. Tyagi. 2008. Imaging individual mRNA molecules using multiple singly labeled probes. *Nat. Methods*. 5:877–879. doi:10.1038/nmeth.1253.
Rubin-Bejerano, I., S. Mandel, K. Robzyk, and Y. Kassir. 1996. Induction of meiosis in Saccharomyces cerevisiae depends on conversion of the transcriptional represssor Ume6 to a positive regulator by its regulated association with the transcriptional activator Ime1. *Mol. Cell. Biol.* 16:2518–2526. doi:10.1128/mcb.16.5.2518.
Rubin-Bejerano, I., S. Sagee, O. Friedman, L. Pnueli, and Y. Kassir. 2004. The In Vivo Activity of Ime1, the Key Transcriptional Activator of Meiosis-Specific Genes in Saccharomyces cerevisiae, Is Inhibited by the Cyclic AMP/Protein Kinase A Signal Pathway through the Glycogen Synthase Kinase 3- Homolog Rim11. *Mol. Cell. Biol.* 24:6967–6979. doi:10.1128/mcb.24.16.6967-6979.2004.
Rundlett E., S., A. Carmen A., N. Suka, B. Turner M., and M. Grunstein. 2003. Transcriptional repression byUME6 involves deacetylationof lysine5 of histoneH4byRPD3. *Nature*. 426:181–186.
Sagee, S., A. Sherman, G. Shenhar, K. Robzyk, N. Ben-Doy, G. Simchen, and Y. Kassir. 1998. Multiple and Distinct Activation and Repression Sequences Mediate the Regulated Transcription of IME1 , a Transcriptional Activator of Meiosis-Specific Genes in Saccharomyces cerevisiae . *Mol. Cell. Biol.* 18:1985–1995. doi:10.1128/mcb.18.4.1985.
Schindelin, J., I. Arganda-Carreras, E. Frise, V. Kaynig, M. Longair, T. Pietzsch, S. Preibisch, C. Rueden, S. Saalfeld, B. Schmid, J.Y. Tinevez, D.J. White, V. Hartenstein, K. Eliceiri, P. Tomancak, and A. Cardona. 2012. Fiji: An open-source platform for biological-image analysis. *Nat. Methods*. 9:676–682. doi:10.1038/nmeth.2019.
Schmoller, K.M., J.J. Turner, M. Kõivomägi, and J.M. Skotheim. 2015. Dilution of the cell cycle inhibitor Whi5 controls budding-yeast cell size. *Nature*. 526:268–272. doi:10.1038/nature14908.
Shin, M.E., A. Skokotas, and E. Winter. 2010. The Cdk1 and Ime2 Protein Kinases Trigger Exit from Meiotic Prophase in Saccharomyces cerevisiae by Inhibiting the Sum1 Transcriptional Repressor . *Mol. Cell. Biol.* 30:2996–3003. doi:10.1128/mcb.01682-09.
Sidorova, J.M., and L.L. Breeden. 2002. Precocious S-phase entry in budding yeast prolongs replicative state and increases dependence upon Rad53 for viability. *Genetics*. 160:123–136.
Siegmund, R.F., and K.A. Nasmyth. 1996. The Saccharomyces cerevisiae Start-Specific Transcription Factor Swi4 Interacts through the Ankyrin Repeats with the

Mitotic Clb2/Cdc28 Kinase and through Its Conserved Carboxy Terminus with Swi6. *Mol. Cell. Biol.* 16:2647–2655. doi:10.1128/MCB.16.6.2647.
Simon, I., J. Barnett, N. Hannett, C.T. Harbison, N.J. Rinaldi, T.L. Volkert, J.J. Wyrick, J. Zeitlinger, D.K. Gifford, T.S. Jaakkola, and R.A. Young. 2001. Serial Regulation of Transcriptional Regulators in the Yeast Cell Cycle. 106:697–708.
Sing, T.L., G.A. Brar, and E. Ünal. 2022. Gametogenesis: Exploring an Endogenous Rejuvenation Program to Understand Cellular Aging and Quality Control. *Annu. Rev. Genet.* 56:89–112. doi:10.1146/annurev-genet-080320-025104.
Smith, A., M.P. Ward, and S. Garrett. 1998. Yeast PKA represses Msn2p/Msn4p-dependent gene expression to regulate growth, stress response and glycogen accumulation. *EMBO J.* 17:3556–3564. doi:10.1093/emboj/17.13.3556.
Smith, H.E., S.E. Driscoll, R.A.L. Sia, H.E. Yuan, and A.P. Mitchell. 1993. Genetic evidence for transcriptional activation by the yeast IME1 gene product. *Genetics*. 133:775–784. doi:10.1093/genetics/133.4.775.
Smolka, M.B., F.M. Bastos De Oliveira, M.R. Harris, and R.A.M. De Bruin. 2012. The checkpoint transcriptional response: Make sure to turn it off once you are satisfied. *Cell Cycle*. 11:3166–3174. doi:10.4161/cc.21197.
Spellman, P., G. Sherlock, M. Zhang, V. Iyer, K. Anders, M. Eisen, P. Brown, D. Botstein, and B. Futcher. 1998. Comprehensive identification of cell cycle-regulated genes of the yeast Saccharomyces cerevisiae by microarray hybridization. *Mol. Biol. Cell*. 9:3273–3297. doi:10.1091/mbc.9.12.3273.
Strich, R., R.T. Surosky, C. Steber, E. Dubois, F. Messenguy, and R.E. Esposito. 1994. UME6 is a key regulator of nitrogen repression and meiotic development. *Genes Dev.* 8:796–810. doi:10.1101/gad.8.7.796.
Taberner, F.J., and J.C. Igual. 2010. Yeast karyopherin Kap95 is required for cell cycle progression at Start. *BMC Cell Biol.* 11:1–13. doi:10.1186/1471-2121-11-47.
Talarek, N., E. Cameroni, M. Jaquenoud, X. Luo, S. Bontron, S. Lippman, G. Devgan, M. Snyder, J.R. Broach, and C. De Virgilio. 2010. Initiation of the TORC1-Regulated G0 Program Requires Igo1/2, which License Specific mRNAs to Evade Degradation via the 5′-3′ mRNA Decay Pathway. *Mol. Cell*. 38:345–355. doi:10.1016/j.molcel.2010.02.039.
Travesa, A., T.I. Kalashnikova, R.A.M. de Bruin, S.R. Cass, C. Chahwan, D.E. Lee, N.F. Lowndes, and C. Wittenberg. 2013. Repression of G1/S Transcription Is Mediated via Interaction of the GTB Motifs of Nrm1 and Whi5 with Swi6. *Mol. Cell. Biol.* 33:1476–1486. doi:10.1128/MCB.01333-12.
Tresenrider, A., K. Morse, V. Jorgensen, M. Chia, H. Liao, F.J. van Werven, and E. Ünal. 2021. Integrated genomic analysis reveals key features of long undecoded transcript isoform-based gene repression. *Mol. Cell*. 81:2231-2245.e11. doi:10.1016/j.molcel.2021.03.013.
Tresenrider, A., and E. Ünal. 2017. One-two punch mechanism of gene repression: a fresh perspective on gene regulation. *Curr. Genet.* 0:1–8. doi:10.1007/s00294-017-0793-5.
Tsuchiya, D., Y. Yang, and S. Lacefield. 2014. Positive Feedback of NDT80 Expression Ensures Irreversible Meiotic Commitment in Budding Yeast. *PLoS Genet.* 10. doi:10.1371/journal.pgen.1004398.
Verma, R., R.S. Annan, M.J. Huddleston, S.A. Carr, G. Reynard, and R.J. Deshaies.

1997. Phosphorylation of Sic1p by G1 Cdk required for its degradation and entry into S phase. *Science (80-.).* 278:455–460. doi:10.1126/science.278.5337.455.
Vidan, S., and A.P. Mitchell. 1997. Stimulation of yeast meiotic gene expression by the glucose-repressible protein kinase Rim15p. *Mol. Cell. Biol.* 17:2688–2697. doi:10.1128/mcb.17.5.2688.
Wagner, M. V., M.B. Smolka, R.A.M. de Bruin, H. Zhou, C. Wittenberg, and S.F. Dowdy. 2009. Whi5 regulation by site specific CDK-phosphorylation in Saccharomyces cerevisiae. *PLoS One*. 4. doi:10.1371/journal.pone.0004300.
Weidberg, H., F. Moretto, G. Spedale, A. Amon, and F.J. van Werven. 2016. Nutrient Control of Yeast Gametogenesis Is Mediated by TORC1, PKA and Energy Availability. *PLoS Genet.* 12:1–26. doi:10.1371/journal.pgen.1006075.
Vander Wende, H.M., M. Gopi, M. Onyundo, C. Medrano, T. Adanlawo, and G.A. Brar. 2022. Meiotic resetting of the cellular Sod1 pool is driven by protein aggregation, degradation, and transient LUTI-mediated repression. *J. Cell Biol.* 222. doi:10.1101/2022.06.28.498006.
van Werven, F.J., and A. Amon. 2011. Regulation of entry into gametogenesis. *Philos. Trans. R. Soc. B Biol. Sci.* 366:3521–3531. doi:10.1098/rstb.2011.0081.
van Werven, F.J., A. Lardenois, G. Neuert, N. Hendrick, A. Lardenois, S. Buratowski, A. van Oudenaarden, M. Primig, and A. Amon. 2012. Transcription of Two Long Noncoding RNAs Mediates Mating-Type Control of Gametogenesis in Budding Yeast. *Cell*. 150:1170–1181. doi:10.1016/j.cell.2012.06.049.
Van Werven, F.J., G. Neuert, N. Hendrick, A. Lardenois, S. Buratowski, A. Van Oudenaarden, M. Primig, and A. Amon. 2012. Transcription of two long noncoding RNAs mediates mating-type control of gametogenesis in budding yeast. *Cell*. 150:1170–1181. doi:10.1016/j.cell.2012.06.049.
Williams, R.M., M. Primig, B.K. Washburn, E.A. Winzeler, M. Bellis, C. Sarrauste de Menthiere, R.W. Davis, and R.E. Esposito. 2002. The Ume6 regulon coordinates metabolic and meiotic gene expression in yeast. *Proc. Natl. Acad. Sci. U. S. A.* 99:13431–13436. doi:10.1073/pnas.202495299.
Winter, E. 2012. The Sum1/Ndt80 Transcriptional Switch and Commitment to Meiosis in Saccharomyces cerevisiae. *Microbiol. Mol. Biol. Rev.* 76:1–15. doi:10.1128/mmbr.05010-11.
Xie, J., M. Pierce, V. Gailus-Durner, M. Wagner, E. Winter, and A.K. Vershon. 1999. Sum1 and Hst1 repress middle sporulation-specific gene expression during mitosis in Saccharomyces cerevisiae. *EMBO J.* 18:6448–6454. doi:10.1093/emboj/18.22.6448.